MR Imaging and Spectroscopy of Brain Plasticity after Experimental Stroke

Jet van der Zijden

ISBN 978 90 311 3024 5

Cover Design: Boekhorst Design, Culemborg
Produced by: Gertjan Verhoog & Caroline ter Meulen
Automatische opmaak: Pre Press, Zeist

MR Imaging and Spectroscopy of Brain Plasticity after Experimental Stroke

MR beeldvorming en spectroscopie van hersenplasticiteit na een experimentele beroerte

(met een samenvatting in het Nederlands)

Proefschrift ter verkrijging van de graad van doctor aan
de Universiteit Utrecht op gezag van
de rector magnificus, prof.dr. J.C. Stoof,
ingevolge het besluit van het college voor promoties
in het openbaar te verdedigen op donderdag 3 juli 2008
des middags te 2.30 uur

door

Johanna Petra van der Zijden
geboren op 18 mei 1979 te Tiel

Promotor: Prof. dr. M.A. Viergever

Co-promotor: Dr. R.M. Dijkhuizen

The research described in this thesis was carried out at the Department of Biomedical MR Imaging and Spectroscopy (BMRIS) of the Image Sciences Institute, University Medical Center Utrecht (Utrecht, The Netherlands), under the auspices of ImagO, the Utrecht Graduate School for Biomedical Image Sciences. Financial support for publication of this thesis was kindly provided by Philips Medical Systems, Röntgen Stichting Utrecht and ImagO Research School for Biomedical Image Sciences.

Table of contents

Chapter 1 General Introduction

1 General Introduction

Stroke and brain plasticity

Ischemic stroke is a major cause of death and long-term disability in the Western society. It leaves more than half of the patients dependent on daily assistance and is considered to be a substantial social burden.

Cerebral ischemia is defined as loss of blood supply to the brain, typically caused by occlusion of a cerebral artery. The reduction in regional blood flow restricts the delivery of nutrients, particularly oxygen and glucose, which triggers a series of biochemical and metabolic changes, ultimately leading to neuronal cell death (see Dirnagl et al. (1999)). At acute stages after focal cerebral ischemia, the irreversibly damaged ischemic core, where blood flow is severely reduced, is commonly surrounded by an area with lesser blood flow deficits, which remains viable for an extent of time. This area is referred to as the penumbra and may be salvageable with timely treatment (Hakim, 1987; Baron et al., 1995; Fisher, 2004). Without therapeutic intervention, however, the penumbra will also become part of the irreversibly damaged core.

The only effective drug approved for early treatment of clinical stroke, tissue plasminogen activator (tPA), is aimed at restoration of perfusion through thrombolysis. However, thrombolytic treatment with tPA is restricted to the hyperacute stage after stroke (up to 3 hours) (Marler, 1995; Hacke et al., 1995). Beyond this time-window, thrombolytic treatment carries a substantial risk of inducing reperfusion injury and/or cerebral hemorrhage. Therefore, there is an urgent need for additional therapies with an extended treatment time-window.

Even beyond the acute stages, when the penumbra has become part of the irreversibly damaged lesion core, most patients exhibit a certain degree of spontaneous functional recovery in the the following weeks or months after stroke. Functional recovery at these stages, when potentially salvageable areas within ischemic tissue have dissolved, is thought to be related to brain plasticity, which refers to the capability of the brain to compensate for loss of function through reorganization of neural networks.

Brain plasticity after injury involves a variety of short- and long-term changes in structure and physiology of neuronal networks that may lead to

functional recovery (see for reviews Nudo and Friel (1999); Kreisel et al. (2006); Rodriguez-Gonzalez et al. (2007)). Several short-term phenomena may lead to unmasking or strengthening of existing pathways that were previously functionally inactive or less involved. Modulation of GABAergic inhibition, neuronal excitability and/or synaptic transmission may be responsible for enhanced activation in ipsi- and contralateral areas remote from the lesion site (see for reviews Weiller (1998); Rossini and Pauri (2000)). As functional recovery progresses, initially dysfunctional perilesional brain areas may regain neuronal function (Dijkhuizen et al., 2001; Dijkhuizen et al., 2003; Tombari et al., 2004; Jaillard et al., 2005; Weber et al., 2008). Then, during chronic stages of post-stoke recovery, long-term structural changes start to reveal and may result in the formation of new connections. Such neuroanatomical plasticity may involve a complex pattern of molecular and cellular events ultimately leading to the establishment of new networks, including induction of growth-promoting genes, reduction of growth-inhibiting proteins, axonal and dendritic sprouting, synaptogenesis and neurogenesis (Cramer and Chopp, 2000; Keyvani and Schallert, 2002; Carmichael, 2006; Nudo, 2006).

A schematic overview of the short- and long-term changes in neuronal networks during the time course of functional recovery is shown in Table 1.

Table 1 **A schematic categorization of the time course of structural and functional adaptations after stroke (see for reviews Nudo and Friel (1999); Kreisel et al. (2006); Rodriguez-Gonzalez et al. (2007)).**

Time after stroke	***Mechanisms of plasticity***
Acute (hours-days)	*Alterations in excitation and inhibition* Neuronal excitability ↑ Synaptic transmission ↑ GABAergic disinhibition ↓
Subacute (days-weeks)	*Restitution of neuronal function* Strengthening of existing pathways Unmasking of alternative pathways
Chronic (days-months)	*Formation of new pathways* Growth-promoting gene expression ↑ Reduction of growth-inhibiting proteins Axonal sprouting ↑ Dendritic sprouting ↑ Synaptogenesis ↑

A great deal of studies suggest that structural plasticity in regions adjacent and remote to the lesion plays a significant role in functional recovery after focal brain injury (for reviews see Nudo (1999); Keyvani and Schallert (2002); Carmichael (2003)). Regions that are prone to plastic changes interact with the ischemic zone, either through network connections or metabolically. Connected areas may be acutely affected, for example because of compression through edema (within the ipsilesional hemisphere) or metabolic stress, but may be capable to reinstate or take over lost functions more chronically.

The large variety of time-dependent post-stroke anatomical and functional alterations may improve functioning and organization of neuronal connections leading to gradual functional recovery. Although many studies have described plastic changes after stroke (see Lee and van Donkelaar (1995); Nudo and Friel (1999) for a review), the exact mechanisms involved in plasticity and their specific contribution to functional recovery are still unclear.

The prolonged time-course of brain plasticity in relation to spontaneous functional recovery may hold great potential for long-term therapeutic interventions that are aimed at facilitating plastic adaptation. Knowledge about the mechanisms responsible for functional recovery may aid in the development of new rehabilitation strategies directed at the improvement of functional outcome.

Much of the progress in understanding the dynamics of stroke has been derived from animal studies (see for review McAuley (1995)). Experimental stroke models enable controllable assessment of the temporal characteristics of brain damage and recovery. In addition, animal studies allow combination of multiple experimental methods, including invasive techniques, to study (changes in) brain physiology and anatomy. In our laboratory, various stroke models, including the well-established technique for induction of transient focal cerebral ischemia in the rat by intraluminal occlusion of the middle cerebral artery (Longa et al., 1989), have been successfully applied for many years.

Magnetic resonance imaging and spectroscopy to study brain plasticity

Many experimental animal studies on stroke are based on invasive experimental techniques (e.g., immunohistochemistry) at single time-points, or investigate a restricted part of the brain (e.g., electrophysiology measurements). Magnetic resonance imaging (MRI) and spectroscopy (MRS), however, allow *in vivo* and repetitive measurements. Because multiple parameters can be measured with MRI and MRS, different pathophysiologic aspects of the evolution of stroke may be studied in the same experiment. In particular, T_2- (T_2W-MRI), diffusion- (DW-MRI) and perfusion-weighted MRI (PW-MRI) have proven their value in stroke diagnosis and experimental research (see for review Dijkhuizen and Nicolay (2003)). T_2W-MRI is sensitive to changes in interstitial water content and can detect tissue changes after stroke due to spongiosis and/or vasogenic edema (van Bruggen et al., 1994; Baird and Warach, 1998). It serves as a

reliable tool to determine the extent and location of the ischemic lesion at subacute and chronic stages (Figure 1, left).

However, changes in T_2 at the hyperacute stage are minimal. Then again, DW-MRI has been shown to be able to detect early-ischemia induced reduction of the apparent diffusion coefficient (ADC) of tissue water, most likely associated with early cytotoxic cell swelling (Moseley et al., 1990). In addition, DW-MRI applied in combination with PW-MRI, permits early identification of tissue-at-risk from the mismatch between diffusion changes and perfusion deficits, which may provide an important guideline for thrombolytic therapy (Sunshine et al., 1999). At chronic stages after stroke, ADC of tissue water is elevated due to cellular lysis and excessive accumulation of edematous water (Figure 1, right).

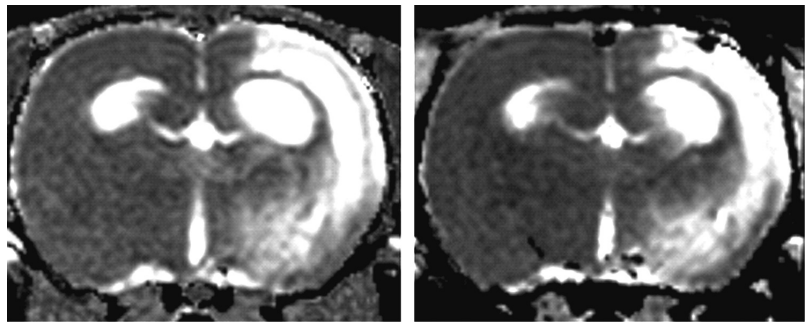

Figure 1

T_2 map (left) and ADC map (right) of a coronal rat brain slice at 3 weeks after transient focal cerebral ischemia. The hyperintense tissue represents the lesion area.

While MR has proven to be able to visualize the area of ischemic damage, the detection of neuronal reorganization in areas outside the infarction remains challenging. In recent years, promising results have been obtained with functional MRI (fMRI) to study changes in brain activation patterns in stroke patients (see reviews by Cramer and Bastings (2000); Rijntjes and Weiller (2002); Calautti and Baron (2003)) and animal models of stroke (Dijkhuizen et al., 2001; Dijkhuizen and Nicolay, 2003).

MRI and MRS of brain function

fMRI, which is based on the detection of the hemodynamic response to neuronal activity, allows whole-brain mapping of stimulus-induced cerebral activation. It can be executed with blood oxygenation level-dependent (BOLD), cerebral blood flow (CBF)-weighted, or cerebral blood volume (CBV)-weighted MRI (Mandeville et al., 2001). In brain pathologies, fMRI enables detection of loss of functional activation, shifts in activation patterns, and evaluation of the functional efficacy of therapies. Moreover, multi-parametric MRI in combination with behavioral studies and histology enables

intra-individual assessment of the interrelationship between brain activation patterns, tissue and perfusion conditions, and functional status. By applying this experimental approach in a rat stroke model, our research team has demonstrated that at acute stages activation in the contralesional hemisphere during stimulation of the stroke-affected forelimb is associated with large lesions, and that restoration of function depends on preservation or reinstatement of ipsilesional activity (Dijkhuizen and Nicolay, 2003) (see Figure 2).

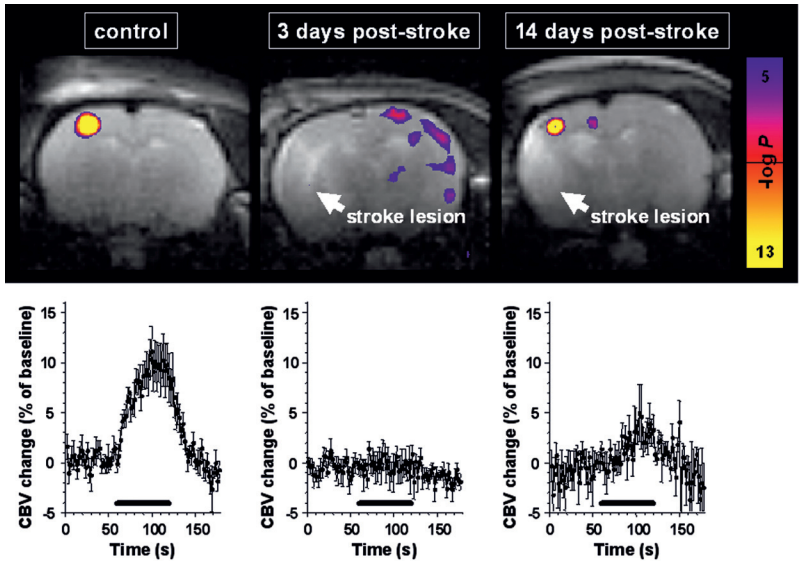

Figure 2

T_2-weighted MR images of a rat brain slice overlaid by statistical activation maps. Contrast-enhanced CBV-weighted functional MRI was performed in combination with an electrical forelimb stimulation paradigm as described by Dijkhuizen et al. (2001) (block design; 60 s stimulation on, 300 s stimulation off) (Dijkhuizen et al., 2001). The colour-coded activation maps represent P values calculated by voxel-wise Student's t-testing of the difference in CBV response between stimulated and non-stimulated conditions. Left forelimb stimulation induced significant activation responses in the right sensorimotor cortex in control rats. At 3 days after right-sided stroke, activation responses in the right, ipsilesional sensorimotor cortex were largely absent, however, responses were found in the left, contralesional hemisphere. After 14 days, partial restoration of activation was detected in the right, ipsilesional sensorimotor cortex. Modified from Van der Zijden and Dijkhuizen (2007).

Changes in neuronal and glial metabolism may play a central role in post-stroke loss and recovery of brain function. Ischemia causes distortion of key metabolic processes in the brain, such as glucose metabolism and glutamatergic neurotransmission (Haberg et al., 1998; Pascual et al., 1998; Haberg et al., 2001; Haberg et al., 2006; Thoren et al., 2006), which may underlie structural and functional plasticity in tissue recovering from stroke. MRS

offers a tool to detect changes in metabolite levels as well as to measure active metabolic pathways, both in humans and animal models (Novotny et al., 2003; Choi et al., 2007), and may provide insights into the metabolic status of tissue affected by cerebral ischemia. In particular, ^{13}C MRS or ^{1}H-observed, ^{13}C-edited (^{1}H/^{13}C) MRS, allows measurement of actively formed ^{13}C-labeled metabolic products after infusion of ^{13}C-labeled metabolic precursors, e.g. glucose (Pfeuffer et al., 1999; de Graaf et al., 2003b), which informs on active metabolic pathways in the brain. A few earlier studies have successfully applied *ex vivo* ^{13}C MRS to characterize regionally specific differences in glucose metabolism after focal cerebral ischemia (Haberg et al., 2001; Haberg et al., 2006). These have demonstrated that differences in Glu and Gln synthesis may distinguish the penumbra zone from the lesion core in the first 4 hour after stroke. Using *in vivo* ^{1}H/^{13}C MRS, dynamic incorporation of the ^{13}C-label into metabolic products 4-^{13}C glutamate and 4-^{13}C glutamine can be measured in order to characterize neuronal and glial metabolism. Hence, the advanced method of *in vivo* ^{1}H/^{13}C MRS may hold great potential to acquire information on metabolic changes underlying neuronal dysfunction and recovery after stroke.

MRI of neuroanatomical reorganization

In vivo diffusion tensor imaging (DTI) (Basser et al., 1994) or manganese-enhanced MRI (MEMRI) (Pautler et al., 1998) can be applied to detect neuroanatomical alterations in the ischemic brain that may be associated with brain plasticity. DTI enables the assessment of the three-dimensional displacement of tissue water. Scalar indices of water diffusion anisotropy can be calculated which inform on structural integrity of gray and white matter (Basser and Pierpaoli, 1996). DTI has shown to be able to reveal a specific temporal profile of changes in mean diffusivity (ADC_{av}) and fractional anisotropy (FA) in the lesion area after stroke, which may be related to specific pathophysiological processes. At the (hyper)acute stage after stroke, reduced ADC_{av}, reflective of cytotoxic edema, is paralleled by increased FA, suggestive of increased tortuosity (Sotak, 2002; Liu et al., 2007). More chronically, ADC_{av} increases and FA declines as a result of loss of structural integrity of brain tissue (Sotak, 2002; Liu et al., 2007), which has shown to be most prominent in white matter areas (Munoz Maniega et al., 2004). In two recent studies, DTI revealed an increase in FA in non-lesioned white matter areas at chronic time points after stroke, which may point towards white matter reorganization (Jiang et al., 2006; Wang et al., 2006). Hence, longitudinal DTI measurements may enable the assessment of long-term changes in tissue microstructure in- and outside the lesion area that may be associated with degenerative and restorative processes.

Alternatively, connective pathways may be visualized with MEMRI. Manganese (Mn^{2+}) is a Ca^{2+} analogue that can enter neurons through Ca^{2+} channels and can be transported along axons (Sloot and Gramsbergen, 1994). Another property of Mn^{2+}, is that it is paramagnetic and shortens T_1 thereby

allowing visualization using MRI (Mendonca-Dias et al., 1983; Fornasiero et al., 1987). Importantly, calculation of the difference between pre- and post-contrast R_1 ($1/T_1$) (ΔR_1), which is proportional to the local manganese concentration (Silva et al., 2004), provides quantitative information on accumulation of manganese. MEMRI has already successfully been applied as *in vivo* tract tracing method to visualize neuronal connections in the visual, olfactory, and sensorimotor system of mice and rats (Pautler et al., 1998; Watanabe et al., 2001; Pautler and Koretsky, 2002; Leergaard et al., 2003). More recently, the potential of MEMRI to study plasticity in the songbird (Van der Linden et al., 2004), and to detect changes in neuronal pathways after stroke in a rat model (Allegrini and Wiessner, 2003) has been demonstrated.

In conclusion, MRI offers a versatile tool to study the spatiotemporal pattern of functional and anatomical changes after stroke. The combination of MR techniques with behavioural experiments can provide unique information on the correlation between different aspects of reorganization in the brain and post-stroke recovery of function. Thus, multi-parametric experimental MR studies may significantly contribute to unravelling underlying neural correlates of functional recovery after stroke.

Aims and Outline

As discussed in the previous paragraphs, there is increasing evidence that spontaneous functional recovery after stroke is associated with structural and functional changes in non-injured brain circuitry. Unravelling the mechanisms of plasticity that contribute to functional recovery may provide important targets for development and optimization of rehabilitative therapies. Nevertheless, characterization of plasticity after stroke remains challenging, because it involves a complex pattern of long-term functional and structural changes in the brain. Yet, MR techniques may offer an effective tool for this purpose, since it allows i) *in vivo*, ii) multi-parametric and iii) longitudinal assessment of morphology, physiology and metabolism in the functioning brain.

The main objective of this thesis was to elucidate spatial and temporal characteristics of brain plasticity underlying post-stroke functional recovery. To that aim, different *in vivo* MR techniques were combined in order to obtain detailed information on long-term changes in morphology and physiology, particularly in brain regions outside the lesion area.

Chapter 2 was aimed at the validation of MEMRI as a tool to study neuronal connectivity changes within the sensorimotor network after unilateral stroke in rats. The spatiotemporal pattern of intracerebral manganese distribution after injection in the ipsilesional sensorimotor cortex was depicted at 2 weeks after stroke. *In vivo* manganese enhancement was compared with *post mortem* wheat-germ agglutinin horseradish peroxidase (WGA-HRP) staining, a conventional tract tracing method.

In **Chapter 3**, the temporal pattern of changes in neuronal connectivity from 2 to 10 weeks following unilateral stroke in rats was characterized using MEMRI. Changes in manganese enhancement were correlated with changes in functional status.

In **Chapter 4**, the temporal profile of structural remodelling of perilesional tissue was characterized using longitudinal T_2 and DTI measurements from 3 hours up to 10 weeks after experimental stroke. These data were correlated with the extent of neuronal connectivity within the perilesional sensorimotor network, as measured with MEMRI.

Chapter 5 was aimed at elucidating lesional and perilesional alterations in glycolysis and glutamatergic neurotransmitter metabolism at 24 hours and 3 weeks after stroke using *in vivo* $^{1}H/^{13}C$ MRS combined with ^{13}C-labeled glucose infusion.

Finally, in **Chapter 6** the findings described in Chapters 2-5 are discussed, and future potentials and pitfalls are outlined.

References

Allegrini PR, Wiessner C (2003). Three-dimensional MRI of cerebral projections in rat brain in vivo after intracortical injection of MnCl2. NMR Biomed 16:252-256.

Baird AE, Warach S (1998). Magnetic resonance imaging of acute stroke. J Cereb Blood Flow Metab 18:583-609.

Baron JC, von Kummer R, del Zoppo GJ (1995). Treatment of acute ischemic stroke. Challenging the concept of a rigid and universal time window. Stroke 26:2219-2221.

Basser PJ, Pierpaoli C (1996). Microstructural and physiological features of tissues elucidated by quantitative-diffusion-tensor MRI. J Magn Reson B 111:209-219.

Basser PJ, Mattiello J, LeBihan D (1994). MR diffusion tensor spectroscopy and imaging. Biophys J 66:259-267.

Calautti C, Baron JC (2003). Functional neuroimaging studies of motor recovery after stroke in adults: a review. Stroke 34:1553-1566.

Carmichael ST (2003). Plasticity of cortical projections after stroke. Neuroscientist 9:64-75.

Carmichael ST (2006). Cellular and molecular mechanisms of neural repair after stroke: making waves. Ann Neurol 59:735-742.

Choi JK, Dedeoglu A, Jenkins BG (2007). Application of MRS to mouse models of neurodegenerative illness. NMR Biomed 20:216-237.

Cramer SC, Chopp M (2000). Recovery recapitulates ontogeny. Trends Neurosci 23:265-271.

Cramer SC, Bastings EP (2000). Mapping clinically relevant plasticity after stroke. Neuropharmacology 39:842-851.

de Graaf RA, Brown PB, Mason GF, Rothman DL, Behar KL (2003a). Detection of [1,6-13C2]-glucose metabolism in rat brain by in vivo 1H-[13C]-NMR spectroscopy. Magn Reson Med 49:37-46.

de Graaf RA, Mason GF, Patel AB, Behar KL, Rothman DL (2003b). In vivo 1H-[13C]-NMR spectroscopy of cerebral metabolism. NMR Biomed 16:339-357.

de Graaf RA, Mason GF, Patel AB, Rothman DL, Behar KL (2004). Regional glucose metabolism and glutamatergic neurotransmission in rat brain in vivo. Proc Natl Acad Sci U S A 101:12700-12705.

Dijkhuizen RM, Nicolay K (2003). Magnetic resonance imaging in experimental models of brain disorders. J Cereb Blood Flow Metab 23:1383-1402.

Dijkhuizen RM, Ren J, Mandeville JB, Wu O, Ozdag FM, Moskowitz MA, Rosen BR, Finklestein SP (2001). Functional magnetic resonance imaging of reorganization in rat brain after stroke. Proc Natl Acad Sci U S A 98:12766-12771.

Dijkhuizen RM, Singhal AB, Mandeville JB, Wu O, Halpern EF, Finklestein SP, Rosen BR, Lo EH (2003). Correlation between brain reorganization, ischemic damage, and neurologic status after transient focal cerebral ischemia in rats: a functional magnetic resonance imaging study. J Neurosci 23:510-517.

Dirnagl U, Iadecola C, Moskowitz MA (1999). Pathobiology of ischaemic stroke: an integrated view. Trends Neurosci 22:391-397.

Fisher M (2004). The ischemic penumbra: identification, evolution and treatment concepts. Cerebrovasc Dis 17 Suppl 1:1-6.

Fornasiero D, Bellen JC, Baker RJ, Chatterton BE (1987). Paramagnetic complexes of manganese(II), iron(III), and gadolinium(III) as contrast agents for magnetic resonance imaging. The influence of stability constants on the biodistribution of radioactive aminopolycarboxylate complexes. Invest Radiol 22:322-327.

Gruetter R, Seaquist ER, Ugurbil K (2001). A mathematical model of compartmentalized neurotransmitter metabolism in the human brain. Am J Physiol Endocrinol Metab 281: E100-112.

Haberg A, Qu H, Sonnewald U (2006). Glutamate and GABA metabolism in transient and permanent middle cerebral artery occlusion in rat: importance of astrocytes for neuronal survival. Neurochem Int 48:531-540.

Haberg A, Qu H, Haraldseth O, Unsgard G, Sonnewald U (1998). In vivo injection of [1-13C]glucose and [1,2-13C]acetate combined with ex vivo 13C nuclear magnetic resonance spectroscopy: a novel approach to the study of middle cerebral artery occlusion in the rat. J Cereb Blood Flow Metab 18:1223-1232.

Haberg A, Qu H, Saether O, Unsgard G, Haraldseth O, Sonnewald U (2001). Differences in neurotransmitter synthesis and intermediary metabolism between glutamatergic and GABAergic neurons during 4 hours of middle cerebral artery occlusion in the rat: the role of astrocytes in neuronal survival. J Cereb Blood Flow Metab 21:1451-1463.

Hacke W, Kaste M, Fieschi C, Toni D, Lesaffre E, von Kummer R, Boysen G, Bluhmki E, Hoxter G, Mahagne MH, et al. (1995). Intravenous thrombolysis with recombinant tissue plasminogen activator for acute hemispheric stroke. The European Cooperative Acute Stroke Study (ECASS). Jama 274:1017-1025.

Hakim AM (1987). The cerebral ischemic penumbra. Can J Neurol Sci 14:557-559.

Jaillard A, Martin CD, Garambois K, Lebas JF, Hommel M (2005). Vicarious function within the human primary motor cortex? A longitudinal fMRI stroke study. Brain 128: 1122-1138.

Jiang Q, Zhang ZG, Ding GL, Silver B, Zhang L, Meng H, Lu M, Pourabdillah-Nejed DS, Wang L, Savant-Bhonsale S, Li L, Bagher-Ebadian H, Hu J, Arbab AS, Vanguri P, Ewing JR, Ledbetter KA, Chopp M (2006). MRI detects white matter reorganization after neural progenitor cell treatment of stroke. Neuroimage 32:1080-1089.

Keyvani K, Schallert T (2002). Plasticity-associated molecular and structural events in the injured brain. J Neuropathol Exp Neurol 61:831-840.

Kreisel SH, Bazner H, Hennerici MG (2006). Pathophysiology of stroke rehabilitation: temporal aspects of neuro-functional recovery. Cerebrovasc Dis 21:6-17.

Lee RG, van Donkelaar P (1995). Mechanisms underlying functional recovery following stroke. Can J Neurol Sci 22:257-263.

Leergaard TB, Bjaalie JG, Devor A, Wald LL, Dale AM (2003). In vivo tracing of major rat brain pathways using manganese-enhanced magnetic resonance imaging and three-dimensional digital atlasing. Neuroimage 20:1591-1600.

Liu Y, D'Arceuil HE, Westmoreland S, He J, Duggan M, Gonzalez RG, Pryor J, de Crespigny AJ (2007). Serial diffusion tensor MRI after transient and permanent cerebral ischemia in nonhuman primates. Stroke 38:138-145.

Longa EZ, Weinstein PR, Carlson S, Cummins R (1989). Reversible middle cerebral artery occlusion without craniectomy in rats. Stroke 20:84-91.

Mandeville JB, Jenkins BG, Kosofsky BE, Moskowitz MA, Rosen BR, Marota JJ (2001). Regional sensitivity and coupling of BOLD and CBV changes during stimulation of rat brain. Magn Reson Med 45:443-447.

Marler JR for The National Institute of Neurological Disorders and Stroke rt-PA Stroke Study Group (1995). Tissue plasminogen activator for acute ischemic stroke. N Engl J Med 333:1581-1587.

Mason GF, Rothman DL (2004). Basic principles of metabolic modeling of NMR (13)C isotopic turnover to determine rates of brain metabolism in vivo. Metab Eng 6:75-84.

McAuley MA (1995). Rodent models of focal ischemia. Cerebrovasc Brain Metab Rev 7:153-180.

Mendonca-Dias MH, Gaggelli E, Lauterbur PC (1983). Paramagnetic contrast agents in nuclear magnetic resonance medical imaging. Semin Nucl Med 13:364-376.

Moseley ME, Cohen Y, Mintorovitch J, Chileuitt L, Shimizu H, Kucharczyk J, Wendland MF, Weinstein PR (1990). Early detection of regional cerebral ischemia in cats: comparison of diffusion- and T2-weighted MRI and spectroscopy. Magn Reson Med 14:330-346.

Munoz Maniega S, Bastin ME, Armitage PA, Farrall AJ, Carpenter TK, Hand PJ, Cvoro V, Rivers CS, Wardlaw JM (2004). Temporal evolution of water diffusion parameters is different in grey and white matter in human ischaemic stroke. J Neurol Neurosurg Psychiatry 75:1714-1718.

Novotny EJ, Jr., Fulbright RK, Pearl PL, Gibson KM, Rothman DL (2003). Magnetic resonance spectroscopy of neurotransmitters in human brain. Ann Neurol 54 Suppl 6: S25-31.

Nudo RJ (1999). Recovery after damage to motor cortical areas. Curr Opin Neurobiol 9: 740-747.

Nudo RJ (2006). Mechanisms for recovery of motor function following cortical damage. Curr Opin Neurobiol 16:638-644.

Nudo RJ, Friel KM (1999). Cortical plasticity after stroke: implications for rehabilitation. Rev Neurol (Paris) 155:713-717.

Pascual JM, Carceller F, Roda JM, Cerdan S (1998). Glutamate, glutamine, and GABA as substrates for the neuronal and glial compartments after focal cerebral ischemia in rats. Stroke 29:1048-1056; discussion 1056-1047.

Pautler RG, Koretsky AP (2002). Tracing odor-induced activation in the olfactory bulbs of mice using manganese-enhanced magnetic resonance imaging. Neuroimage 16:441-448.

Pautler RG, Silva AC, Koretsky AP (1998). In vivo neuronal tract tracing using manganese-enhanced magnetic resonance imaging. Magn Reson Med 40:740-748.

Petersen KF, Krssak M, Navarro V, Chandramouli V, Hundal R, Schumann WC, Landau BR, Shulman GI (1999). Contributions of net hepatic glycogenolysis and gluconeogenesis to glucose production in cirrhosis. Am J Physiol 276:E529-535.

Pfeuffer J, Tkac I, Choi IY, Merkle H, Ugurbil K, Garwood M, Gruetter R (1999). Localized in vivo 1H NMR detection of neurotransmitter labeling in rat brain during infusion of [1-13C] D-glucose. Magn Reson Med 41:1077-1083.

Rijntjes M, Weiller C (2002). Recovery of motor and language abilities after stroke: the contribution of functional imaging. Prog Neurobiol 66:109-122.

Rodriguez-Gonzalez R, Hurtado O, Sobrino T, Castillo J (2007). Neuroplasticity and cellular therapy in cerebral infarction. Cerebrovasc Dis 24 Suppl 1:167-180.

Rossini PM, Pauri F (2000). Neuromagnetic integrated methods tracking human brain mechanisms of sensorimotor areas 'plastic' reorganisation. Brain Res Brain Res Rev 33: 131-154.

Shen J, Petersen KF, Behar KL, Brown P, Nixon TW, Mason GF, Petroff OA, Shulman GI, Shulman RG, Rothman DL (1999). Determination of the rate of the glutamate/glutamine cycle in the human brain by in vivo 13C NMR. Proc Natl Acad Sci U S A 96:8235-8240.

Sibson NR, Dhankhar A, Mason GF, Behar KL, Rothman DL, Shulman RG (1997). In vivo 13C NMR measurements of cerebral glutamine synthesis as evidence for glutamate-glutamine cycling. Proc Natl Acad Sci U S A 94:2699-2704.

Silva AC, Lee JH, Aoki I, Koretsky AP (2004). Manganese-enhanced magnetic resonance imaging (MEMRI): methodological and practical considerations. NMR Biomed 17:532-543.

Sloot WN, Gramsbergen JB (1994). Axonal transport of manganese and its relevance to selective neurotoxicity in the rat basal ganglia. Brain Res 657:124-132.

Sotak CH (2002). The role of diffusion tensor imaging in the evaluation of ischemic brain injury - a review. NMR Biomed 15:561-569.

Sunshine JL, Tarr RW, Lanzieri CF, Landis DM, Selman WR, Lewin JS (1999). Hyperacute stroke: ultrafast MR imaging to triage patients prior to therapy. Radiology 212:325-332.

Thoren AE, Helps SC, Nilsson M, Sims NR (2006). The metabolism of C-glucose by neurons and astrocytes in brain subregions following focal cerebral ischemia in rats. J Neurochem 97:968-978.

Tombari D, Loubinoux I, Pariente J, Gerdelat A, Albucher JF, Tardy J, Cassol E, Chollet F (2004). A longitudinal fMRI study: in recovering and then in clinically stable sub-cortical stroke patients. Neuroimage 23:827-839.

van Bruggen N, Roberts TP, Cremer JE (1994). The application of magnetic resonance imaging to the study of experimental cerebral ischaemia. Cerebrovasc Brain Metab Rev 6:180-210.

Van der Linden A, Van Meir V, Tindemans I, Verhoye M, Balthazart J (2004). Applications of manganese-enhanced magnetic resonance imaging (MEMRI) to image brain plasticity in song birds. NMR Biomed 17:602-612.

Van der Zijden J, Dijkhuizen RM (2007). Assessment of functional and neuroanatomical reorganization after experimental stroke using MRI. In: Tavitian, Leroy-Willig and Ntziachristos, eds. International Textbook on in vivo Imaging in Vertebrates, 239-242. Chichester: John Wiley & Sons, Ltd.

Wang C, Stebbins GT, Nyenhuis DL, deToledo-Morrell L, Freels S, Gencheva E, Pedelty L, Sripathirathan K, Moseley ME, Turner DA, Gabrieli JD, Gorelick PB (2006). Longitudinal changes in white matter following ischemic stroke: a three-year follow-up study. Neurobiol Aging 27:1827-1833.

Watanabe T, Michaelis T, Frahm J (2001). Mapping of retinal projections in the living rat using high-resolution 3D gradient-echo MRI with Mn2+–induced contrast. Magn Reson Med 46:424-429.

Weber R, Ramos-Cabrer P, Justicia C, Wiedermann D, Strecker C, Sprenger C, Hoehn M (2008). Early prediction of functional recovery after experimental stroke: functional magnetic resonance imaging, electrophysiology, and behavioral testing in rats. J Neurosci 28:1022-1029.

Weiller C (1998). Imaging recovery from stroke. Exp Brain Res 123:13-17.

Chapter 2 Changes in Neuronal Connectivity after Stroke in Rats as studied by Serial Manganese-Enhanced MRI

[1]Jet P. van der Zijden, [1,2]Ona Wu, [1]Annette van der Toorn, [3]Tom P. Roeling, [3]Ronald L.A.W. Bleys, MD, [1]Rick M. Dijkhuizen

[1]Image Sciences Institute, University Medical Center Utrecht, Utrecht, the Netherlands
[2]Athinoula A. Martinos Center for Biomedical Imaging, Massachusetts General Hospital/Massachusetts Institute of Technology/Harvard Medical School, Charlestown, MA, United States
[3]Rudolf Magnus Institute of Neuroscience, University Medical Center Utrecht, Utrecht, the Netherlands

Published in NeuroImage 34, pp. 1650-1657 (2007)

2 Changes in Neuronal Connectivity after Stroke in Rats as studied by Serial Manganese-Enhanced MRI

Abstract

Loss of function and subsequent spontaneous recovery after stroke have been associated with physiological and anatomical alterations in neuronal networks in the brain. However, the spatiotemporal pattern of such changes has been incompletely characterized. Manganese-enhanced MRI (MEMRI) provides a unique tool for *in vivo* investigation of neuronal connectivity.

In this study, we measured manganese-induced changes in longitudinal relaxation rate, R_1, to assess the spatiotemporal pattern of manganese distribution after focal injection into the intact sensorimotor cortex in control rats (n = 10), and in rats at 2 weeks after 90-min unilateral occlusion of the middle cerebral artery (n = 10). MEMRI data were compared with results from conventional tract tracing with wheat-germ agglutinin horseradish peroxidase (WGA-HRP).

Distinct areas of the sensorimotor pathway were clearly visualized with MEMRI. At two weeks after stroke, manganese-induced changes in R_1 were significantly delayed and diminished in the ipsilateral caudate putamen, thalamus and substantia nigra. Loss of connectivity between areas of the sensorimotor network was also identified from reduced WGA-HRP staining in these areas on *post mortem* brain sections. This study demonstrates that MEMRI enables *in vivo* assessment of spatiotemporal alterations in neuronal connectivity after stroke, which may lead to improved insights in mechanisms underlying functional loss and recovery after stroke.

Introduction

Stroke is the leading cause of disability in the western society. Despite acute loss of function after stroke, most patients demonstrate partial functional recovery over time. Interruption and subsequent spontaneous restoration of function has been associated with anatomical and physiological alterations of neuronal networks in the brain (Lee and van Donkelaar, 1995; Seil, 1997; Steinberg and Augustine, 1997; Weiller, 1998; Johansson, 2000). However,

the spatial and temporal characteristics of neural reorganization remain largely unresolved.

In recent years, neuroimaging tools, in particular functional magnetic resonance imaging (fMRI), have been successfully applied for *in vivo*, whole-brain studies on changes in functional activation patterns in stroke patients (see reviews by Cramer and Bastings (2000); Rijntjes and Weiller (2002); Calautti and Baron (2003)) and animal models of stroke (Dijkhuizen et al., 2001; Dijkhuizen and Nicolay, 2003). Studies on anatomical alterations in neuronal connectivity after stroke, have been mostly confined to invasive axonal tract tracing techniques (Kataoka et al., 1989; Carmichael et al., 2001; Carmichael, 2003). Manganese-enhanced MRI (MEMRI) provides a unique tool to assess changes in neuronal connections *in vivo* (Pautler et al., 1998). MEMRI is based on the detection of paramagnetic manganese (Mn^{2+}), a calcium analogue that enters active neurons through Ca^{2+} channels and is transported axonally and transsynaptically (Sloot and Gramsbergen, 1994; Pautler et al., 1998; Saleem et al., 2002). Focal injection of manganese in animal brain is followed by neuronal uptake and subsequent transport along afferent and efferent connective pathways, thereby allowing *in vivo* mapping of neuronal connections (Pautler, 2004). Allegrini and Wiessner (2003), have recently demonstrated that MEMRI has the potential to detect alterations in brain circuitry after cortical injury in rats.

The goal of our study was to depict changes in neuronal connectivity within the sensorimotor network in a rat stroke model at a time-point when ischemic damage is complete and dynamic alterations in sensorimotor function have largely ceased, i.e. two weeks after stroke (Kawamata et al., 1997). To that aim, we characterized the spatiotemporal pattern of manganese accumulation by means of serial brain mapping of changes in the longitudinal relaxation rate R_1 ($1/T_1$), which are proportional to the local manganese concentration (Silva et al., 2004). In addition, MEMRI data were compared with a conventional neuronal tract tracing technique based on the immunohistochemical detection of the tracer wheat-germ agglutinin horseradish peroxidase (WGA-HRP) (Gong and LeDoux, 2003).

Materials and Methods

Animals

All animal procedures were approved by the local ethical committee of Utrecht University and met governmental guidelines. A total of 31 male Wistar rats weighing 250-340 g were included in the study. Rats were divided into two experimental groups. Group 1 animals (n = 20) were subjected to *in vivo* tract tracing using MEMRI; Group 2 animals (n = 11) were subjected to conventional tract tracing using WGA-HRP immunohistochemistry. In both groups, rats were divided in two subgroups. Experimental stroke was induced in Groups 1A (n = 10) and 2A (n = 5). Normal rats in Groups 1B (n = 10) and 2B (n = 6) served as controls.

Figure 1 shows the time schedule for experimental procedures in Groups 1 and 2.

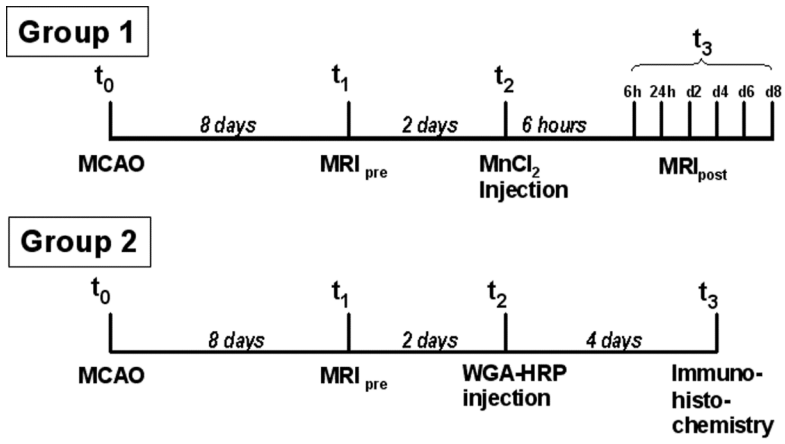

Figure 1

Schematic representation of the time schedule of experimental procedures for Groups 1 and 2. t_0: MCA occlusion (MCAO); t_1: MRI of ischemic lesion (MRI_{pre}); t_2: injection of tracer ($MnCl_2$ or WGA-HRP); t_3: tracer detection with MRI or immunohistochemistry.

Stroke model

Rats were anesthetized with 2.5% isoflurane in N_2O/O_2 (70:30) under spontaneous respiration. Blood oxygen saturation and heart rate were continuously monitored during surgical procedures. Body temperature was maintained at 37.0 ± 0.5 °C. Transient focal cerebral ischemia was induced by 90-min occlusion of the right middle cerebral artery (MCA) with an intraluminal filament (Longa et al., 1989). In brief, a 4.0 silicon-coated polypropylene suture (Ethicon, Piscataway, NJ, USA) was introduced into the external carotid artery and advanced through the internal carotid artery until a slight resistance was felt, indicating that the MCA was occluded. After 90 minutes, the filament was withdrawn from the internal carotid artery to allow reperfusion. After surgery, rats received a subcutaneous injection of 0.3 mg/kg buprenorphin (Schering-Plough, Utrecht, The Netherlands) for post-surgical pain relief, and 5 ml saline to compensate for loss of water and minerals.

Tracer injection

Neuronal tract tracer was injected at ten days after MCA occlusion. Animals were anesthetized by subcutaneous injection of a mixture of 0.55 mg/kg midazolam, and 0.315 mg/ml fentanyl citrate and 10 mg/ml fluanisone (0.55 mg/kg). Rats were placed in a stereotactic holder and immobilized by ear-

plugs and a toothholder. Blood oxygen saturation and heart rate were continuously monitored. Body temperature was maintained at 37.0 ± 0.5 °C.

A burr hole was drilled in the skull at 0.5 mm anterior and 1.5-3.0 mm lateral to bregma (according to Paxinos and Watson (1998)). Lateral coordinates were adapted based on the extent of the lesion, as determined by T_2-weighted MRI prior to tracer injection (see below), and chosen as such that tracer was injected in spared sensorimotor cortical tissue bordering the T_2-defined infarct. Injections sites for control animals were adjusted correspondingly. Mean lateral coordinates were the same for control rats (2.5 ± 0.7 mm) and for rats with a stroke (2.5 ± 0.7 mm).

0.2 µl 1 M isotonic $MnCl_2$ (Group 1) or 0.2 µl 5% WGA-HRP (Group 2) was injected at 1.5 mm below the dura, with a 2.0 µl Hamilton syringe at a rate of 0.05 µl/min. After injection, the needle was left in place for 3 minutes to prevent leakage.

MRI

MRI measurements were performed on a 4.7 T horizontal bore MR system (Varian, Palo Alto, CA, USA) with use of a Helmholtz volume coil (90-mm diameter) and an inductively coupled surface coil (35-mm diameter) for signal excitation and detection, respectively.

Prior to MRI, rats were anaesthetized with 4% isoflurane for endotracheal intubation, followed by mechanical ventilation with 2.5% isoflurane in N_2O/O_2 (70:30). Rats were placed in a MR-compatible stereotactic holder and immobilized with earplugs and a toothholder. Blood oxygen saturation and heart rate were monitored during MRI measurements, and body temperature was maintained at 37.0 ± 0.5 °C.

First, T_2-weighted MRI (multi-echo acquisition with repetition time (TR) = 3 s; echo time (TE) = 17.5 ms; echo train length = 8; acquisition matrix = 128 x 128; voxel dimensions = 0.25 x 0.25 x 1.2 mm^3; 15 coronal slices; number of averages = 2; total acquisition time = 12 min and 48 s) was performed in all rats with a stroke at 2 days prior to tracer injection to determine the extent of the ischemic lesion. In addition, in rats of Group 1, pre-contrast T_1-weighted MRI was performed using a saturation recovery gradient-echo sequence with seven TRs (TR/TE = 55 - 3000/18 ms; acquisition matrix = 128 x 128; voxel dimensions = 0.25 x 0.25 x 1.2 mm^3; 15 coronal slices; number of averages = 2; total acquisition time = 26 min and 16 s). Subsequently, T_2- and T_1-weighted MRI were performed at day 2, 4, 6, and 8 after manganese injection. In a number of animals (Group 1A, n = 5; Group 1B, n = 5), MRI was also done at 6 and 24 h after manganese injection.

Immunohistochemistry

At 4 days after WGA-HRP injection, Group 2 rats were deeply anesthetized by intraperitoneal injection of pentobarbital (120 mg/kg), and immediately transcardially perfused with saline followed by 4% paraformaldehyde in 0.1 M phosphate-buffered saline (PBS). Brains were removed and post-fixed in

4% paraformaldehyde in 0.1 M PBS for an additional 2 h and subsequently stored in 20% sucrose in 0.1 M PBS at 4 °C. Brains were cut in 40-μm thick coronal sections on a freezing microtome, and stored in 20% sucrose in 0.1 M PBS. Free-floating sections were processed for immunohistochemical detection of WGA-HRP using the following protocol: (1) 3x 10-min rinsing in Tris-buffered saline (TBS) (0.05 M; pH = 7.6); (2) 60-min rinsing in 3% H_2O_2 in TBS; (3) 3x 10-min rinsing in TBS; (4) 60-min pre-incubation with 3% normal rabbit serum in TBS; (5) overnight incubation with primary antibody (goat anti-WGA (Vector Laboratories, Burlingame, CA, USA); 1:500), 0.1% bovine serum albumin and 0.1% Triton X-100 in TBS at 4 °C; (6) 3x 10-min rinsing in TBS; (7) 60-min incubation with secondary antibody (polyclonal rabbit anti-goat IgG (DakoCytomation, Glostrup, Denmark); 1:250), 0.1% bovine serum albumin and 0.1% Triton X-100 in TBS; (8) 3x 10-min rinsing in TBS; (9) 90-min incubation with peroxidase-antiperoxidase complex (1:600), 0.1% Triton X-100 in TBS; (10) 3x 10-min rinsing in TBS; (11) development using a diaminobenzidine peroxidase substrate kit (Vector Laboratories Burlingame, CA, USA) with nickel intensification according to manufacturer's instructions; (12) 3x 10-min rinsing in TBS; (13) overnight air drying, dehydration and coverslipping with Entallan (Merck, Darmstadt, Germany).

Data analysis

MRI Quantitative T_2 maps were calculated on a voxel-wise basis by weighted linear least-squares fit of the logarithm of the signal intensity at different echo times versus TE.

Lesion volumes were determined from 11 adjacent slices on quantitative T_2 maps as ipsilateral tissue greater than the mean + 2 SD of T_2 in contralateral tissue. The edema-corrected hemispheric lesion volume (%HLV^e) was calculated as described by Gerriets et al. (2004):

%HLV^e = (HV_c- (HV_i- LV^u))/HV_c x 100%, where HV_c and HV_i are the contralateral and ipsilateral hemispheric volumes, respectively; and LV^u is the uncorrected lesion volume.

Quantitative T_1 maps were calculated on a voxel-wise basis by performing a non-linear least-squares fit using the Levenberg-Marquardt method (Press and Vetterling, 1992). Longitudinal relaxation rate R_1 (= $1/T_1$) maps were coregistered to an averaged brain T_2-weighted MRI data set from 6 control rats using semi-automated image registration software (MNI Autoreg (Collins et al., 1994)). To correct for misregistration as a result of edema-induced brain distortion, anatomic landmarks were manually selected on brains with a stroke lesion, followed by a second registration procedure. Changes in R_1 after manganese administration are proportional to the local manganese concentration (Silva et al., 2004). Hence, manganese accumulation was measured in specific regions-of-interest (ROIs) from the difference between pre- and post-contrast R_1 (ΔR_1). We selected four ipsi- and contralateral ROIs within the sensorimotor corticostriatonigral-thalamocortical pathway. Based on the extent of the lesion in animals with a stroke, ROI size and shape were adjusted, so that the ROI included that part of the particular brain

region that was invariably outside the lesion area for all animals. Contralateral ROIs were exactly matched in size and shape with respect to their ipsilateral counterparts. There were no significant differences between T_2 values in the ipsi- and contralateral ROIs (paired Student's *t*-test; $P < 0.05$), which confirms that ROIs were not part of the infarcted area. Thus, for all animals, ROIs were the same in location, size and shape, and only included the non-infarcted part of the specific anatomical structure.

The selected ROIs were the sensorimotor cortex (SMCX; 36 voxels; center at 1.0 mm posterior, 1.5 mm lateral and 1.5 mm depth from bregma (Paxinos and Watson, 1998), caudate putamen (CPu; 34 voxels; center at 1.0 mm posterior, 3.0 mm lateral and 5.5 mm depth from bregma), thalamus (Th; 87 voxels; center at 2.5 mm posterior, 2.5 mm lateral and 6.0 mm depth from bregma), and substantia nigra (SN; 15 voxels; center at 5.5 mm posterior, 1.5 mm lateral and at a depth of 8.5 mm from bregma) (see Figure 2A). An ROI was also placed in the visual cortex (VCX; 45 voxels; center at 5.5 mm posterior, 3.0 mm lateral and 1.5 mm depth from bregma) to check for non-specific distribution of manganese.

Immunohistochemistry WGA-HRP-stained brain slices were studied with a light microscope (Zeiss Axiophot with Sony 3 CCD Color Video Camera) under bright- and dark-field illumination. WGA-HRP labeled cells were counted with Kontron KS 400 software in anatomical areas that matched the ROIs used for MRI analysis (5 adjacent sections were analyzed for each ROI).

Statistics All values are expressed as mean ± SD. Differences in the temporal pattern of manganese enhancement were analyzed using a one- (within ROIs) or two-way (between ROIs, and between groups) repeated measures analysis-of-variance (ANOVA) with post-hoc multiple comparison *t*-testing with Bonferroni correction. Differences in lesion volumes, T_2 values and WGA-HRP staining were statistically analyzed with a paired or unpaired Student's *t*-test. $P < 0.05$ was considered significant.

Results

Ischemic damage In rats with a stroke, the unilateral ischemic lesion was characterized by a prolonged T_2 (see Figure 2C). The mean $\%HLV^e$ was 12.3 ± 4.8%, with no significant difference in lesion volumes between Groups 1 and 2 (13.1 ± 3.2% and 11.0 ± 6.9%, respectively).

Injection site Lateral coordinates of tracer injection site varied between 1.5 and 3.0 mm from bregma (see Methods section), but were invariably in the forelimb area of the sensorimotor cortex. To determine if variations in injection site influence the pattern of tracer distribution, control animals in Groups 1B en 2B were divided into 2 subgroups, based on the lateral coordinates of the injection site. In subgroup I, lateral coordinates were 1.5-2.5 mm from bregma (n = 4 in Group 1B; n = 3 in Group 2B). In subgroup II: lateral

coordinates were 3.0 mm from bregma (n = 6 in Group 1B; n = 3 in Group 2B). There was only a significant difference in manganese-induced ΔR_1 in SMCX, i.e. nearby the injection site, between the two subgroups. In all other ROIs, there were no significant differences in ΔR_1 values between the subgroups. Moreover, there were no significant differences between the subgroups in any of the ROIs with regard to number of WGA-HRP labeled cells. Therefore, we conclude that the small variation in site of injection did not result in different global patterns of manganese enhancement or WGA-HRP staining.

MEMRI The spatial pattern of manganese enhancement was clearly visualized on R_1 maps (Figure 2A and B). R_1 increase was observed in all four ROIs of the ipsilateral sensorimotor network in control rats as well as after stroke. The temporal pattern of manganese-induced R_1 changes in ipsilateral ROIs is shown in Figure 3. R_1 values were significantly increased from baseline R_1 as early as 6 h after manganese injection in SMCX, CPu and Th. In SN, manganese-induced R_1 change became significant after 24 h. After a peak, ΔR_1 subsequently declined. In SMCX in control rats, post-manganese R_1 values were not significantly elevated after $\geq$4 days. For each ROI, we defined the time-point of maximal ΔR_1 as the time-point at which ΔR_1 was significantly higher than ΔR_1 values at the largest number of other time-points. Close to the injection site in SMCX, ΔR_1 was maximal at 6 h after manganese administration in control and stroke rats. In CPu, ΔR_1 was maximal after 24 h/2 days in control rats and after 2 days in stroke rats. In Th and SN, ΔR_1 was maximal after 2 days in control and stroke rats. ΔR_1 values in the ROIs at later time-points were significantly reduced as compared to the maximal ΔR_1: In SMCX after $\geq$24 h in control and stroke rats; in CPu after $\geq$4 days in

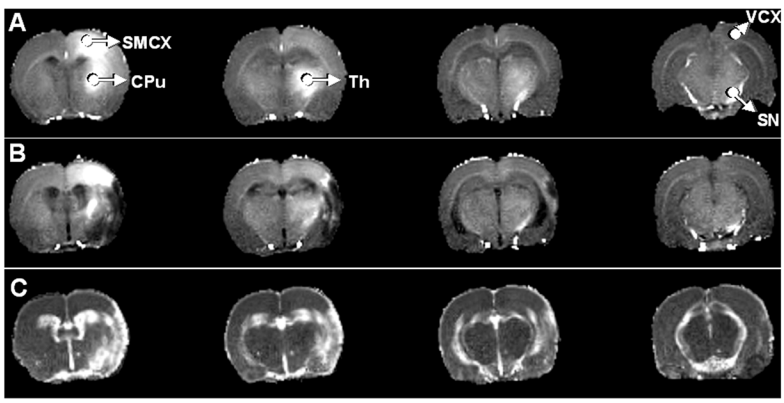

Figure 2

R_1 maps of four adjacent coronal brain slices at 2 days after $MnCl_2$ injection in the ipsilateral sensorimotor cortex of a control rat (A), and 2 weeks after unilateral stroke (B). C: T_2 maps of the same animal as in (B) at 2 days before manganese injection (i.e., 8 days after stroke). Manganese-induced contrast enhancement is clear in the ipsilateral sensorimotor cortex (SMCX), caudate putamen (CPu), thalamus (Th) and substantia nigra (SN). After stroke, manganese enhancement was less in subcortical areas. The lesion is characterized by reduced R_1 and prolonged T_2.

control rats, and after ≥6 days in stroke rats; in Th after ≥4 days in control rats, and after ≥8 days in stroke rats; and in SN after ≥4 days in control rats. In SN in stroke rats, ΔR_1 did not significantly decrease within the 8 days of MEMRI measurements.

Small but significant manganese-induced R_1 increases were also detected in VCX (Figure 3) and in contralateral sensorimotor ROIs (Figure 4). ΔR_1 changes in ipsi- and contralateral VCX, however, were significantly lower than ΔR_1 changes in sensorimotor ROIs within the same hemisphere. For example, in control rats maximal ΔR_1 in ipsi- and contralateral VCX were 0.16 ± 0.06 s^{-1} and 0.10 ± 0.04 s^{-1}, as compared to1.34 ± 0.21 s^{-1} and 0.26 ± 0.16 s^{-1} in ipsi- and contralateral CPu, respectively.

After stroke, manganese-induced ΔR_1 changes were significantly reduced in the CPu at 24 h, in the Th at 24 h and 2 days, and in the SN at 2 days after manganese injection (Figure 3). A significant main group effect (stroke vs. control rats) was found for ΔR_1 in Th ($P < 0.05$). We found no significant correlation between lesion volume and decrease in ΔR_1 at any time point in

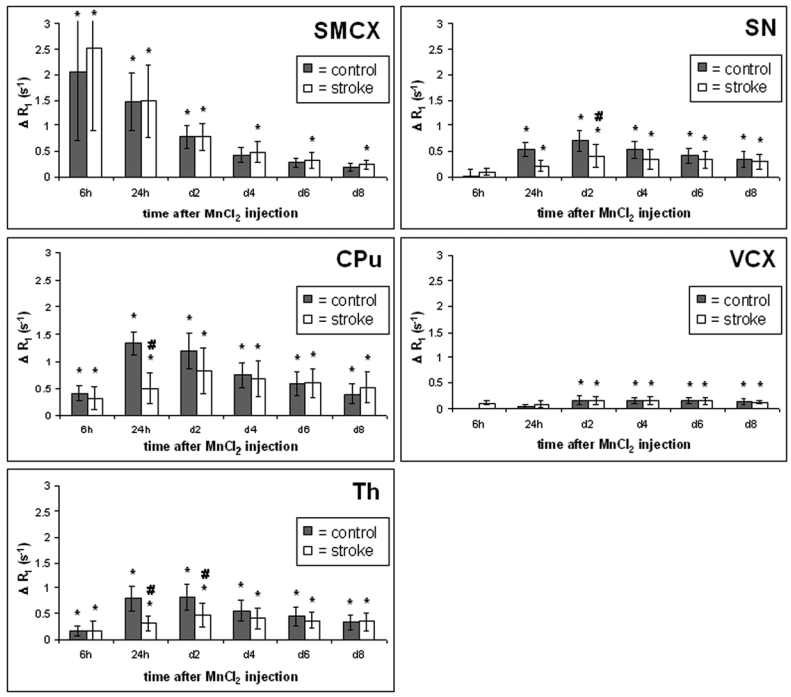

Figure 3

Manganese-induced ΔR_1 (s^{-1}) ± SD in ipsilateral ROIs as a function of time (6 h and 24 h (n = 5), and 2, 4, 6 and 8 days (n = 10)) after $MnCl_2$ injection in the ipsilateral sensorimotor cortex in control rats (■) and after stroke (□). SMCX: sensorimotor cortex; CPu: caudate putamen; Th: thalamus; SN: substantia nigra; VCX: visual cortex. *$P < 0.05$, post-manganese R_1 larger than pre-manganese R_1. #$P < 0.05$, stroke vs. control group. Among all time-points, there was an overall significant difference in ΔR_1 in Th between control rats and rats with a stroke ($P < 0.05$).

any of the ROIs. Also, we found no statistically significant differences in contralateral ROIs between control rats and rats with a stroke, however, there was a trend for larger ΔR_1 values in contralateral CPu and Th after stroke, as compared to control animals (P = 0.10 and P = 0.07, respectively).

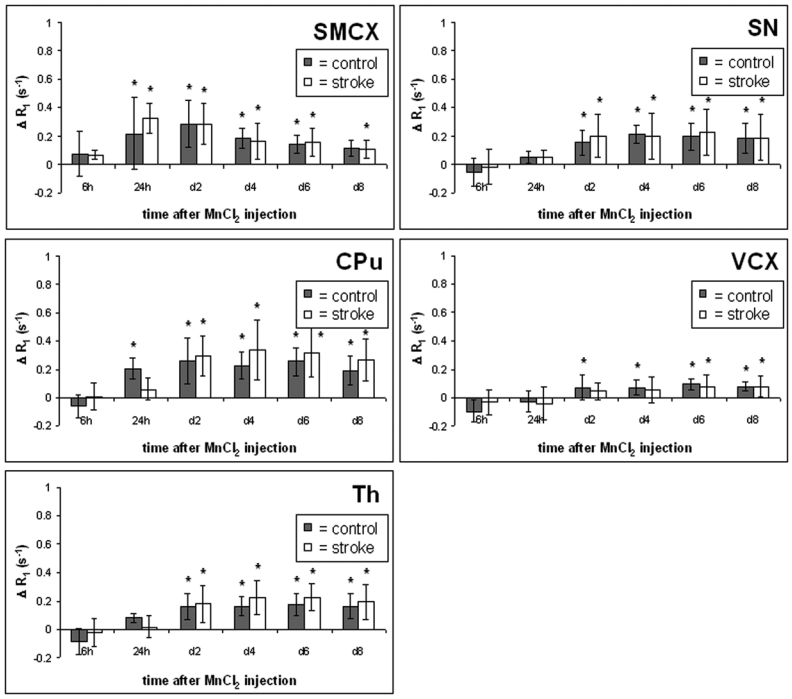

Figure 4

Manganese-induced ΔR_1 (s^{-1}) ± SD in contralateral ROIs as a function of time (6 h and 24 h (n = 5), and 2, 4, 6 and 8 days (n = 10)) after $MnCl_2$ injection in the ipsilateral sensorimotor cortex in control rats (■) and after stroke (□). SMCX: sensorimotor cortex; CPu: caudate putamen; Th: thalamus; SN: substantia nigra; VCX: visual cortex. *P < 0.05, post-manganese R_1 larger than pre-manganese R_1.

Immunohistochemistry The spatial pattern of WGA-HRP staining corresponded well with that of manganese enhancement. WGA-HRP-labeled cells were found in all ROIs in the ipsilateral sensorimotor network, both in control rats and after stroke (Figure 5). There were, however, differences in the degree of tracer accumulation when comparing WGA-HRP staining with MEMRI data. For example, the spatial extent of manganese enhancement was larger than that of WGA-HRP labeling. Furthermore, at variance with MEMRI data, in control rats WGA-HRP labeling was strongest in the thalamus (147 ± 59 cells) as compared to other ROIs (SMCX: 81 ± 29 cells; CPu: 51 ± 30 cells; SN: 20 ± 10 cells) (P < 0.05). Also, we found no WGA-HRP-labeled cells in ipsilateral VCX and in contralateral ROIs. After stroke, WGA-HRP

staining was significantly reduced in the ipsilateral CPu ($P = 0.01$), Th ($P = 0.01$) and SN ($P = 0.004$) as compared to control rats (Figure 6).

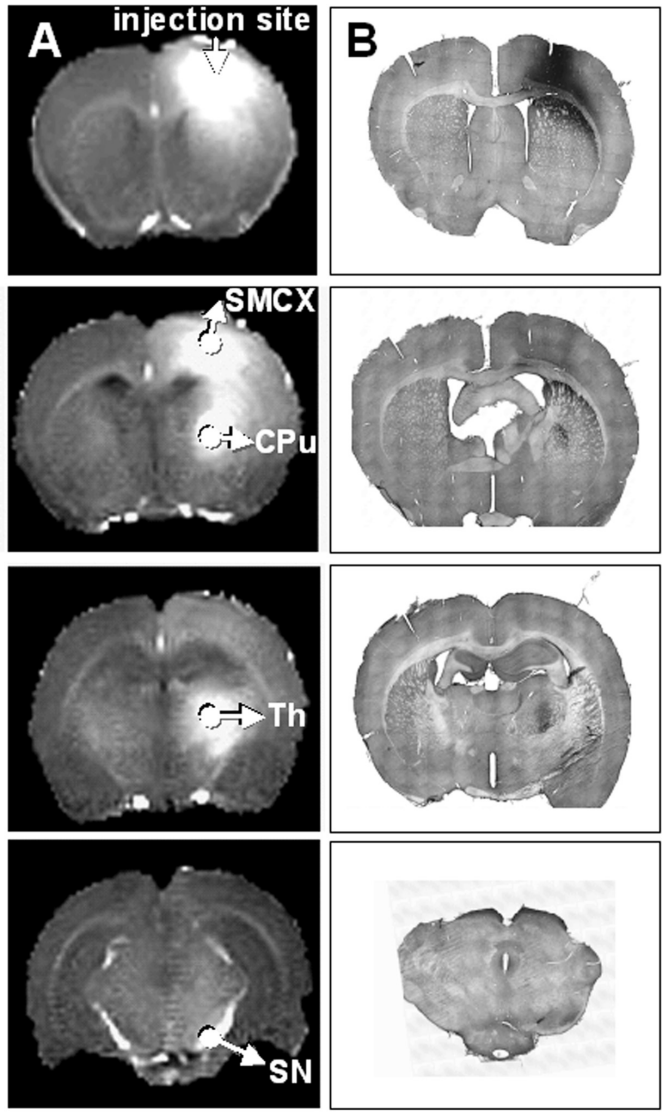

Figure 5

R_1 maps (A) and corresponding histological sections (B) of five adjacent slices of control rat brains at 2 days after $MnCl_2$ injection and at 4 days after WGA-HRP injection, respectively, into the ipsilateral sensorimotor cortex. Manganese-induced R_1 increase and WGA-HRP cell labeling are evident at the injection site and in the sensorimotor cortex (SMCX), caudate putamen (CPu), thalamus (Th) and substantia nigra (SN). Note that upper cerebral tissue was detached during preparation of the most posterior histological section.

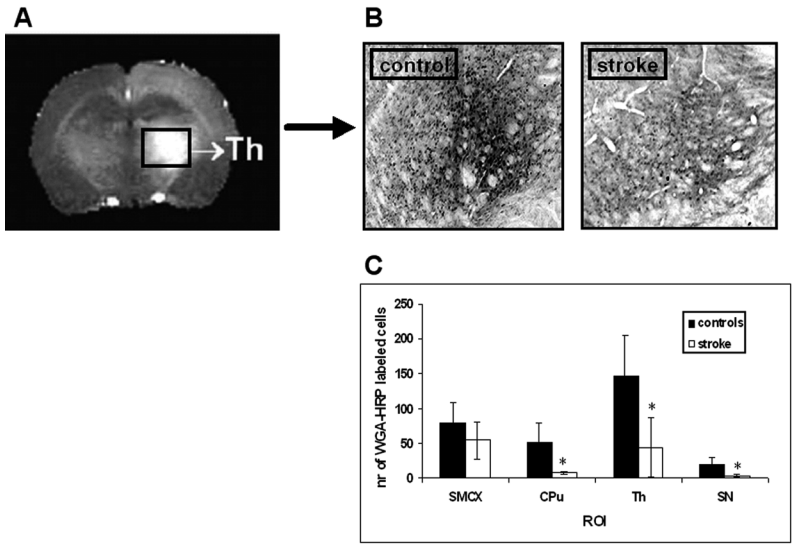

Figure 6

R_1 map (A) and corresponding histological sections of a control and a stroke rat brain (magnification 16x) (B) showing increased R_1 and cell labelling in the ipsilateral thalamus at 2 days after injection of $MnCl_2$ and 4 days after injection of WGA-HRP. After stroke, the number of WGA-HRP-labeled cells was significantly reduced in the ipsilateral CPu, Th and SN (B, C). *P < 0.05, stroke vs. control group.

Discussion

In this study we characterized the spatiotemporal distribution of the paramagnetic neuronal tract tracer manganese using *in vivo* MRI, in order to assess changes in neuronal connectivity within the sensorimotor network at two weeks after unilateral stroke in rats. In addition, MEMRI data were compared with results from a conventional tract tracing method based on *post mortem* detection of WGA-HRP labeling in the brain.

Manganese-induced R_1 changes were detected in distinct regions of the connective pathway between cortex, caudate putamen, substantia nigra and thalamus after injection of manganese in the sensorimotor cortex. Manganese is taken up by neurons through calcium channels and may be transported anterogradely and retrogradely along the axons (Pautler et al., 2003). The manganese-induced R_1 increase that we observed in the substantia nigra, which mostly receives indirect projections from the sensorimotor cortex, confirms the findings by Pautler et al. (1998) and Saleem et al. (2002), that manganese can be transferred transsynaptically. In control rats, maximal cortical contrast enhancement occurred within 6 h after manganese administration, followed by maximal R_1 increase in the caudate putamen around 24 h, and in the thalamus and substantia nigra at two days. R_1 changes diminished thereafter, but were still evident at 8 days after manganese in-

jection. In rats with a two-week old unilateral stroke, manganese-induced ΔR_1 was significantly diminished at the time-points of maximal manganese enhancement in subcortical areas, i.e. the caudate putamen, substantia nigra and, in particular, the thalamus. The reduced build-up of manganese in these regions points toward disturbed connectivity within the sensorimotor network, even though manganese was injected in preserved cortical tissue.

WGA-HRP labeling was found in the same regions of the ipsilateral sensorimotor pathway as detected with MEMRI, which is in agreement with a previous study in monkeys by Saleem et al. (2002). The spatial extent of manganese enhancement, however, was larger than that of WGA-HRP labeling. This may be explained by a relatively higher concentration and/or more diffusion of manganese at the injection site. In addition, partial volume effects on MRI slices that were about thirty-fold thicker than histological sections may have caused more blurring. WGA-HRP labeling was strongest in the thalamus, which is probably due to the relatively high number of thalamocortical afferents. Although WGA-HRP is transported antero- and retrogradely, our results indicate that transport was predominantly in retrograde direction (see also Kobbert et al. (2000)). In correspondence with our MEMRI data, after stroke a reduction of WGA-HRP-labeled cells was found in subcortical areas. The reduced build-up of manganese in these regions points toward disturbed connectivity within the sensorimotor network, even though manganese was injected in preserved cortical tissue.

Our results correspond with earlier reports on post-stroke loss of efferent thalamocortical pathways based on *ex vivo* detection of neuronal tract tracer (Kataoka et al., 1989; Iizuka et al., 1990; Carmichael et al., 2001). Cerebral ischemia has been shown to affect remote areas that are connected to the lesion site through anterograde and/or retrograde axonal degeneration (Iizuka et al., 1989; Kataoka et al., 1989). In addition to axonal disconnection, breakdown of axonal cytoskeletal components and disruption of axoplasmic transport, which have been described after MCA occlusion in rats (Yam et al., 1998), may account for the observed loss of tracer accumulation within the sensorimotor network.

Importantly, serial *in vivo* MEMRI may provide exclusive information on axonal transport dynamics. For example, in ipsilateral CPu of rats with a stroke maximal manganese-induced ΔR_1 occurred somewhat later than in control rats. Moreover, in all subcortical ROIs subsequent ΔR_1 decrease was significantly delayed. These results point toward delayed neuronal tracer arrival and clearance after stroke.

Slight, but significant manganese enhancement was detected in areas outside the sensorimotor network, e.g the visual cortex. This may be explained by passive diffusion and/or systemic reabsorption into the microvessels and cerebral spinal fluid (CSF) (see also Watanabe et al. (2004); Thuen et al. (2005)). Non-specific passive manganese distribution, however, was minor as compared to the network-specific axonal transport to sensorimotor areas. Small, but significant manganese enhancement was also observed in contralateral sensorimotor cortex, caudate putamen, thalamus and substantia nigra. Manganese-induced R_1 changes in these contralateral sensorimotor

regions were significantly higher than R_1 changes in ipsi- and contralateral visual cortex. Maximal manganese-induced ΔR_1 in contralateral caudate putamen was about a factor 1.5-2 higher than ΔR_1 in the ipsilateral visual cortex, while these ROIs are at comparable distance from the manganese injection site (5.7 mm and 6.0 mm respectively (Paxinos and Watson, 1998)). These findings suggest that manganese enhancement in the contralateral sensorimotor network cannot be merely explained by non-specific manganese accumulation, and anyway involves transhemispheric axonal transport.

We detected slightly elevated contralateral manganese enhancement in rats with a stroke as compared to controls, however, differences were not statistically significant. Increased transhemispheric connectivity after stroke has been previously described, but was observed at stages much later than two weeks post-stroke (Carmichael et al., 2001; Allegrini and Wiessner, 2003). To assess potential plasticity-associated changes in connectivity between the injured and unaffected hemisphere after stroke with MEMRI, future studies should include more chronic time-points after stroke.

Conclusion

Our study demonstrates that MEMRI allows unique spatiotemporal assessment of alterations in neuronal connectivity after stroke. We have detected decreased and delayed manganese enhancement in brain network regions that are connected to the sensorimotor cortex where manganese was injected. Loss or dysfunction of neuronal connections, even outside the ischemic lesion, may explain lasting impairment of function. MEMRI thereby provides a unique *in vivo* tool that can give important new insights in neural correlates of functional loss and recovery after stroke.

Acknowledgements

- Dr. Dijkhuizen is financially supported by a fellowship of the Royal Netherlands Academy of Arts and Sciences.

References

Allegrini PR, Wiessner C (2003). Three-dimensional MRI of cerebral projections in rat brain in vivo after intracortical injection of MnCl2. NMR Biomed 16:252-256.

Calautti C, Baron JC (2003). Functional neuroimaging studies of motor recovery after stroke in adults: a review. Stroke 34:1553-1566.

Carmichael ST (2003). Plasticity of cortical projections after stroke. Neuroscientist 9:64-75.

Carmichael ST, Wei L, Rovainen CM, Woolsey TA (2001). New patterns of intracortical projections after focal cortical stroke. Neurobiol Dis 8:910-922.

Collins DL, Neelin P, Peters TM, Evans AC (1994). Automatic 3D intersubject registration

of MR volumetric data in standardized Talairach space. J Comput Assist Tomogr 18:192-205.

Cramer SC, Bastings EP (2000). Mapping clinically relevant plasticity after stroke. Neuropharmacology 39:842-851.

Dijkhuizen RM, Nicolay K (2003). Magnetic resonance imaging in experimental models of brain disorders. J Cereb Blood Flow Metab 23:1383-1402.

Dijkhuizen RM, Ren J, Mandeville JB, Wu O, Ozdag FM, Moskowitz MA, Rosen BR, Finklestein SP (2001). Functional magnetic resonance imaging of reorganization in rat brain after stroke. Proc Natl Acad Sci U S A 98:12766-12771.

Gerriets T, Stolz E, Walberer M, Muller C, Rottger C, Kluge A, Kaps M, Fisher M, Bachmann G (2004). Complications and pitfalls in rat stroke models for middle cerebral artery occlusion: a comparison between the suture and the macrosphere model using magnetic resonance angiography. Stroke 35:2372-2377.

Gong S, LeDoux MS (2003). Immunohistochemical detection of wheat germ agglutinin-horseradish peroxidase (WGA-HRP). J Neurosci Methods 126:25-34.

Iizuka H, Sakatani K, Young W (1989). Corticofugal axonal degeneration in rats after middle cerebral artery occlusion. Stroke 20:1396-1402.

Iizuka H, Sakatani K, Young W (1990). Neural damage in the rat thalamus after cortical infarcts. Stroke 21:790-794.

Johansson BB (2000). Brain plasticity and stroke rehabilitation. The Willis lecture. Stroke 31:223-230.

Kataoka K, Hayakawa T, Yamada K, Mushiroi T, Kuroda R, Mogami H (1989). Neuronal network disturbance after focal ischemia in rats. Stroke 20:1226-1235.

Kawamata T, Dietrich WD, Schallert T, Gotts JE, Cocke RR, Benowitz LI, Finklestein SP (1997). Intracisternal basic fibroblast growth factor enhances functional recovery and up-regulates the expression of a molecular marker of neuronal sprouting following focal cerebral infarction. Proc Natl Acad Sci U S A 94:8179-8184.

Kobbert C, Apps R, Bechmann I, Lanciego JL, Mey J, Thanos S (2000). Current concepts in neuroanatomical tracing. Prog Neurobiol 62:327-351.

Lee RG, van Donkelaar P (1995). Mechanisms underlying functional recovery following stroke. Can J Neurol Sci 22:257-263.

Longa EZ, Weinstein PR, Carlson S, Cummins R (1989). Reversible middle cerebral artery occlusion without craniectomy in rats. Stroke 20:84-91.

Pautler RG (2004). In vivo, trans-synaptic tract-tracing utilizing manganese-enhanced magnetic resonance imaging (MEMRI). NMR Biomed 17:595-601.

Pautler RG, Silva AC, Koretsky AP (1998). In vivo neuronal tract tracing using manganese-enhanced magnetic resonance imaging. Magn Reson Med 40:740-748.

Pautler RG, Mongeau R, Jacobs RE (2003). In vivo trans-synaptic tract tracing from the murine striatum and amygdala utilizing manganese enhanced MRI (MEMRI). Magn Reson Med 50:33-39.

Paxinos G, Watson C (1998). The rat brain in stereotaxic coordinates, 4th Edition. San Diego: Academic Press.

Press WH, Vetterling WT (1992). Numerical recipes in FORTRAN : the art of scientific computing, 2nd Edition. Cambridge, England: Cambridge University Press.

Rijntjes M, Weiller C (2002). Recovery of motor and language abilities after stroke: the contribution of functional imaging. Prog Neurobiol 66:109-122.

Saleem KS, Pauls JM, Augath M, Trinath T, Prause BA, Hashikawa T, Logothetis NK (2002). Magnetic resonance imaging of neuronal connections in the macaque monkey. Neuron 34:685-700.

Seil FJ (1997). Recovery and repair issues after stroke from the scientific perspective. Curr Opin Neurol 10:49-51.

Silva AC, Lee JH, Aoki I, Koretsky AP (2004). Manganese-enhanced magnetic resonance imaging (MEMRI): methodological and practical considerations. NMR Biomed 17:532-543.

Sloot WN, Gramsbergen JB (1994). Axonal transport of manganese and its relevance to selective neurotoxicity in the rat basal ganglia. Brain Res 657:124-132.

Steinberg BA, Augustine JR (1997). Behavioral, anatomical, and physiological aspects of recovery of motor function following stroke. Brain Res Brain Res Rev 25:125-132.

Thuen M, Singstad TE, Pedersen TB, Haraldseth O, Berry M, Sandvig A, Brekken C (2005). Manganese-enhanced MRI of the optic visual pathway and optic nerve injury in adult rats. J Magn Reson Imaging 22:492-500.

Watanabe T, Frahm J, Michaelis T (2004). Functional mapping of neural pathways in rodent brain in vivo using manganese-enhanced three-dimensional magnetic resonance imaging. NMR Biomed 17:554-568.

Weiller C (1998). Imaging recovery from stroke. Exp Brain Res 123:13-17.

Yam PS, Dewar D, McCulloch J (1998). Axonal injury caused by focal cerebral ischemia in the rat. J Neurotrauma 15:441-450.

Chapter 3 Manganese-Enhanced MRI of Brain Plasticity in Relation to Functional Recovery after Experimental Stroke

[1]Jet P. van der Zijden, [1]Mark J.R.J. Bouts, [1,2]Ona Wu, [3]Tom A.P. Roeling, [3]Ronald L.A.W. Bleys, [1]Annette van der Toorn, [1]Rick M. Dijkhuizen

[1]Image Sciences Institute, University Medical Center Utrecht, Utrecht, the Netherlands
[2]Athinoula A. Martinos Center for Biomedical Imaging, Massachusetts General Hospital/Massachusetts Institute of Technology/Harvard Medical School, Charlestown, MA, United States
[3]Rudolf Magnus Institute of Neuroscience, University Medical Center Utrecht, Utrecht, the Netherlands

Published in Journal of Cerebral Blood Flow and Metabolism 28 (4), pp. 832-840 (2008)

3 Manganese-Enhanced MRI of Brain Plasticity in Relation to Functional Recovery after Experimental Stroke

Abstract

Restoration of function after stroke may be associated with structural remodelling of neuronal connections outside the infarcted area. However, the spatiotemporal profile of post-stroke alterations in neuroanatomical connectivity in relation to functional recovery is still largely unknown. We performed *in vivo* magnetic resonance imaging (MRI)-based neuronal tract tracing with manganese in combination with immunohistochemical detection of the neuronal tracer wheat-germ agglutinin horseradish peroxidase (WGA-HRP), to assess changes in intra- and interhemispheric sensorimotor network connections from 2 to 10 weeks after unilateral stroke in rats. In addition, functional recovery was measured by repetitive behavioural testing. Four days after tracer injection in perilesional sensorimotor cortex, manganese enhancement and WGA-HRP staining were decreased in subcortical areas of the ipsilateral sensorimotor network at 2 weeks post-stroke, which was restored at later time-points. At 4-10 weeks after stroke we detected significantly increased manganese enhancement in the contralateral hemisphere. Behaviourally, sensorimotor functions were initially disturbed but subsequently recovered and plateaud 17 days after stroke.

This study shows that manganese-enhanced MRI can provide unique *in vivo* information on the spatiotemporal pattern of neuroanatomical plasticity after stroke. Our data suggest that the plateau stage of functional recovery is associated with restoration of ipsilateral sensorimotor pathways and enhanced interhemispheric connectivity.

Introduction

Stroke causes acute loss of function due to damage of neuronal tissue. Yet, most patients exhibit a certain degree of functional recovery in the succeeding months, which may be associated with neuronal repair and/or neuroplasticity. Plasticity describes the capability of undamaged brain tissue to alter its neuronal organization to compensate for loss of function, e.g.

through unmasking or strengthening of existing pathways or by formation of new connections. A great deal of studies suggests that structural plasticity in adjacent and remote regions plays a significant role in functional recovery after focal brain injury (for reviews see Nudo (1999); Keyvani and Schallert (2002); Carmichael (2003)). Processes involved in post-stroke structural reorganization are characterized by a complex pattern of molecular and cellular events, including induction of growth-promoting genes, reduction of growth-inhibiting proteins, axonal and dendritic sprouting, synaptogenesis and neurogenesis (Cramer and Chopp, 2000; Keyvani and Schallert, 2002; Carmichael, 2006; Nudo, 2006). These events have been detected in ipsi- as well as contralesional tissue, and may enhance intra- and interhemisperic connectivity, which could provide a substrate for post-stroke improvement in cerebral function. Still, the spatiotemporal profile of alterations in neuroanatomical connectivity in relation to functional recovery after stroke has not yet been fully clarified.

We and others have recently shown that changes in neuronal connectivity after experimental stroke can be assessed *in vivo* with manganese-enhanced MRI (MEMRI) (Allegrini and Wiessner, 2003; van der Zijden et al., 2007). Upon intracerebral injection, the paramagnetic ion manganese (Mn^{2+}) acts as a neuronal tracer, as it enters neurons through Ca^{2+} channels and moves along axons (Sloot and Gramsbergen, 1994; Pautler et al., 1998). In addition, manganese can be transported transsynaptically (Pautler et al., 1998; Saleem et al., 2002). Hence, MRI of the distribution of intracerebrally injected manganese allows *in vivo* mapping of connective pathways within neuronal networks. In our previous MEMRI study, we have demonstrated that manganese accumulation is decreased and delayed in ipsilesional subcortical regions connected to peri-infarct sensorimotor cortical tissue, at 2 weeks after stroke in rats (van der Zijden et al., 2007). In the current study, we hypothesized that restoration of sensorimotor function at more chronic time-points is associated with recovery of connectivity within the ipsilesional sensorimotor network and increased connectivity with the contralesional hemisphere. To test our hypotheses we performed neuronal tract tracing with MEMRI and WGA-HRP immunohistochemistry at different time points after stroke along with repetitive behavioural testing, and we correlated post-stroke changes in neuronal connectivity with functional recovery.

Materials and Methods

Animals

All animal procedures were approved by the local ethical committee of Utrecht University and met governmental guidelines. A total of 28 male Wistar rats weighing 250-350 g were included in this study. Animals were divided into four experimental groups. In stroke groups, *in vivo* tract tracing using MEMRI was performed at 2 (Group S-2w; n = 7), 4 (Group S-4w; n = 7)

or 10 (Group S-10w; n = 7) weeks after experimental stroke. In a control group, MEMRI was done at 4 weeks after sham operation (Group C-4w; n = 7). Four animals of each group were also subjected to conventional tract tracing using wheat-germ agglutinin horseradish peroxidase (WGA-HRP) immunohistochemistry.

Stroke model

Animals were anesthetized by subcutaneous injection of a mixture of 0.315 mg/ml fentanyl citrate and 10 mg/ml fluanisone (0.55 mg/kg), and 0.55 mg/kg midazolam. Blood oxygen saturation and heart rate were continuously monitored during surgical procedures. Body temperature was maintained at 37.0 ± 0.5 °C. Transient focal cerebral ischemia was induced by 90-min occlusion of the right middle cerebral artery (MCA) with an intraluminal filament (Longa et al., 1989). In brief, a 4.0 silicon-coated polypropylene suture (Ethicon, Piscataway, NJ, USA) was introduced into the right external carotid artery and advanced through the internal carotid artery until a resistance was felt, indicating that the MCA bifurcation was reached. Sham-operated animals were subjected to the same surgical procedures, except that the suture was advanced for only 1 mm, thereby not occluding the MCA. After 90 minutes, the filament was withdrawn from the internal carotid artery to allow reperfusion. After surgery, rats received a subcutaneous injection of 0.3 mg/kg buprenorphin (Schering-Plough, Utrecht, The Netherlands) for post-surgical pain relief, and 5 ml saline to compensate for loss of water and minerals.

Functional examination

Animals were subjected to two behavioural tests to assess sensorimotor function. First, we applied a battery of motor, sensory and tactile tests, which provided a neurological score on a scale of 0 to 20 points, with 20 as maximal deficit score (see Table 1) (modified from Reglodi et al. (2003)). Second, an adhesive removal test was performed (Schallert et al., 2000). A small circular sticky tape was attached to the distal-radial region of the wrist of either the left or right forelimb (Schallert et al., 2000), and the sticky tape removal time was measured for each forelimb with a maximally allowed removal time of 60 seconds.

Animals were trained at 4 and 3 days before stroke. Subsequently, behavioural examination was performed on days 0, 4, 7 and 10 after stroke, and every week thereafter.

Table 1 **Neurological score grading scale for rats.**

Sign	*Description*	*Score*
Motility, spontaneous activity	Normal or slightly reduced exploratory behavior	0 - 1
	Moving limbs without proceeding	2
	Moving only to stimuli	3
	Unresponsive to stimuli, normal muscle tone	4
	Severely reduced muscle tone, premortal signs	5
Gait disturbances	Straight walking	0
	Walking towards contralateral side	1
	Alternate circling and walking straight	2
	Alternate circling and walking towards paretic side	3
	Circling and/or other gait disturbances	4
	Constant circling towards paretic side	5
Postural signs		
– Forelimb flexion	Degree of limb flexion when held by tail	0 - 2
– Thorax twisting	Degree of body rotation when held by tail	0 - 2
Lateral resistance	Degree of resistance against lateral push	0 - 2
Limb placing		
– Ipsilesional forelimb	Normal, weak, or no placing	0 - 2
– Contralateral forelimb	Normal, weak, or no placing	0 - 2
TOTAL SCORE		0 - 20

Tracer injection

Neuronal tract tracer was injected 4 days before MEMRI and subsequent removal of the brain for WGA-HRP immunohistochemistry. This time-point was chosen to allow optimal combined detection of the two tracers.

Animals were anesthetized by subcutaneous injection of a mixture of 0.315 mg/ml fentanyl citrate and 10 mg/ml fluanisone (0.55 mg/kg), and 0.55 mg/kg midazolam, and placed in a stereotactic holder. Blood oxygen saturation and heart rate were continuously monitored. Body temperature was maintained at 37.0 ± 0.5 °C.

Using a 2.0-µl Hamilton syringe, 0.2 µl of a solution containing either 1 M $MnCl_2$ (n = 3 for all groups) or a combination of 1 M isotonic $MnCl_2$ and 5% WGA-HRP (Sigma Aldrich, Munich, Germany) (n = 4 for all groups) was injected at a rate of 0.05 µl/min into the sensorimotor cortex through a burr hole in the skull (0.5 mm anterior, 1.5-3.0 mm lateral and at a depth of 1.5 mm relative to bregma (Paxinos and Watson, 1998)). After injection, the

needle was left in place for 3 minutes to prevent leakage along the injection track. Lateral coordinates were adjusted based on the lesion location determined by T_2-weighted MRI prior to tracer injection, to arrive at an injection site at approximately 0.5 mm from the lesion border. In the stroke groups, tracer was invariably injected into intact sensorimotor cortex, outside the T_2-defined lesion area. Injections sites for sham-operated rats were adjusted correspondingly. Mean lateral coordinates were 2.4 ± 0.7 mm, 2.2 ± 0.6 mm, 2.3 ± 0.6 mm and 2.6 ± 0.5 mm for Groups S-2w, S-4w, S-10w and C-4w, respectively. As shown in our previous study, such small variation in lateral position of the injection site does not result in significant differences in the pattern of manganese enhancement in subcortical regions of the sensorimotor network (van der Zijden et al., 2007).

MRI

MRI measurements were performed on a 4.7 T horizontal bore MR spectrometer (Varian instruments (Palo Alto, CA, USA)) using a Helmholtz volume coil (90-mm diameter) and an inductively coupled surface coil (25-mm diameter) for signal excitation and detection, respectively.

Before MRI, rats were anesthetized with 4% isoflurane for endotracheal intubation, followed by mechanical ventilation with 2.5% isoflurane in N_2O/O_2 (70:30). Rats were placed in a home-built plastic holder and immobilized with earplugs and a toothholder. Blood oxygen saturation and heart rate were monitored during MRI measurements. Body temperature was maintained at 37.0 ± 0.5 °C.

Multi-echo, multi-slice T_2-weighted MRI (repetition time (TR)/echo spacing = 3000/17.5 ms; echo train length = 8; acquisition matrix = 128 x 128; voxel dimension = 0.2 x 0.2 x 1.2 mm^3; 15 coronal slices; number of averages = 2) was performed at i) 1 week after stroke, ii) 2 days prior to tracer injection, and iii) 4 days after tracer injection. Quantitative T_2 maps were calculated on a voxel-wise basis by weighted linear least-squares fit of the logarithm of the signal intensity versus echo time (TE).

Saturation recovery T_1-weighted gradient-echo MRI with seven TRs (TR/TE = 55 - 3000/18 ms; acquisition matrix = 128 x 128; voxel dimensions = 0.2 x 0.2 x 1.2 mm^3; 15 coronal slices; number of averages = 2) was performed 2 days prior to tracer injection and 4 days after tracer injection. Quantitative pre- and post-injection R_1 ($1/T_1$) maps were calculated on a voxel-wise basis by performing a non-linear least-squares fit using the Levenberg-Marquardt method (Press and Vetterling, 1992).

Immunohistochemistry

At 4 days after tracer injection, rats that had received the mixture of $MnCl_2$ and WGA-HRP were deeply anesthetized by intraperitoneal injection of pentobarbital (120 mg/kg), and immediately transcardially perfused with saline followed by 4% paraformaldehyde in 0.1 M phosphate-buffered saline (PBS) (pH = 7). Brains were removed and post-fixed in 4% paraformaldehyde

in 0.1 M PBS for an additional 2 h and subsequently stored in 20% sucrose in 0.1 M PBS at 4 °C. Brains were cut in 40-μm thick coronal sections on a freezing microtome, and every fifth section was collected in 5 containers consecutively and stored in 20% sucrose in 0.1 M PBS. Thus each container consisted of 10-15 slices covering the whole brain. Free-floating sections were processed for immunohistochemical detection of WGA-HRP using goat anti-WGA (Vector Laboratories, Burlingame, CA, USA) as a primary antibody and development using a diaminobenzidine peroxidase substrate kit (Vector Laboratories Burlingame, CA, USA) as described before (van der Zijden et al., 2007).

Data analysis

MRI Lesion volumes were determined from 11 adjacent slices of the T_2 dataset acquired at 1 week after stroke and defined as ipsilesional tissue greater than the mean + 2 SD of T_2 in contralateral tissue. The edema-corrected hemispheric lesion volume (%HLV^e) was calculated as described by Gerriets et al. (2004):

$\%HLV^e = (HV_c - (HV_i - LV^u))/HV_c \times 100\%$, where HV_c and HV_i are the contralesional and ipsilesional hemispheric volumes, respectively; and LV^u is the uncorrected lesion volume.

Longitudinal relaxation rate R_1 (= $1/T_1$) maps were coregistered to an averaged T_2-weighted brain MRI data set from 6 control rats using semi-automated image registration software (MNI Autoreg (Collins et al., 1994)). Erroneous registration as a result of edema-induced brain distortion was corrected by a second registration procedure after manually selecting specific landmarks on brains with a stroke lesion. Co-registered pre- and post-injection R_1 maps were subtracted to generate ΔR_1 maps. As manganese-induced changes in R_1 are proportional to the local manganese concentration (Silva et al., 2004), manganese accumulation was measured from the difference between pre- and post-contrast R_1 (ΔR_1). Mean ΔR_1 values were determined in ipsi- and contralateral subcortical regions that are connected to the sensorimotor cortex, i.e. striatum (St), thalamus (Th) and substantia nigra (SN), and corpus callosum (CC). Non-specific distribution of manganese was verified in the ipsilateral visual cortex (VCX). Regions-of-interest (ROIs), shown in Figs. 2 and 3A (top row), were identical for all animals and selected to be invariably outside the T_2-defined lesion area.

To measure the total volume of manganese enhancement in the ipsi- and contralateral hemisphere we performed cluster-based segmentation of manganese-enhanced brain areas on ΔR_1 maps. Image intensity scale was standardized to correct for intensity variations between rats due to small differences in $MnCl_2$ concentration at the injection site. The average multi-slice ΔR_1 map of the control group was used to calculate a 'standard' intensity histogram to which intensity histograms of ΔR_1 maps of individual rats were transformed (Nyul and Udupa, 1999; Nyul et al., 2000). Subsequently, segmentation was performed using a fuzzy *c*-means method based on a clustering algorithm in which four classes (not enhanced; not likely enhanced;

likely enhanced; very likely enhanced) were defined (Pham and Prince, 1999). Pixels segmented into class 1 and 2 were considered non-enhanced, pixels segmented into class 3 and 4 were considered as manganese-enhanced. The volume of manganese enhancement was determined from the total number of manganese-enhanced pixels in the ipsi- and contralesional hemisphere of six adjacent brain slices posterior to the injection site.

Immunohistochemistry WGA-HRP-stained brain slices were studied with a light microscope (Zeiss Axiophot with Sony 3 CCD Color Video Camera) under bright- and dark-field illumination. WGA-HRP-labeled neuronal profiles were counted on single brain sections that were at the same anterior-posterior position as the MRI slices used for ROI analysis. Counting of labeled profiles was performed in the anatomical area that best matched the corresponding ROI used for MRI analysis, where WGA-HRP staining was most pronounced. The number of labeled neurons was calculated using the formula: $N = nT/(T+h)$, where N = number of neurons; n = number of neuronal profiles; T = slice thickness; and h = mean neuronal profile diameter (Abercrombie and Johnson, 1946). For each rat, mean neuronal profile diameter (h) was determined from 10 random labeled somata per ROI. The number of labeled neurons per 40 μm brain section was then multiplied by 30 to estimate the number of labeled neurons per 1.2-mm slice (i.e., the MRI slice thickness).

Statistics All values are expressed as mean ± SD. The temporal pattern of sensorimotor function was analyzed using a one-way repeated measures analysis-of-variance (ANOVA) with post-hoc multiple comparison *t*-testing with Bonferroni correction. Differences in lesion volumes, ROI ΔR_1 values, manganese-enhanced volumes, segmentation class ΔR_1 values and WGA-HRP staining between groups were analyzed using a one-way ANOVA with post-hoc multiple comparison *t*-testing with Bonferroni correction. Differences between pre- and post-injection R_1 values for each ROI were analyzed with a paired Student's *t*-test. $P < 0.05$ was considered significant.

Results

Functional status Figure 1 shows the changes in neurological score (Figure 1A) and adhesive removal time (Figure 1B) as a function of time after stroke. All rats demonstrated substantial functional deficits at day 4 after stroke. Functional recovery was reflected by a significant improvement of neurological score on day 17 and adhesive removal time on day 10 as compared to day 4 after stroke. Plateau functional recovery, defined as the time point after which behavioural scores did not significantly change, occurred for both functional tests on day 17 after stroke.

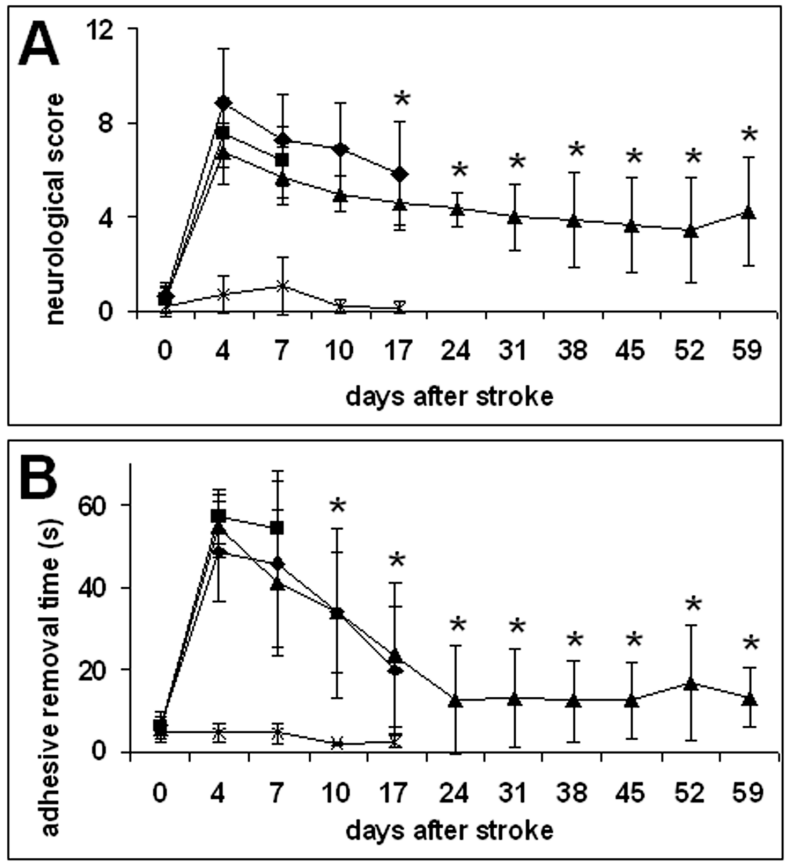

Figure 1

Neurological score ± SD (A) and adhesive removal time ± SD (B) as a function of time after stroke. x: Group C-4w (controls, 4 weeks after sham operation); ■: Group S-2w (2 weeks after stroke); ◆: Group S-4w (4 weeks after stroke); ▲: Group S-10w (10 weeks after stroke). *P < 0.05 vs. score at first time-point post-stroke (i.e., day 4).

Ischemic damage Unilateral ischemic lesions, characterized by a significant increase in T_2, included part of the somatosensory cortex and the lateral striatum (Figure 2). Mean %HLV[e] at 1 week post-stroke was 17.1 ± 10.1%, 21.0 ± 8.3% and 16.6 ± 8.1% for Groups S-2w, S-4w and S-10w, respectively. There was no significant difference in lesion volumes between groups.

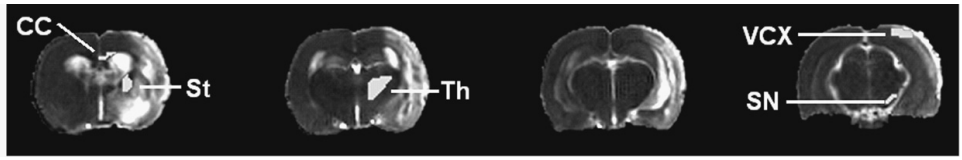

Figure 2
T_2 maps of four adjacent coronal brain slices at 4 weeks after stroke. The lesion is characterized by an increased T_2. Overlaid on the T_2 maps are ipsilateral regions-of-interest (ROIs): striatum (St), corpus callosum (CC), thalamus (Th), substantia nigra (SN) and visual cortex (VCX).

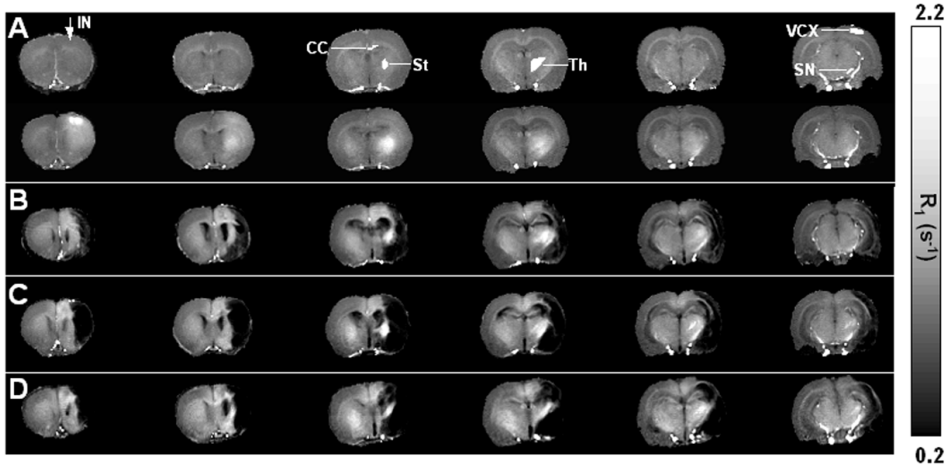

Figure 3
R_1 maps of six adjacent coronal brain slices. A: Before (top row), and at 4 days after $MnCl_2$ injection in the ipsilateral sensorimotor cortex in a rat after sham-operation (bottom row). B, C, D: Post-manganese R_1 maps at 2, 4, and 10 weeks after stroke, respectively. Injection site (IN) and regions-of-interest (ROIs) are displayed on the pre-contrast control R_1 maps in the ipsilateral hemisphere (A, top row): Striatum (St), corpus callosum (CC), thalamus (Th), substantia nigra (SN) and visual cortex (VCX). Matching ROIs were positioned in the contralateral hemisphere. The stroke lesion is characterized by reduced R_1 (B, C, D).

MEMRI In all groups, 4 days after manganese injection into the sensorimotor cortex, R_1 maps clearly visualized manganese-enhanced regions that are connected to the site of injection, i.e. striatum, thalamus, substantia nigra and corpus callosum (Figure 3).

Pre-injection R_1 values in striatum, thalamus, corpus callosum and visual cortex were not significantly different between groups. A small but statistically significant R_1 increase in the ipsilesional substantia nigra was found between Groups C-4w and S-10w ($0.95 \pm 0.02\ s^{-1}$ and $1.06 \pm 0.04\ s^{-1}$, respectively). However this difference was minor compared to the post-injection R_1 values in this ROI ($1.60 \pm 0.25\ s^{-1}$ and $1.71 \pm 0.24\ s^{-1}$ for Groups C-4w and S-10w, respectively).

In the ipsilateral hemisphere of control rats, R_1 values were significantly increased from baseline in all subcortical ROIs of the sensorimotor network after manganese injection ($P < 0.05$). There was no significant R_1 increase in the visual cortex, which lies outside the sensorimotor network. Post-manganese R_1 values in subcortical sensorimotor regions were also significantly elevated in all stroke groups ($P < 0.05$), except for the ipsilateral substantia nigra at 2 weeks post-stroke. In the contralateral ROIs, manganese-induced R_1 changes were much smaller than in their ipsilateral counterparts. Nevertheless, a significant R_1 increase was detected in contralateral striatum in controls and at 2 weeks after stroke. At 4 and 10 weeks after stroke, R_1 was significantly increased in all sensorimotor ROIs of the contralateral hemisphere.

Figure 4 shows manganese-induced ΔR_1 values in ipsi- and contralateral ROIs. At 2 weeks after stroke, ΔR_1 was significantly reduced in the ipsilateral substantia nigra as compared to control rats. Thereafter, ΔR_1 values increased and were again similar to control values at 10 weeks after stroke. A signifi-

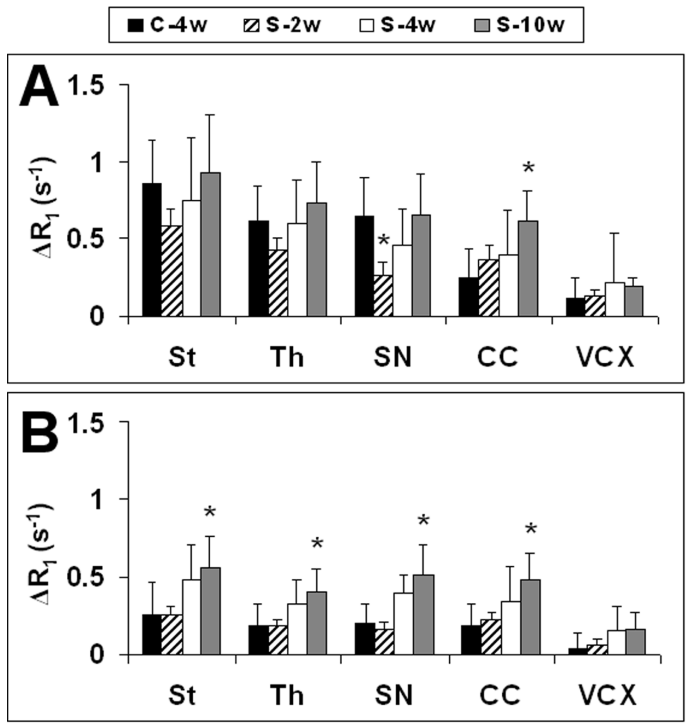

Figure 4

Manganese-induced ΔR_1 (s^{-1}) in ipsi- (A) and contralateral ROIs (B) at 4 days after $MnCl_2$ injection in the ipsilateral sensorimotor cortex of rats after sham-operation, and at 2, 4, and 10 weeks after stroke. St: striatum; Th: thalamus; SN: substantia nigra; CC: corpus callosum; VCX: visual cortex. *$P < 0.05$ vs. sham-operated group.

cant increase in manganese-induced ΔR_1 as compared to controls was found at 10 weeks after stroke in the contralateral striatum, thalamus and substantia nigra, as well as ipsi- and contralateral corpus callosum at 10 weeks post-stroke.

With a fuzzy *c*-means algorithm we segmented ΔR_1 maps. For each of the four segmentation classes, mean non-normalized ΔR_1 values were not significantly different between groups (Table 2). Class 3 and 4 were considered to represent manganese-enhanced areas and were used for calculation of ipsi- and contralateral volume of manganese enhancement. Examples of segmented rat brain ΔR_1 maps of controls and at 4 weeks after stroke are shown in Figure 5. We found no significant differences in total volume of manganese enhancement in the ipsilateral hemispheres between control and all stroke groups (Figure 6). However, in the contralateral hemisphere, total volume of manganese enhancement was significantly larger at 4 weeks after stroke as compared to controls.

Table 2	**Mean $\Delta R_1 \pm$ SD (s^{-1}) of segmentation classes in control and stroke groups.**			
Class	*Group*			
	C-4w	*S-2w*	*S-4w*	*S-10w*
1	0.07 ± 0.09	0.02 ± 0.05	0.11 ± 0.12	0.10 ± 0.13
2	0.26 ± 0.12	0.22 ± 0.06	0.33 ± 0.16	0.41 ± 0.18
3	0.58 ± 0.18	0.52 ± 0.12	0.57 ± 0.14	0.67 ± 0.24
4	1.36 ± 0.34	1.36 ± 0.29	1.28 ± 0.40	1.37 ± 0.43

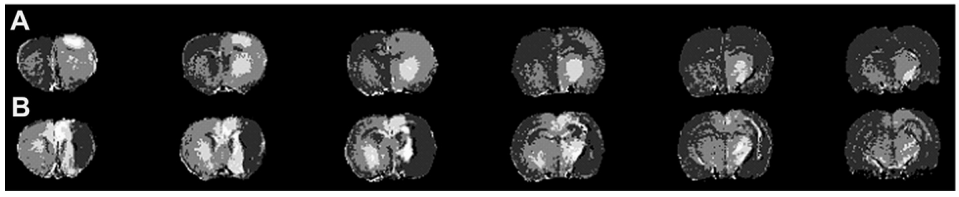

Figure 5

Fuzzy c-means-based segmentation of ΔR_1 maps of six adjacent coronal brain slices at 4 weeks after sham-operation (A) or stroke induction (B). Four segmentation classes were discerned: ■: not enhanced; ■: not likely enhanced; ■: likely enhanced; □: very likely enhanced.

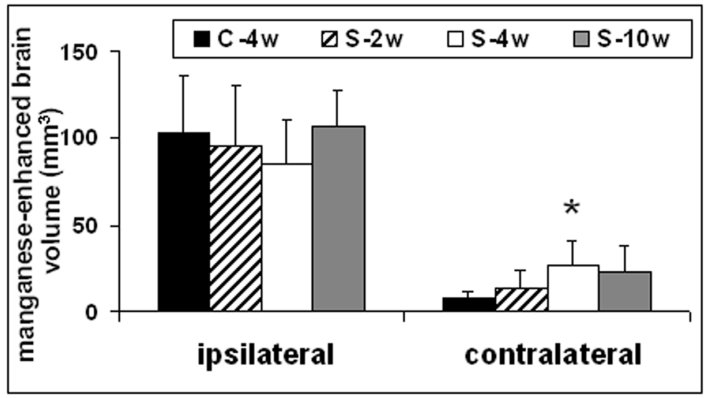

Figure 6

Ipsi- and contralateral brain volumes of manganese enhancement as calculated from ΔR_1 segmentation maps. *P < 0.05 vs. sham-operated group.

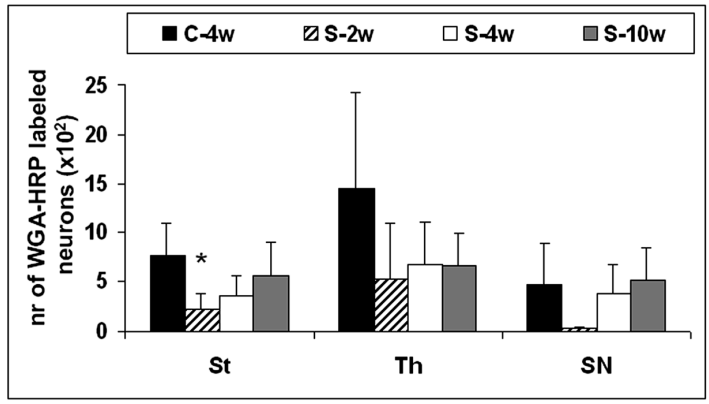

Figure 7

Number of labeled neurons (x 10^2) in ipsilateral subcortical ROIs of the sensorimotor network at 4 days after WGA-HRP injection in the ipsilateral sensorimotor cortex in rats after sham-operation, and at 2, 4, and 10 weeks after stroke. St: striatum; Th: thalamus; SN: substantia nigra. $^*P < 0.05$ vs. sham-operated group.

Immunohistochemistry In correspondence with our previous study (van der Zijden et al., 2007), the spatial distribution of WGA-HRP staining in the ipsilateral hemisphere was largely similar to the pattern of manganese enhancement. In agreement with the above-described MEMRI findings, the degree of WGA-HRP staining in ipsilateral subcortical ROIs was reduced at 2 weeks after stroke, which was statistically significant in the striatum, and returned to control values after 4 and 10 weeks (Figure 7). However, we found no WGA-HRP-labeled neurons in contralateral ROIs.

Discussion

In this study we applied MEMRI to assess temporal changes in neuroanatomical connectivity in relation to sensorimotor recovery after unilateral stroke in rats. We measured the spatial distribution of the paramagnetic neuronal tracer manganese 4 days after injection in the perilesional sensorimotor cortex at 2, 4 and 10 weeks post-stroke. After 4 and 10 weeks, when rats had reached a plateau stage of functional recovery, we observed increased manganese enhancement in connected ipsi- and contralateral regions. These findings point toward re-establishment of ipsilateral connections with the perilesional sensorimotor cortex and enhanced interhemispheric connectivity, in association with post-stroke restoration of sensorimotor function.

Restoration of ipsilateral connectivity In agreement with our previous study (van der Zijden et al., 2007), reduced MEMRI and WGA-HRP staining in subcortical ROIs demonstrated loss of connectivity between the perilesional sensorimotor cortex and ipsilateral subcortical sensorimotor network regions at 2 weeks after stroke. Numerous afferent and efferent cortical projections pass through or end in the infarcted zone, which included part of the somatosensory cortex and lateral striatum. After unilateral MCA occlusion in rats, prominent axonal and terminal degeneration has been demonstrated in cortical, striatal, thalamic and nigral areas adjacent to the infarct (Iizuka et al., 1989; Kataoka et al., 1989). Furhermore, Yam et al. (1998) have reported breakdown of axonal cytoskeleton and disruption of axonal transport inside and around the infarct after cerebral ischemia in rats. Clearly, these alterations give explanation to the disrupted tracer transport.

Significant ipsilateral loss of manganese enhancement and WGA-HRP labeling in subcortical ROIs at 2 weeks after stroke, however, was not present at later time-points. These results suggest a re-establishment of connectivity between the perilesional cortex and subcortical regions, which may be explained by recovery of existing neuronal pathways and/or structural alterations such as regenerative growth of axons, collateral sprouting, and formation of new synaptic connections. Yet it may also be possible that increased ipsilesional tracer accumulation represents enhanced take up and/or transport of manganese or WGA-HRP as compared to earlier time-points post-stroke. Nevertheless various histological studies have provided evidence for structural plasticity in the lesion border zone. An increase of the growth cone marker, growth-associated protein 43 (GAP-43) has been detected in perilesional tissue from the first days up to 4 weeks after unilateral stroke in rats (Stroemer et al., 1995; Li et al., 1998). This was followed by an increase in synaptophysin, a marker of mature synapses, between days 14 and 60 (Stroemer et al., 1995). Ito and others recently reported elevated density of synapses and axon terminals in ischemic borderzone from 1 to 12 weeks post-stroke, subsequent to initial degeneration of neurites in the first week (Ito et al., 2006). Moreover, during the same period, dendritic spine formation is also increased in this area (Brown et al., 2007). Actual formation of new connections with the perilesional cortex through axonal sprouting within

the ipsilateral hemisphere has been demonstrated by Carmichael et al. (2001). They injected the neuroanatomical tracer biotinylated dextran amine (BDA) into the perilesional cortex and observed new intracortical projections at 3 weeks after focal ischemia in rats. Similarly, using the same tracer, Dancause et al. (2005) detected corticocortical sprouting near a chronic ischemic lesion in monkey brain. Our data are in correspondence with these findings and further suggest that perilesional cortical connections with subcortical regions are also restored after a few weeks following stroke.

Enhanced interhemispheric connectivity In addition to re-establishment of manganese enhancement in ipsilateral regions, we detected a significant increase in the total contralateral volume of manganese enhancement at 4 weeks after stroke, and significantly increased manganese accumulation in the contralateral sensorimotor ROIs at 10 weeks. Our results correspond with earlier studies that have provided evidence for structural remodeling in the contralesional hemisphere after unilateral ischemic damage. For example, Jones and others have reported increased dendritic arborization and a larger number of synapses per neuron within the contralesional sensorimotor cortex between 18 and 30 days after lesion of the ipsilateral sensorimotor cortex in rats (Jones and Schallert, 1992; Jones et al., 1996). In addition, Stroemer et al. (1995) detected significantly elevated levels of synaptophysin in contralesional sensorimotor cortex at 14, 30 and 60 days after unilateral cortical infarction. Studies with an anterograde neuroanatomical tracer have demonstrated axonal sprouting from the contralesional cortex to the ipsilesional striatum and to the perilesional cortex (Napieralski et al., 1996; Uryu et al., 2001; Carmichael, 2003). Since manganese is transported in both anterograde and retrograde direction (Pautler et al., 2003), and can be transferred transsynaptically (Pautler et al., 1998; Saleem et al., 2002). MEMRI allows visualization of wide-ranging neuronal networks, and not sole afferent or efferent projections. This explains why we have found increased manganese enhancement in multiple contralateral regions. The enhanced transhemispheric manganese transfer may be explained by retrograde transport via newly formed or unmasked corticocortical (Allegrini and Wiessner, 2003; Carmichael, 2003), corticostriatal (Napieralski et al., 1996; Uryu et al., 2001) and corticothalamic projections (Yu et al., 1995). Evidence for increased manganese transport in crossing white matter fibres was found in the corpus callosum. This is in correspondence with findings by Allegrini and Wiessner (2003), who detected manganese enhancement in transhemispheric callosal fibres after manganese injection in the sensorimotor cortex contralateral to a cortical photothrombotic lesion. Also, increased manganese transport to the contralateral olfactory cortex has recently been detected at 4 weeks after a lesion in the lateral olfactory tract (Cross et al., 2006).

Despite the clear MRI-based detection of manganese in contralateral regions, marked WGA-HRP staining was not evident in the contralateral hemisphere in our study. The tracer survival time of 4 days, which was optimized for MEMRI, may have been too short for WGA-HRP transport to distant contralateral areas. In addition, WGA-HRP staining is not easily

discernible because of punctate and incomplete filling of neuronal processes with this tracer (Ferguson et al., 2001) and may be a less sensitive method to detect tracer accumulation at more remote sites.

Correlation between brain reorganization and functional recovery The time at which we detected increase in and intra- and interhemispheric neuroanatomical connectivity corresponded with the stage of plateau recovery of sensorimotor function, i.e. more than 2 weeks after stroke. Although our study does not provide direct evidence of a relationship between functional recovery and neuroanatomical reorganization, previous studies have shown that the temporal pattern of functional recovery correlates with neuroanatomical alterations, such as peri- and contralesional synaptogenesis (Stroemer et al., 1995) and contralesional dendritic sprouting (Jones and Schallert, 1992) after cortical brain injury. Furthermore, pharmacological stimulation of neuronal sprouting has been shown to improve behavioural performance (Kawamata et al., 1997; Stroemer et al., 1998; Chen et al., 2002). The lack of a direct correlation between early functional recovery and neuroanatomical changes in our study may be explained by insensitivity of the neuroanatomical tracer techniques to detect initial changes in projection patterns. Nonetheless, our MEMRI results suggest that plateau functional recovery is upheld by effective (re-)establishment of connections. Moreover, the maturation of newly formed network ties in with recovery of cortical function adjacent to a unilateral infarct. With functional MRI, we have shown that neuronal activation responses in perilesional sensorimotor cortex, which are largely lost in the first days post-stroke, are restored after 2 weeks (Dijkhuizen et al., 2001; Dijkhuizen et al., 2003; Weber et al., 2006).

In conclusion, in line with studies on the bird song control system (Van der Linden et al., 2004) and mossy fibre sprouting in a rat epilepsy model (Nairismagi et al., 2006), our results demonstrate the unique potential of MEMRI for *in vivo* detection of structural plasticity in the brain. Our MEMRI data on spatiotemporal changes in neuroanatomical connectivity after stroke suggest that remodelling of intra- and interhemispheric neuronal networks effectively contributes to post-stroke functional recovery.

Acknowledgements

- Dr. Dijkhuizen was financially supported by a fellowship of the Royal Netherlands Academy of Arts and Sciences.
- We thank Gerard van Vliet and Jan-Willem de Groot for excellent technical assistance.

References

Abercrombie M, Johnson ML (1946). Quantitative histology of Wallerian degeneration: I. Nuclear population in rabbit sciatic nerve. J Anat 80:37-50.

Allegrini PR, Wiessner C (2003). Three-dimensional MRI of cerebral projections in rat brain in vivo after intracortical injection of MnCl2. NMR Biomed 16:252-256.

Brown CE, Li P, Boyd JD, Delaney KR, Murphy TH (2007). Extensive turnover of dendritic spines and vascular remodeling in cortical tissues recovering from stroke. J Neurosci 27: 4101-4109.

Carmichael ST (2003). Plasticity of cortical projections after stroke. Neuroscientist 9:64-75.

Carmichael ST (2006). Cellular and molecular mechanisms of neural repair after stroke: making waves. Ann Neurol 59:735-742.

Carmichael ST, Wei L, Rovainen CM, Woolsey TA (2001). New patterns of intracortical projections after focal cortical stroke. Neurobiol Dis 8:910-922.

Chen P, Goldberg DE, Kolb B, Lanser M, Benowitz LI (2002). Inosine induces axonal rewiring and improves behavioral outcome after stroke. Proc Natl Acad Sci U S A 99: 9031-9036.

Collins DL, Neelin P, Peters TM, Evans AC (1994). Automatic 3D intersubject registration of MR volumetric data in standardized Talairach space. J Comput Assist Tomogr 18:192-205.

Cramer SC, Chopp M (2000). Recovery recapitulates ontogeny. Trends Neurosci 23:265-271.

Cross DJ, Flexman JA, Anzai Y, Morrow TJ, Maravilla KR, Minoshima S (2006). In vivo imaging of functional disruption, recovery and alteration in rat olfactory circuitry after lesion. Neuroimage 32:1265-1272.

Dancause N, Barbay S, Frost SB, Plautz EJ, Chen D, Zoubina EV, Stowe AM, Nudo RJ (2005). Extensive cortical rewiring after brain injury. J Neurosci 25:10167-10179.

Dijkhuizen RM, Ren J, Mandeville JB, Wu O, Ozdag FM, Moskowitz MA, Rosen BR, Finklestein SP (2001). Functional magnetic resonance imaging of reorganization in rat brain after stroke. Proc Natl Acad Sci U S A 98:12766-12771.

Dijkhuizen RM, Singhal AB, Mandeville JB, Wu O, Halpern EF, Finklestein SP, Rosen BR, Lo EH (2003). Correlation between brain reorganization, ischemic damage, and neurologic status after transient focal cerebral ischemia in rats: a functional magnetic resonance imaging study. J Neurosci 23:510-517.

Ferguson IA, Xian C, Barati E, Rush RA (2001). Comparison of wheat germ agglutinin-horseradish peroxidase and biotinylated dextran for anterograde tracing of corticospinal tract following spinal cord injury. J Neurosci Methods 109:81-89.

Gerriets T, Stolz E, Walberer M, Muller C, Rottger C, Kluge A, Kaps M, Fisher M, Bachmann G (2004). Complications and pitfalls in rat stroke models for middle cerebral artery occlusion: a comparison between the suture and the macrosphere model using magnetic resonance angiography. Stroke 35:2372-2377.

Iizuka H, Sakatani K, Young W (1989). Corticofugal axonal degeneration in rats after middle cerebral artery occlusion. Stroke 20:1396-1402.

Ito U, Kuroiwa T, Nagasao J, Kawakami E, Oyanagi K (2006). Temporal profiles of axon terminals, synapses and spines in the ischemic penumbra of the cerebral cortex: ultrastructure of neuronal remodeling. Stroke 37:2134-2139.

Jones TA, Schallert T (1992). Overgrowth and pruning of dendrites in adult rats recovering from neocortical damage. Brain Res 581:156-160.

Jones TA, Kleim JA, Greenough WT (1996). Synaptogenesis and dendritic growth in the cortex opposite unilateral sensorimotor cortex damage in adult rats: a quantitative electron microscopic examination. Brain Res 733:142-148.

Kataoka K, Hayakawa T, Yamada K, Mushiroi T, Kuroda R, Mogami H (1989). Neuronal network disturbance after focal ischemia in rats. Stroke 20:1226-1235.

Kawamata T, Dietrich WD, Schallert T, Gotts JE, Cocke RR, Benowitz LI, Finklestein SP (1997). Intracisternal basic fibroblast growth factor enhances functional recovery and up-regulates the expression of a molecular marker of neuronal sprouting following focal cerebral infarction. Proc Natl Acad Sci U S A 94:8179-8184.

Keyvani K, Schallert T (2002). Plasticity-associated molecular and structural events in the injured brain. J Neuropathol Exp Neurol 61:831-840.

Li Y, Jiang N, Powers C, Chopp M (1998). Neuronal damage and plasticity identified by microtubule-associated protein 2, growth-associated protein 43, and cyclin D1 immunoreactivity after focal cerebral ischemia in rats. Stroke 29:1972-1980; discussion 1980-1971.

Longa EZ, Weinstein PR, Carlson S, Cummins R (1989). Reversible middle cerebral artery occlusion without craniectomy in rats. Stroke 20:84-91.

Nairismagi J, Pitkanen A, Narkilahti S, Huttunen J, Kauppinen RA, Grohn OH (2006). Manganese-enhanced magnetic resonance imaging of mossy fiber plasticity in vivo. Neuroimage 30:130-135.

Napieralski JA, Butler AK, Chesselet MF (1996). Anatomical and functional evidence for lesion-specific sprouting of corticostriatal input in the adult rat. J Comp Neurol 373:484-497.

Nudo RJ (1999). Recovery after damage to motor cortical areas. Curr Opin Neurobiol 9: 740-747.

Nudo RJ (2006). Mechanisms for recovery of motor function following cortical damage. Curr Opin Neurobiol 16:638-644.

Nyul LG, Udupa JK (1999). On standardizing the MR image intensity scale. Magn Reson Med 42:1072-1081.

Nyul LG, Udupa JK, Zhang X (2000). New variants of a method of MRI scale standardization. IEEE Trans Med Imaging 19:143-150.

Pautler RG, Silva AC, Koretsky AP (1998). In vivo neuronal tract tracing using manganese-enhanced magnetic resonance imaging. Magn Reson Med 40:740-748.

Pautler RG, Mongeau R, Jacobs RE (2003). In vivo trans-synaptic tract tracing from the murine striatum and amygdala utilizing manganese enhanced MRI (MEMRI). Magn Reson Med 50:33-39.

Paxinos G, Watson C (1998). The rat brain in stereotaxic coordinates, 4th Edition. San Diego: Academic Press.

Pham DL, Prince JL (1999). Adaptive fuzzy segmentation of magnetic resonance images. IEEE Trans Med Imaging 18:737-752.

Press WH, Vetterling WT (1992). Numerical recipes in FORTRAN : the art of scientific computing, 2nd Edition. Cambridge, England: Cambridge University Press.

Reglodi D, Tamas A, Lengvari I (2003). Examination of sensorimotor performance following middle cerebral artery occlusion in rats. Brain Res Bull 59:459-466.

Saleem KS, Pauls JM, Augath M, Trinath T, Prause BA, Hashikawa T, Logothetis NK

(2002). Magnetic resonance imaging of neuronal connections in the macaque monkey. Neuron 34:685-700.

Schallert T, Fleming SM, Leasure JL, Tillerson JL, Bland ST (2000). CNS plasticity and assessment of forelimb sensorimotor outcome in unilateral rat models of stroke, cortical ablation, parkinsonism and spinal cord injury. Neuropharmacology 39:777-787.

Silva AC, Lee JH, Aoki I, Koretsky AP (2004). Manganese-enhanced magnetic resonance imaging (MEMRI): methodological and practical considerations. NMR Biomed 17:532-543.

Sloot WN, Gramsbergen JB (1994). Axonal transport of manganese and its relevance to selective neurotoxicity in the rat basal ganglia. Brain Res 657:124-132.

Stroemer RP, Kent TA, Hulsebosch CE (1995). Neocortical neural sprouting, synaptogenesis, and behavioral recovery after neocortical infarction in rats. Stroke 26:2135-2144.

Stroemer RP, Kent TA, Hulsebosch CE (1998). Enhanced neocortical neural sprouting, synaptogenesis, and behavioral recovery with D-amphetamine therapy after neocortical infarction in rats. Stroke 29:2381-2393; discussion 2393-2385.

Uryu K, MacKenzie L, Chesselet MF (2001). Ultrastructural evidence for differential axonal sprouting in the striatum after thermocoagulatory and aspiration lesions of the cerebral cortex in adult rats. Neuroscience 105:307-316.

Van der Linden A, Van Meir V, Tindemans I, Verhoye M, Balthazart J (2004). Applications of manganese-enhanced magnetic resonance imaging (MEMRI) to image brain plasticity in song birds. NMR Biomed 17:602-612.

van der Zijden JP, Wu O, van der Toorn A, Roeling TP, Bleys RL, Dijkhuizen RM (2007). Changes in neuronal connectivity after stroke in rats as studied by serial manganese-enhanced MRI. Neuroimage 34:1650-1657.

Weber R, Ramos-Cabrer P, Wiedermann D, van Camp N, Hoehn M (2006). A fully non-invasive and robust experimental protocol for longitudinal fMRI studies in the rat. Neuroimage 29:1303-1310.

Yam PS, Dewar D, McCulloch J (1998). Axonal injury caused by focal cerebral ischemia in the rat. J Neurotrauma 15:441-450.

Yu XH, Moret V, Rouiller EM (1995). Re-examination of the plasticity of the corticothalamic projection after unilateral neonatal lesion of the sensorimotor cortex in the rat: a phaseolus vulgaris-leucoagglutinin tracing study. J Hirnforsch 36:123-133.

Chapter 4 Longitudinal *in vivo* MRI of Alterations in Perilesional Tissue after Transient Ischemic Stroke in Rats

[1]Jet P. van der Zijden, [1]Annette van der Toorn, [1]Kajo van der Marel, [1]Rick M. Dijkhuizen

[1]Image Sciences Institute, University Medical Center Utrecht, Utrecht, the Netherlands

In press in Journal of Experimental Neurology

4 Longitudinal *in vivo* MRI of Alterations in Perilesional Tissue after Transient Ischemic Stroke in Rats

Abstract

Spontaneous restoration of function after stroke is associated with remodelling of functional neuronal networks in and around the ischemic lesion. However, the spatiotemporal profile of structural alterations in (peri)lesional tissue in relation to post-stroke recovery of neuronal function remains largely to be elucidated.

We performed neurological testing in combination with *in vivo* serial T_2-weighted magnetic resonance imaging (MRI) and diffusion tensor imaging (DTI) to assess functional recovery in relation to longitudinal changes in tissue integrity from 3 hours up to 9 weeks after experimental unilateral stroke in rats (n = 7). Subsequently, to evaluate perilesional neuronal connectivity, we conducted manganese-enhanced MRI after $MnCl_2$ injection in cortical tissue at the boundary of the lesion at 10 weeks post-stroke (n = 5).

All animals showed significant improvement of neurological function over time. Normalization of tissue T_2 and fractional diffusion anisotropy (FA) after significant subacute change was observed in cortical and subcortical lesion borderzones between 3 and 9 weeks post-stroke. Progressive FA increase above baseline levels was detected in perilesional white matter areas (n = 4). In these animals particularly, significant manganese enhancement appeared within the neuronal network around the chronic lesion, including areas that were part of the lesion at day 3 post-stroke.

This longitudinal multi-parametric MRI study suggests that resolution of early ischemic damage and reorganization of white matter in perilesional tissue is chronically accompanied by preservation or restoration of neuronal connectivity, which may significantly contribute to post-stroke functional recovery.

Introduction

Spontaneous restoration of function generally occurs in patients recovering from ischemic brain injury, which could be the direct result of reorganization in and around affected tissue. Various physiological and morphological changes occur in post-ischemic brain. Effective functional recovery requires preservation, restitution and/or remodelling of functional neuronal networks. In a neuroanatomical tracer study, which included *in vivo* manganese-enhanced MRI (MEMRI) and immunohistochemical neuronal tract tracing with wheat-germ agglutinin horseradish peroxidase (WGA-HRP), we have recently demonstrated that neuronal connectivity in perilesional tissue is enhanced at chronic time-points after stroke in rats, in association with significant improvement of neurological function (van der Zijden et al., 2008). Following injection of neuronal tracer in intact sensorimotor cortex at the border of an ischemic lesion, increased tracer accumulation was found in subcortical regions of the sensorimotor network at 10 weeks post-stroke. In a separate group of animals, tracer distribution was significantly less at 2 weeks after stroke. These findings suggest time-dependent modification of ischemic borderzone tissue. However, the precise evolution of structural changes that lead to recovery of neuronal function remains to be clarified.

Longitudinal alterations in post-stroke brain tissue may be ideally assessed with serial *in vivo* MRI experiments. For example, T_2-weighted MRI allows measurement of changes in the extent of edema (van Bruggen et al., 1994; Baird and Warach, 1998), while diffusion tensor imaging (DTI) informs on structural integrity of gray and white matter after experimental and clinical stroke (Le Bihan et al., 2001; Sotak, 2002). Earlier longitudinal multiparametric MRI studies have shown specific temporal profiles of changes in T_2 and diffusion characteristics in ischemic borderzone tissue, which have been related to pathophysiological as well as restorative processes (Knight et al., 1994; Virley et al., 2000; Jiang et al., 2006). For example, normalization of T_2 after initial prolongation has been associated with resolution of edema (Lin et al., 2002a; Lin et al., 2002b) as well as with glial proliferation (Ishii et al., 1998; Wegener et al., 2006). Recent DTI studies have shown increase of diffusion anisotropy in perilesional areas, which may be explained by white matter reorganization (Jiang et al., 2006). The aim of our study was to further characterize the long-term evolution of changes in perilesional tissue after unilateral stroke, and to establish whether neuronal connectivity was preserved or recovered in these areas. To that aim we applied serial *in vivo* T_2-weighted MRI and DTI, together with behavioural testing, from acute to chronic stages after experimental transient stroke, concluded with *in vivo* MEMRI after 10 weeks.

Materials and Methods

Animals

All animal procedures were approved by the local ethical committee of Utrecht University and met governmental guidelines. A total of seven male Wistar rats weighing 250-350 g were included in the study. Animals were subjected to serial MRI measurements at 3 hours, 3 days, 3 weeks and 9 weeks after stroke. Five out of seven animals were also subjected to MEMRI at 10 weeks after stroke.

Stroke model

Rats were anesthetized with 2.5% isoflurane in N_2O/O_2 (70:30) under spontaneous respiration. Blood oxygen saturation and heart rate were continuously monitored during surgical procedures. Body temperature was maintained at 37.0 ± 0.5 °C. Transient focal cerebral ischemia was induced by 30-min occlusion of the right middle cerebral artery (MCA) with an intraluminal filament (Longa et al., 1989). In brief, a 4.0 silicon-coated polypropylene suture (Ethicon, Piscataway, NJ, USA) was introduced into the external carotid artery and advanced through the internal carotid artery until a slight resistance was felt, indicating that the MCA was occluded. After 30 minutes, the filament was withdrawn from the internal carotid artery to allow reperfusion. After surgery, rats received a subcutaneous injection of 0.3 mg/kg buprenorphine (Schering-Plough, Utrecht, The Netherlands) for post-surgical pain relief, and 5 ml saline to compensate for loss of water and minerals.

Functional examination

Animals were subjected to behavioural testing to assess sensorimotor function. We applied a battery of motor, sensory and tactile tests, which provided a neurological score on a scale of 0 to 20 points, with 20 as maximal deficit score (van der Zijden et al., 2008). Behavioural examination was performed a few hours before and on days 3, 7 and 10 after stroke, and every week thereafter.

MRI experiments

MRI measurements were performed on a 4.7 T horizontal bore MR system (Varian, Palo Alto, CA, USA) with use of a Helmholtz volume coil (90-mm diameter) and an inductively coupled surface coil (35-mm diameter) for signal excitation and detection, respectively.

Prior to MRI, rats were anaesthetized with 4% isoflurane for endotracheal intubation, followed by mechanical ventilation with 2.5% isoflurane in air/O_2 (85:15). Rats were placed in a MR-compatible stereotactic holder and immobilized with earplugs and a toothholder. Blood oxygen saturation and

heart rate were monitored during MRI measurements, and body temperature was maintained at 37.0 ± 0.5 °C.

Serial T_2-weighted MRI and DTI All rats underwent T_2-weighted MRI and DTI, carried out at 3 hours, 3 days, 3 weeks and 9 weeks after stroke. First, multi-echo multi-slice T_2-weighted MRI (repetition time (TR)/echo time (TE) = 3000/17.5 ms; echo train length = 8; acquisition matrix = 128 x 128; voxel resolution = 0.25 x 0.25 x 1.0 mm^3) was performed to measure the edematous ischemic lesion. Quantitative T_2 maps were calculated on a voxel-wise basis by linear least-squares fit of the logarithm of the signal intensity versus TE.

Second, multi-slice, eight-shot, diffusion-weighted echo-planar imaging (EPI) (TR/TE = 3000/32 ms; *b*-values = 303 and 1213 s/mm^2 in 6 directions; acquisition matrix = 128 x 128; voxel resolution = 0.25 x 0.25 x 1.0 mm^3) was performed to assess tissue architecture. Quantitative apparent diffusion coefficient (ADC) maps were calculated on a voxel-wise basis with a linear least-squares fit on the logarithm of the signal intensity versus the b-value for each diffusion direction. Based on the ADC maps, the eigenvalues of the diffusion tensor, quantitative mean diffusivity (ADC_{av}) and fractional anisotropy (FA) maps were generated as described by Kingsley (2006).

MEMRI In addition to the above MRI protocol, five out of seven animals underwent MEMRI at 10 weeks after stroke. First, at 9 weeks after stroke multi-slice, pre-contrast T_1-weighted MRI was performed using a saturation recovery gradient-echo sequence with seven TRs (TR/TE = 55-3000/18 ms; acquisition matrix = 128 x 128; voxel resolution = 0.25 x 0.25 x 1.0 mm^3). Manganese was injected 3 days later, for which animals were anesthetized by subcutaneous injection of 0.55 mg/kg midazolam, and a mixture of 0.315 mg/ml fentanyl citrate and 10 mg/ml fluanisone (0.55 mg/kg). Rats were placed in a stereotactic holder and immobilized by earplugs and a tooth-holder. Blood oxygen saturation and heart rate were continuously monitored. Body temperature was maintained at 37.0 ± 0.5 °C. A burr hole was drilled in the skull at 0.5 mm anterior and 1.2-2.5 mm lateral to bregma, above the sensorimotor cortex (according to Paxinos and Watson (2005)). Lateral coordinates were adjusted based on the extent of the lesion, as determined by T_2-weighted MRI prior to tracer injection, and chosen as such that tracer was injected in spared sensorimotor cortical tissue bordering the T_2-defined lesion. As we have previously shown, such small variation in lateral position of the injection site does not cause significant differences in the pattern of manganese enhancement within the sensorimotor network (van der Zijden et al., 2007). 0.2 µl 1 M $MnCl_2$ was injected with a 2.0 µl Hamilton syringe at a rate of 0.05 µl/min. After injection, the needle was left in place for 3 minutes to prevent leakage.

T_2- and T_1-weighted MRI were performed at 4 days after manganese injection. Quantitative pre- and post-injection R_1 ($1/T_1$) maps were calculated on a voxel-wise basis by performing a non-linear least-squares fit using the Levenberg-Marquardt method (Press and Vetterling, 1992).

Data analysis

T_2, ADC_{av}, FA and R_1 maps were co-registered to a MRI data set from a control rat brain using the FMRIB Linear Image Registration Tool (FLIRT), which optimized a normalized correlation cost function of a 12-parameter affine transformation (Jenkinson and Smith, 2001).

T_2 recovery Ischemic lesion areas were determined from the T_2 dataset and defined as ipsilateral volume with T_2 values greater than the mean + 2 SD of the T_2 in contralateral tissue. In correspondence with previous studies (Neumann-Haefelin et al., 2000; Virley et al., 2000; Jiang et al., 2006; Wegener et al., 2006), T_2 lesion volume reduced in size from subacute to chronic stages after stroke. To identify regions where T_2 normalized, we subtracted T_2 lesion volumes at 9 weeks from T_2 lesion volumes at 3 days, in co-registered brains from individual rats. Next, three regions-of-interest (ROIs) were selected in seven adjacent brain slices: i) permanent lesion (i.e., the volume that was part of the T_2 lesion at both 3 days and 9 weeks after stroke) (Lesion); ii) dorsal cortical region where T_2 normalized between 3 days and 9 weeks post-stroke (Cx_{rec}); and iii) subcortical region, excluding the corpus callosum, where T_2 normalized between 3 days and 9 weeks post-stroke ($subCx_{rec}$). Homologous contralateral regions served as control regions.

FA recovery A recent study has reported recovery of FA in lesion borderzones, chronically after stroke in rats (Jiang et al., 2006). To further investigate this we delineated regions that exhibited progressive increase of FA at chronic time-points following subacute FA reduction. This was done by automated selection of voxels where the time course of FA corresponded to the following pattern: $FA_{3d} < FA_{3h} - 2SD$; $FA_{3w} > FA_{3d} + 2SD$; $FA_{9w} > FA_{3w} + 2SD$, where FA_{3h}, FA_{3d}, FA_{3w} and FA_{9w} represent the FA at 3 hours, 3 days, 3 weeks and 9 weeks, post-stroke, respectively.

Manganese enhancement Manganese accumulation was measured from the difference between pre- and post-contrast R_1 (ΔR_1) in ipsi- and contralateral subcortical ROIs, i.e. thalamus (Th), substantia nigra (SN), and $subCx_{rec}$. Th and SN were automatically selected using home-built, registration-based segmentation software in conjunction with Paxinos' rat brain atlas (Paxinos and Watson, 2005). Only parts of the Th and SN that were outside the T_2-defined lesion at 10 weeks were included for analysis.

Statistics All values are expressed as mean ± SD. The temporal pattern of functional status was analyzed using a one-way repeated measures analysis-of-variance (ANOVA) with post-hoc multiple comparison *t*-testing with Bonferroni correction. The temporal patterns of T_2, ADC_{av}, and FA were analyzed using a two-way repeated measures ANOVA with post-hoc multiple comparison *t*-testing with Bonferroni correction. Differences between ΔR_1 values in ROIs were analyzed with one-way repeated measures ANOVA with post-hoc multiple comparison *t*-testing with Bonferroni correction. Differ-

ences between ipsi- and contralateral T_2, FA and ADC_{av}, and differences between pre- and post-manganese R_1 values, were analyzed with a paired Student's *t*-test. Correlations between change in neurological score and changes in T_2, ADC_{av} and FA in Cx_{rec} and $subCx_{rec}$, between day 3 and week 9, were assessed by Pearson Product Moment Correlation testing. $P < 0.05$ was considered significant.

Results

Functional status All rats demonstrated substantial functional deficits at day 3 after stroke, which significantly improved thereafter and stabilized between 2 and 9 weeks after stroke (Figure 1).

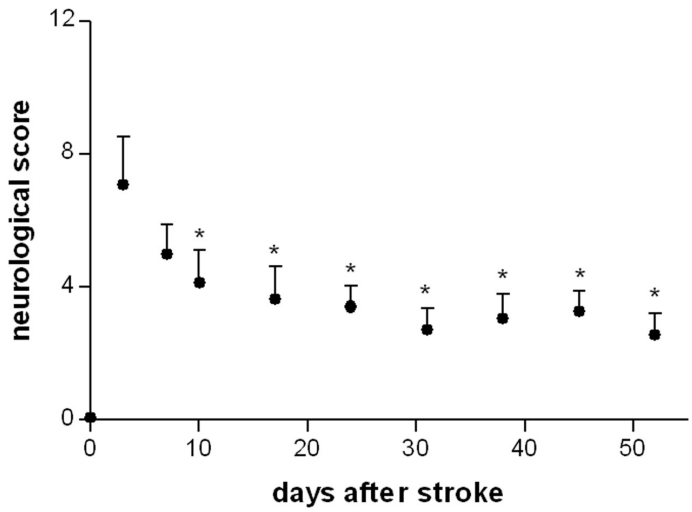

Figure 1
Neurological score (mean + SD) as a function of time after stroke. *P < 0.05 vs. day 3.

T_2 and DTI data The unilateral ischemic lesion was characterized by a prolonged T_2 (Figure 2). The lesion volume on day 3 after stroke as determined from 7 adjacent slices of the T_2 dataset was 27.2 ± 8.8 % of the total brain volume. The area of significant T_2 prolongation was smaller at 9 weeks (Figure 2, right) than at 3 days after stroke (Figure 2, left). Areas where T_2 was recovered after 9 weeks typically included the dorsal cortical region and the lateral subcortical region at the lesion boundaries. The three ROIs, representing the permanent T_2 lesion (Lesion), and the cortical (Cx_{rec}) and subcortical regions where T_2 recovered ($subCx_{rec}$), are overlaid on the T_2 map in Figure 2 (right).

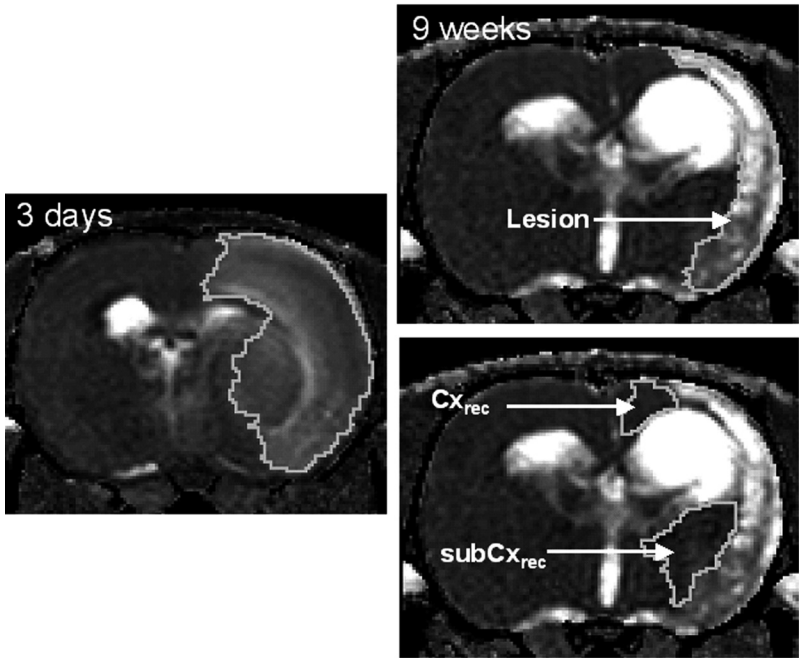

Figure 2

T_2 maps of a rat brain slice at 3 days (left) and 9 weeks (right) after stroke. After 9 weeks, lesion volume was smaller than at 3 days. Regions-of-interest (ROIs) are displayed on the T_2 map at 9 weeks after stroke: lesion area (Lesion), cortical T_2 recovery (Cx_{rec}) and subcortical T_2 recovery ($subCx_{rec}$).

ADC_{av} (A) and FA maps (B) at 3 days (left) and 9 weeks after stroke (right) are shown in Figure 3. At 3 days post-stroke, ADC_{av} and FA were reduced in most part of the lesion, while an increased ADC_{av} was observed around the external capsule. After 9 weeks, ADC_{av} was elevated within the entire remaining lesion area, which was however smaller than at 3 days, similar to the findings on T_2 maps. FA, however, did not appear significantly different from contralateral after 9 weeks. In fact, in some rats, an enhanced FA was detectable subcortically just outside the lesion.

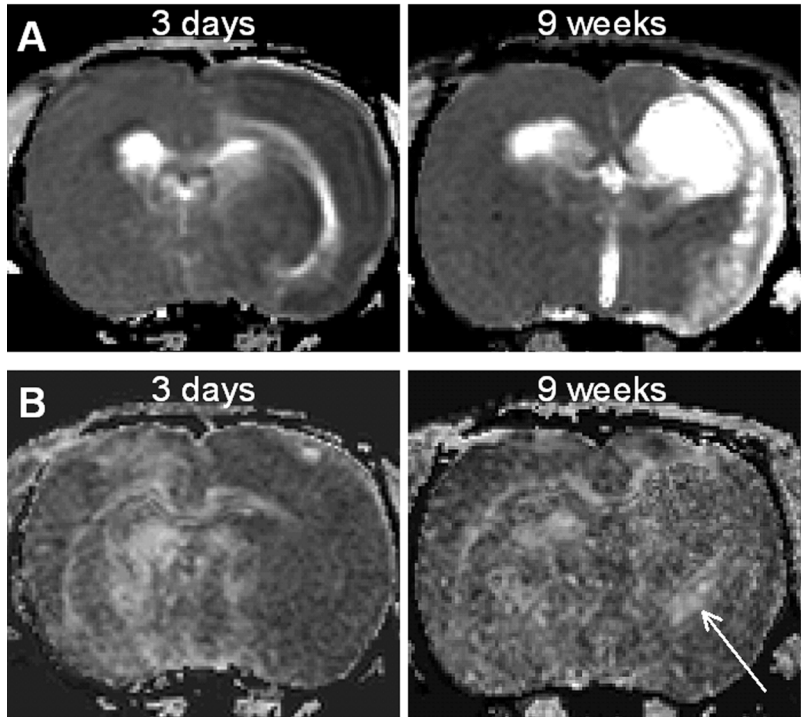

Figure 3
ADC_{av} (A) and FA (B) maps of a rat brain slice at 3 days (left) and 9 weeks (right) after stroke. The arrow indicates the area where FA markedly increased.

Time-courses of relative T_2 (A), ADC_{av} (B) and FA (C) in Lesion, Cx_{rec} and $subCx_{rec}$ are shown in Figure 4. T_2 clearly increased in Lesion over the entire time-period. In Cx_{rec} and $subCx_{rec}$, T_2 normalized after 3 days and reached control levels at 9 weeks after stroke.

ADC_{av} values were slightly increased after 3 hours (i.e. 2.5 hours after reperfusion) in Lesion and Cx_{rec}. At 3 and 9 weeks after stroke, there was a large increase in ADC_{av} inside the lesion. Smaller but significant ADC_{av} increases were detected in Cx_{rec} and $subCx_{rec}$.

FA was reduced in all ipsilateral ROIs at 3 days after stroke. Thereafter, FA increased over time and was not significantly different from contralateral after 9 weeks in all ROIs. In four rats, we identified a distinct area in the lesion borderzone where the FA demonstrated a marked temporal profile as described in the Methods section (Figure 5). This area was typically located outside the 9-weeks lesion and anatomically matched with the internal capsule and/or the corpus callosum.

We analyzed potential relationships between changes in T_2, ADC_{av} and FA and change in neurological score, but found no statistically significant correlations.

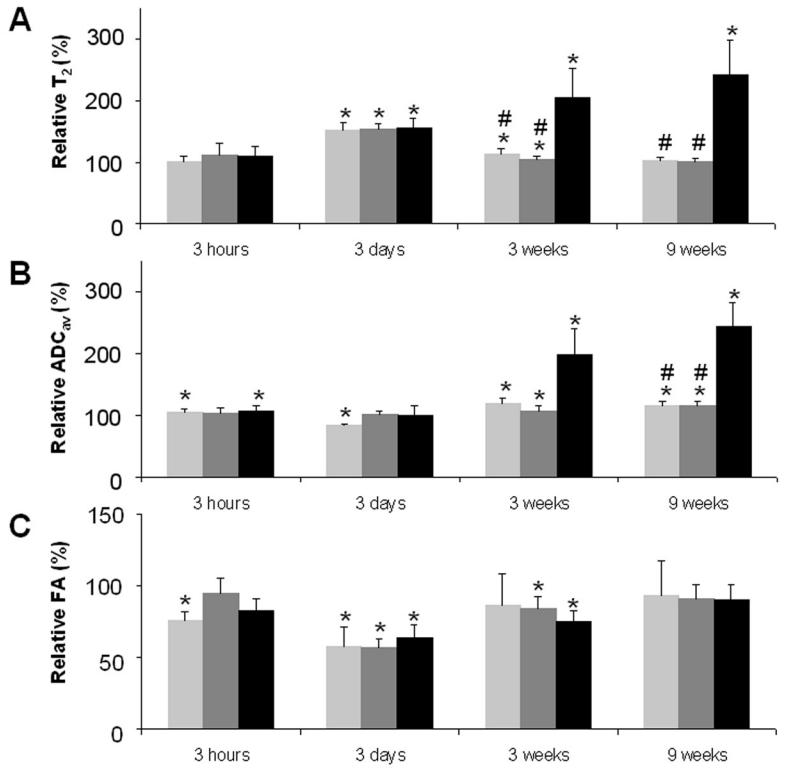

Figure 4

Time-course of T_2 (A), ADC_{av} (B) and FA (C) in Lesion (■), Cx_{rec} (■) and $subCx_{rec}$ (■) after stroke (% of contralateral, mean ± SD). $^{*}P < 0.05$ ipsi- vs. contralateral; $^{\#}P < 0.05$ vs. lesion.

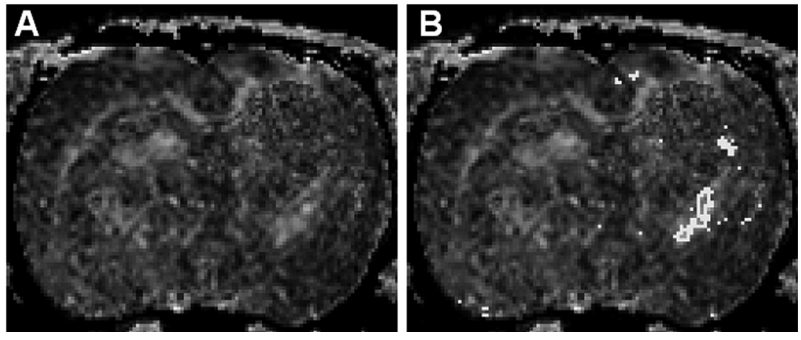

Figure 5

FA maps of a rat brain slice at 9 weeks after stroke without (A) and with marked (white) voxels that exhibited progressive FA increase as described in the Methods section (B).

MEMRI At 10 weeks after stroke, manganese was injected in the intact perilesional sensorimotor cortex of five animals that underwent serial T_2-weighted MRI and DTI. Correct injection into the sensorimotor cortex was confirmed on post-contrast T_1-weighted MR images. In four animals the injection site was part of Cx_{rec}, while in one animal manganese was injected in cortical tissue that was outside the lesion area at all time-points. Post-manganese R_1 maps clearly visualized the spatial pattern of manganese distribution after injection into the intact perilesional sensorimotor cortex (Figure 6A). After four days manganese accumulation was particularly evident in subcortical areas, e.g., the thalamus (Th) and the substantia nigra (SN) (Figure 6B). Significant manganese accumulation was also detected in $subCx_{rec}$.

In rats that demonstrated progressive FA increase after subacute decrease subcortically, manganese-induced ΔR_1 in thalamus and substantia nigra (0.71 ± 0.32 s^{-1} and 0.60 ± 0.36 s^{-1}, respectively (n = 3)) was stronger than in the rat that did not show this particular pattern of subcortical FA changes (0.20 s^{-1} and 0.17 s^{-1}, respectively (n = 1)).

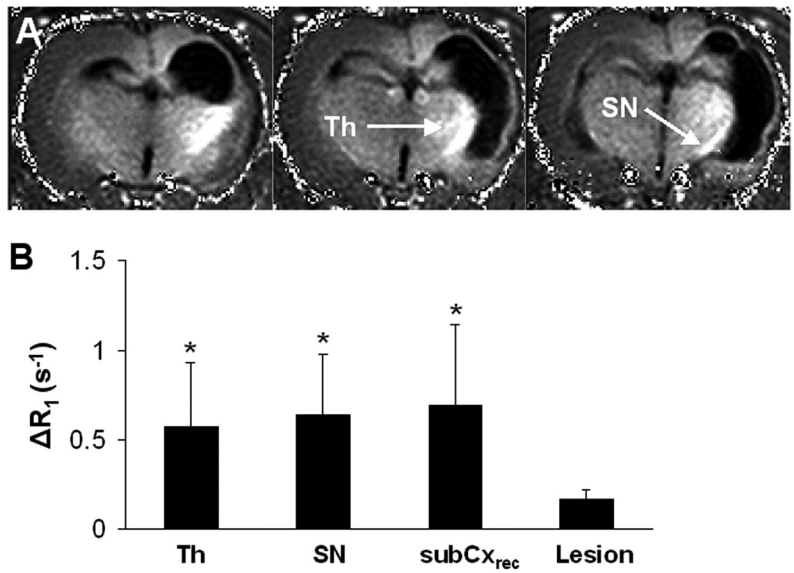

Figure 6

A: R_1 maps of three adjacent coronal brain slices at 4 days after $MnCl_2$ injection in the ipsilateral sensorimotor cortex in a rat at 10 weeks after stroke. The stroke lesion is characterized by reduced R_1. B: Ipsilateral manganese-induced ΔR_1 (s^{-1}) in thalamus (Th), substantia nigra (SN), subcortical T_2 recovery ($subCx_{rec}$) and lesion area (Lesion) at 4 days after $MnCl_2$ injection in the ipsilateral sensorimotor cortex of rats at 10 weeks after stroke. $^*P < 0.05$ versus other ROIs.

Discussion

In this study we combined serial *in vivo* T_2-weighted MRI and DTI with MEMRI to assess temporal changes in tissue architecture in rats recovering from transient unilateral stroke. Early ischemia-induced changes that are reflective of tissue degeneration, i.e. prolonged T_2 and decreased FA, normalized at chronic time-points in cortical and subcortical lesion borderzones. Progressive FA increase was evident in white matter areas, suggestive of alterations in fibre structure. Injection of the neuroanatomical tracer manganese into perilesional sensorimotor cortex where T_2 had recovered after 9 weeks resulted in significant manganese enhancement in subcortical regions that had been part of the T_2 lesion at 3 days after stroke. Our findings suggest that resolution of initial ischemic damage is accompanied by rearrangement of white matter structure and preservation or restoration of neuronal connectivity, which are critical factors in post-stroke functional recovery.

T_2 normalization Inside the permanent, chronic lesion T_2 and ADC_{av} were highly increased, reflective of loss of tissue structure. A larger area of T_2 prolongation was evident subacutely after stroke, most likely resulting from extensive vasogenic edema formation (see Dijkhuizen and Nicolay (2003) and references therein). Partial resolution of vasogenic edema usually occurs over the following weeks, which would explain the T_2 recovery in perilesional areas. Nevertheless, it has been shown that selective neuronal damage and gliosis may develop in tissue that exhibits T_2 recovery after stroke (Ishii et al., 1998; Wegener et al., 2006). We detected a slight but significant ADC_{av} increase in the regions of T_2 recovery, which corroborates the existence of minor tissue injury in these areas. Apparently, perilesional tissue where T_2 normalizes does not necessarily reflect normal, fully recovered tissue. On the other hand several studies have demonstrated plastic changes, e.g. neurite sprouting, in these areas (Nudo, 1999; Keyvani and Schallert, 2002; Carmichael, 2003). In all probability ischemic borderzones continually experience pathological effects as well as restorative processes (Li et al., 1998; Witte et al., 2000; Carmichael, 2006) and improvement of local neuronal function is dependent on the interplay between pathological consequences and tissue repair.

FA recovery The evolution of FA was characterized by a decrease at 3 days after stroke followed by recovery at 3 weeks and return to control values after 9 weeks, both in perilesional areas and in the lesion core. The observed FA increase in lesion borderzone tissue corresponds with previous findings by Jiang et al. (2006). In addition, Wang et al. (2006) has described longitudinal FA increase in normal-appearing white matter in stroke patients. In these studies the FA recovery was associated with improvement of white matter integrity, e.g. due to remyelination. Yet, we also detected rise of FA inside the lesion core. Chronic increase of FA inside stroke lesions has also been observed in a recent serial DTI study in nonhuman primates after transient

MCA occlusion (Liu et al., 2007). This might be associated with glial proliferation and fibrous mesh formation in incompletely infarcted tissue with structurally preserved architecture (Garcia et al., 1997), but could also be caused by relatively low signal-to-noise levels in this area on diffusion-weighted images (Pierpaoli and Basser, 1996).

Since our ROIs where T_2 recovered involved white and gray matter, the anticipated strong effect of white matter reorganization on FA increase may have been diminished. Therefore we performed an additional segmentation procedure that automatically selected regions that exhibited a progressive pattern of FA increase after initial decline at 3 days, which would be reflective of initial loss and subsequent improvement of white matter integrity. In four animals, we found specific FA increase in areas corresponding to the internal capsule and/or corpus callosum, just outside the lesion area. In correspondence, white matter reorganization, such as remyelination and/or axonal sprouting, has been observed in these regions after experimental unilateral stroke (Ishiguro et al., 1993; Tanaka et al., 2003; Jiang et al., 2006). Alternatively, the FA increase may also be related to gliosis, i.e. proliferation of glial cells (reactive astrocytes), in areas bordering the lesion. Using DTI, Schwartz et al. have detected an increased lattice anisotropy index, but not FA, in glial scar tissue surrounding a spinal cord lesion (Schwartz et al., 2005). Future studies that include microscopical histological evaluation are required to establish to what extent white matter reorganization and gliosis contribute to chronic post-stroke FA increase.

Manganese enhancement At 10 weeks after stroke, we injected manganese in the perilesional sensorimotor cortex where T_2 was unchanged (n = 1) or had recovered after initial prolongation (n = 4). In all animals significant manganese-induced R_1 increase was detected in subcortical regions, particularly within the ipsilateral sensorimotor network, which is in agreement with our previous study (van der Zijden et al., 2007). Large portions of the subcortical area where manganese accumulated were part of the lesion area at 3 days after stroke. Correspondingly, we detected significant manganese enhancement in $subCx_{rec}$.

We have recently shown that initially distorted neuronal connectivity within the ipsilateral sensorimotor nework recovers after 10 weeks (van der Zijden et al., 2008). In the current study we demonstrate that perilesional neuronal connectivity was associated with cortical and subcortical T_2 normalization and progressive FA increase in connective white matter regions. Thus our data indicate that connective pathways that are initially affected by cerebral ischemia may be preserved, restored or remodelled at later timepoints after stroke. As animals exhibited significant improvement of neurological function in parallel with the described morphological alterations, we believe that structural modifications in ischemic borderzones are critically involved in functional recovery after stroke. Yet, we found no direct correlation between changes in MRI parameters and changes in neurological score. This may be explained by lack of sensitivity and specificity of the MRI techniques and behavioural tests to detect subtle and specific changes in

neuronal architecture and neurological functions, respectively. Future studies on the correlation between functional recovery and brain remodelling should focus on more detailed assessment of specific neurological functions in relation to neuronal modifications in representational brain regions.

In conclusion, our study demonstrates that longitudinal multi-parametric MRI can provide unique *in vivo* information on structural tissue changes related to damage and recovery after stroke. Our findings, particularly with respect to changes in FA, however, must be interpreted carefully and require detailed histological validation in future studies. Nevertheless, we believe that our results provide significant evidence of structural reorganization in and around ischemic lesions, which may contribute to functional recovery after stroke.

Acknowledgements

- Dr. Dijkhuizen is financially supported by a fellowship of the Royal Netherlands Academy of Arts and Sciences.
- We thank Gerard van Vliet and Jan-Willem de Groot for excellent technical assistance.

References

Baird AE, Warach S (1998). Magnetic resonance imaging of acute stroke. J Cereb Blood Flow Metab 18:583-609.

Carmichael ST (2003). Plasticity of cortical projections after stroke. Neuroscientist 9:64-75.

Carmichael ST (2006). Cellular and molecular mechanisms of neural repair after stroke: making waves. Ann Neurol 59:735-742.

Dijkhuizen RM, Nicolay K (2003). Magnetic resonance imaging in experimental models of brain disorders. J Cereb Blood Flow Metab 23:1383-1402.

Garcia JH, Liu KF, Ye ZR, Gutierrez JA (1997). Incomplete infarct and delayed neuronal death after transient middle cerebral artery occlusion in rats. Stroke 28:2303-2309; discussion 2310.

Ishiguro H, Inuzuka T, Fujita N, Sato S, Nakano R, Tamura A, Kirino T, Miyatake T (1993). Expression of the large myelin-associated glycoprotein isoform in rat oligodendrocytes around cerebral infarcts. Mol Chem Neuropathol 20:173-179.

Ishii H, Arai T, Morikawa S, Inubushi T, Tooyama I, Kimura H, Mori K (1998). Evaluation of focal cerebral ischemia in rats by magnetic resonance imaging and immunohistochemical analyses. J Cereb Blood Flow Metab 18:931-934.

Jenkinson M, Smith S (2001). A global optimisation method for robust affine registration of brain images. Med Image Anal 5:143-156.

Jiang Q, Zhang ZG, Ding GL, Silver B, Zhang L, Meng H, Lu M, Pourabdillah-Nejed DS, Wang L, Savant-Bhonsale S, Li L, Bagher-Ebadian H, Hu J, Arbab AS, Vanguri P, Ewing JR, Ledbetter KA, Chopp M (2006). MRI detects white matter reorganization after neural progenitor cell treatment of stroke. Neuroimage 32:1080-1089.

Keyvani K, Schallert T (2002). Plasticity-associated molecular and structural events in the injured brain. J Neuropathol Exp Neurol 61:831-840.

Kingsley PB (2006). Introduction to diffusion tensor imaging mathematics: Part I. Tensors, rotations, and eigenvectors. Concepts in Magnetic Resonance Part A 28A:101-122.

Knight RA, Dereski MO, Helpern JA, Ordidge RJ, Chopp M (1994). Magnetic resonance imaging assessment of evolving focal cerebral ischemia. Comparison with histopathology in rats. Stroke 25:1252-1261; discussion 1261-1252.

Le Bihan D, Mangin JF, Poupon C, Clark CA, Pappata S, Molko N, Chabriat H (2001). Diffusion tensor imaging: concepts and applications. J Magn Reson Imaging 13:534-546.

Li Y, Jiang N, Powers C, Chopp M (1998). Neuronal damage and plasticity identified by microtubule-associated protein 2, growth-associated protein 43, and cyclin D1 immunoreactivity after focal cerebral ischemia in rats. Stroke 29:1972-1980; discussion 1980-1971.

Lin SP, Schmidt RE, McKinstry RC, Ackerman JJ, Neil JJ (2002a). Investigation of mechanisms underlying transient T2 normalization in longitudinal studies of ischemic stroke. J Magn Reson Imaging 15:130-136.

Lin TN, Sun SW, Cheung WM, Li F, Chang C (2002b). Dynamic changes in cerebral blood flow and angiogenesis after transient focal cerebral ischemia in rats. Evaluation with serial magnetic resonance imaging. Stroke 33:2985-2991.

Liu Y, D'Arceuil HE, Westmoreland S, He J, Duggan M, Gonzalez RG, Pryor J, de Crespigny AJ (2007). Serial diffusion tensor MRI after transient and permanent cerebral ischemia in nonhuman primates. Stroke 38:138-145.

Longa EZ, Weinstein PR, Carlson S, Cummins R (1989). Reversible middle cerebral artery occlusion without craniectomy in rats. Stroke 20:84-91.

Neumann-Haefelin T, Kastrup A, de Crespigny A, Yenari MA, Ringer T, Sun GH, Moseley ME (2000). Serial MRI after transient focal cerebral ischemia in rats: dynamics of tissue injury, blood-brain barrier damage, and edema formation. Stroke 31:1965-1972; discussion 1972-1963.

Nudo RJ (1999). Recovery after damage to motor cortical areas. Curr Opin Neurobiol 9: 740-747.

Paxinos G, Watson C (2005). The rat brain in stereotaxic coordinates, 5 Edition: San Diego: Academic Press.

Pierpaoli C, Basser PJ (1996). Toward a quantitative assessment of diffusion anisotropy. Magn Reson Med 36:893-906.

Press WH, Vetterling WT (1992). Numerical recipes in FORTRAN : the art of scientific computing, 2nd Edition. Cambridge, England: Cambridge University Press.

Schwartz ED, Duda J, Shumsky JS, Cooper ET, Gee J (2005). Spinal cord diffusion tensor imaging and fiber tracking can identify white matter tract disruption and glial scar orientation following lateral funiculotomy. J Neurotrauma 22:1388-1398.

Sotak CH (2002). The role of diffusion tensor imaging in the evaluation of ischemic brain injury - a review. NMR Biomed 15:561-569.

Tanaka K, Nogawa S, Suzuki S, Dembo T, Kosakai A (2003). Upregulation of oligodendrocyte progenitor cells associated with restoration of mature oligodendrocytes and myelination in peri-infarct area in the rat brain. Brain Res 989:172-179.

van Bruggen N, Roberts TP, Cremer JE (1994). The application of magnetic resonance

imaging to the study of experimental cerebral ischaemia. Cerebrovasc Brain Metab Rev 6:180-210.

van der Zijden JP, Wu O, van der Toorn A, Roeling TP, Bleys RL, Dijkhuizen RM (2007). Changes in neuronal connectivity after stroke in rats as studied by serial manganese-enhanced MRI. Neuroimage 34:1650-1657.

van der Zijden JP, Bouts MJ, Wu O, Roeling TA, Bleys RL, van der Toorn A, Dijkhuizen RM (2008). Manganese-enhanced MRI of brain plasticity in relation to functional recovery after experimental stroke. J Cereb Blood Flow Metab 8: 832-840.

Virley D, Beech JS, Smart SC, Williams SC, Hodges H, Hunter AJ (2000). A temporal MRI assessment of neuropathology after transient middle cerebral artery occlusion in the rat: correlations with behavior. J Cereb Blood Flow Metab 20:563-582.

Wang C, Stebbins GT, Nyenhuis DL, deToledo-Morrell L, Freels S, Gencheva E, Pedelty L, Sripathirathan K, Moseley ME, Turner DA, Gabrieli JD, Gorelick PB (2006). Longitudinal changes in white matter following ischemic stroke: a three-year follow-up study. Neurobiol Aging 27:1827-1833.

Wegener S, Weber R, Ramos-Cabrer P, Uhlenkueken U, Sprenger C, Wiedermann D, Villringer A, Hoehn M (2006). Temporal profile of T2-weighted MRI distinguishes between pannecrosis and selective neuronal death after transient focal cerebral ischemia in the rat. J Cereb Blood Flow Metab 26:38-47.

Witte OW, Bidmon HJ, Schiene K, Redecker C, Hagemann G (2000). Functional differentiation of multiple perilesional zones after focal cerebral ischemia. J Cereb Blood Flow Metab 20:1149-1165.

Chapter 5 $^{1}H/^{13}C$ MR Spectroscopic Imaging of Regionally Specific Metabolic Alterations after Experimental Stroke

[1]Jet P. van der Zijden, [2]Pieter van Eijsden, [3]Robin A. de Graaf, [1]Rick M. Dijkhuizen

[1]Image Sciences Institute, University Medical Center Utrecht, Utrecht, The Netherlands
[2]Rudolf Magnus Institute of Neuroscience, Department of Neurosurgery, University Medical Center Utrecht, Utrecht, The Netherlands
[3]Magnetic Resonance Research Center, Yale University School of Medicine, New Haven, CT, USA

Submitted for publication

5 $^{1}H/^{13}C$ MR Spectroscopic Imaging of Regionally Specific Metabolic Alterations after Experimental Stroke

Abstract

Loss of function and subsequent spontaneous recovery after ischemic stroke are associated with functional and structural alterations in brain tissue. Acute functional tissue damage involves distortion of key metabolic processes, such as oxidative glycolysis and neurotransmitter metabolism. Nevertheless, initially perturbed metabolism may be restored at later stages, e.g. in perilesional areas, which could play a key role in post-stroke recovery of brain function. The pattern of metabolic recovery in relation to ischemic tissue damage, however, is basically unknown. The goal of our study was to reveal changes in glycolysis and glutamatergic neurotransmitter metabolism that could underlie post-stroke changes in functional status.

We performed *in vivo* $^{1}H/^{13}C$ magnetic resonance spectroscopic imaging (MRSI) during ^{13}C-labeled glucose infusion, and MRI, at 24 h (n = 6) and 3 weeks (n = 8) after stroke in a rat model to characterize alterations in baseline metabolite levels, glutamate (Glu) and glutamine (Gln) turnover, and active lactate (Lac) formation in areas with different degrees of ischemic injury.

Inside the lesion, we detected significant reductions in baseline metabolite levels, ongoing Lac formation, and seriously diminished Glu and Gln turnover at both time points, indicative of irreversible functional tissue damage. In perilesional areas, significant decrease of *N*-acetyl aspartate (NAA) levels, and Glu and Gln turnover indicated neuronal dysfunction at 24 h. After 3 weeks, when animals showed significant neurological improvement, anaerobic glycolysis had ceased, NAA levels were normalized, Glu turnover was maintained and Gln turnover had recovered. These findings point out that early metabolic impairment in the lesion borderzone can be restored over time. Alterations in brain metabolism in perilesional areas probably contribute significantly to changes in functional status in stroke subjects, and may provide a gateway for therapeutic strategies directed at improvement of functional recovery after stroke.

Introduction

Stroke is the main cause of disability in the Western society. Stroke patients exhibit acute loss of function as a result of neuronal damage, but their functional status can spontaneously recover to at least some extent over time. Acutely after stroke, the ischemic core is surrounded by an area of affected but potentially viable tissue; the penumbra. Without therapeutic intervention, the penumbra will go into infarction within the first hours after stroke. After the disappearance of the penumbra, later functional recovery must be related to other processes, e.g. brain plasticity. With use of neuroimaging techniques, we and others have demonstrated that initially affected perilesional brain areas can later on regain neuronal function (Dijkhuizen et al., 2001; Dijkhuizen et al., 2003; Tombari et al., 2004; Jaillard et al., 2005; Weber et al., 2008), which may be associated with remodeling of structural connections (Keyvani and Schallert, 2002; Carmichael, 2003; Nudo, 2006; van der Zijden et al., 2008). Such brain reorganization is believed to be key to functional recovery after stroke.

Changes in neuronal and glial metabolism may play a fundamental role in post-stroke loss and recovery of brain function. Ischemia causes distortion of key metabolic processes in the brain, i.e. glucose oxidation and glutamate (Glu)-glutamine (Gln) cycling between neurons and astrocytes (Haberg et al., 1998; Pascual et al., 1998; Haberg et al., 2001; Haberg et al., 2006; Thoren et al., 2006), but it is unknown how metabolic activity recovers in relation to restoration of function. It is well conceivable that adaptations in glucose metabolism and glutamatergic neurotransmission underlie structural and functional plasticity in tissue recovering from stroke.

MR spectroscopy (MRS) provides an ideal tool for non-invasive assessment of *in vivo* brain metabolism. It enables detection of baseline metabolite levels as well as measurement of active metabolic pathways in humans and animal models (Novotny et al., 2003; Choi et al., 2007). Longitudinal *in vivo* ^{1}H MRS can detect changes in levels of NAA, a neuronal marker, and lactate, the endproduct of anaerobic glycolysis (Igarashi et al., 2001). This provides insights into the metabolic status of tissue affected by cerebral ischemia. Alternatively, ^{13}C-based MRS methods allow measurement of actively formed ^{13}C-labeled metabolic products after infusion of ^{13}C-labeled glucose (for review see de Graaf et al. (2003b)). With *in vivo* ^{1}H-observed, ^{13}C-edited (^{1}H/^{13}C) MRS during intravenous infusion of ^{13}C-labeled glucose we have previously shown that penumbral tissue may be distinguished from the lesion core based on dynamics in lactate formation after acute experimental focal cerebral ischemia (Dijkhuizen et al., 1999). *Ex vivo* ^{13}C MRS studies have demonstrated that changes in neuronal and glial metabolism can be detected from altered Glu and Gln synthesis after acute focal cerebral ischemia in rats (Haberg et al., 1998; Pascual et al., 1998; Haberg et al., 2001; Haberg et al., 2006). Haberg et al. (2001, 2006) showed that preserved astrocytic metabolism in the first 4 h after cerebral ischemia differentiates the potentially salvageable penumbra zone from the irreversibly damaged lesion core.

The goal of the present study was to characterize alterations in neuronal

and glial metabolism in and around an ischemic lesion in order to elucidate changes in functional tissue status after stroke. To this aim we applied *in vivo* $^{1}H/^{13}C$ MRS imaging (MRSI) at ultrahigh magnetic field strength to assess regionally specific alterations in glucose metabolism and glutamatergic neurotransmission, at semi-acute and chronic stages after experimental stroke. We hypothesized that temporary functional deficit of morphologically intact tissue at the border of an ischemic lesion is reflected in transient dysfunction of neuronal and glial metabolism.

Materials and Methods

Animal Preparation

Animals were studied in accordance with the guidelines established by the Yale Animal Care and Use Committee.

Fourteen male Wistar rats (200-250g) were anesthetized with 1.2% halothane in N_2O/O_2 (70:30) under spontaneous respiration. Blood oxygen saturation and heart rate were continuously monitored during surgical procedures. Body temperature was maintained at 37.0 ± 0.5 °C by means of a heating pad. Additional analgesia was provided by a pre-emptive subcutaneous injection of 1.0 mg/kg Meloxicam (Metacam TM, Sigma Aldrich, St. Louis, MO, USA).

Transient focal cerebral ischemia was induced by 90-min occlusion of the right middle cerebral artery (MCA) with an intraluminal filament (Longa et al., 1989). In brief, a 4.0 silicon-coated polypropylene suture (Ethicon, Piscataway, NJ, USA) was introduced into the right external carotid artery and advanced through the internal carotid artery until a slight resistance was felt, indicating that the MCA was occluded. After 90 minutes, the filament was withdrawn from the internal carotid artery to allow reperfusion. After surgery, rats received a subcutaneous injection of 5 ml saline to compensate for loss of water and minerals. Post-operative analgesia was provided through Meloxicam (1 mg/kg/day) in drinking water up to 48 h after stroke induction.

Animals were fasted for 12-16 h before MR experiments. At 24 h (24h group; n = 6) or 3 weeks (3w group; n = 8) after stroke induction, rats were anesthetized, tracheotomized and mechanically ventilated with 1.5% halothane in N_2O/O_2 (70:30). A femoral artery was cannulated for monitoring of blood gases (arterial pO_2 and pCO_2), pH and blood pressure. Physiological parameters were maintained within normal limits (pCO_2: 33-45 mmHg; pO_2: > 120 mmHg; pH: 7.32-7.57; blood pressure: 90-110 mmHg). Left and right femoral veins were cannulated for infusion of [U-^{13}C]glucose (Cambridge Isotope Laboratories Inc., Andover, MA, USA) and for injection of the intravascular iron oxide contrast agent ferumoxtran-10 (Combidex, Advanced Magnetics, Cambridge, MA, USA). During MR experiments, anesthesia was maintained with 0.3-0.8% halothane in N_2O/O_2 (70:30). Rats were restrained using a head-holder and additional immobilization was

achieved by i.v. injections of D-tubocurarine chloride (0.25 mg/kg every 60 min). Body temperature was measured with a rectal thermosensor and maintained at 37.0 ± 0.5 °C by means of a heating pad. Rats were infused with [U-^{13}C]glucose for 140 minutes according to a protocol previously described (de Graaf et al., 2003a). Blood samples were taken before and every 35 minutes after infusion to quantify ^{13}C fractional enrichment of plasma glucose.

Functional examination

Animals were subjected to two behavioural tests to assess sensorimotor function. First, we applied a series of motor, sensory and tactile tests, which provided a neurological score of 0 to 20 points, with 20 as maximal deficit score (van der Zijden et al., 2008). Second, an adhesive removal test was performed (Schallert et al., 2000). A small circular sticky tape was attached to the distal-radial region of the wrist of either the left or right forelimb, and the sticky tape removal time was measured for each forelimb with a maximally allowed removal time of 60 seconds. Behavioural examination was performed on days 0, 4, 7, 10, 14 and 21 after stroke.

MR acquisition and processing

In vivo MR experiments were performed on an 11.74 T magnet (Magnex Scientific, Oxford, UK) equipped with a 9-cm diameter gradient-set (395 mT/m in 180 μs, Magnex Scientific, Oxford, UK) interfaced to a Bruker Avance console (Bruker, Ettlingen, Germany). Radiofrequency pulse transmission and MR signal detection for ^{1}H (499.814 MHz) were performed with a 14-mm-diameter single-turn surface coil. Radiofrequency pulse transmission on ^{13}C (125.7 MHz) was achieved with two orthogonal 21-mm diameter surface coils driven in quadrature.

T_2-weighted MRI Before MRS experiments, we performed multi-echo, multi-slice T_2-weighted echo planar imaging (EPI) of 9 slices covering the spectroscopic volume (repetition time (TR)/echo time (TE) spacing = 2500/25 ms; echo train length = 8; acquisition matrix = 64 x 64; voxel resolution = 0.3 x 0.3 x 1.0 mm^3).

Quantitative T_2 maps were calculated on a voxel-wise basis by weighted linear least-squares-fit of the logarithm of the signal intensity at different echo times versus TE.

$^{1}H/^{13}C$ MRS Spatial localization of a 10 x 2 x 5 mm^3 volume was achieved with LASER (Garwood and DelaBarre, 2001) using TR/TE = 2500/14 ms. The volume encompassed the ipsilateral as well as the contralateral cortex (see Figure 1). 1D MRSI data were obtained by applying a phase-encoding gradient in the x-direction (16 steps over a 16–mm field-of-view), resulting in a 10 μl nominal voxel size. The magnetic field homogeneity was optimized using

MRI-based B_0 mapping (Koch et al., 2006) and resulted in water linewidths of 16-20 Hz over the localized volume.

^{1}H and $^{1}H/^{13}C$ MR spectra were obtained during infusion of U-^{13}C-labeled glucose by applying a ^{13}C inversion pulse on alternate scans (de Graaf et al., 2003a) and by calculating the difference post-acquisition. With 8 averages per phase-encoding increment, the total duration of one $^{1}H/^{13}C$ MRSI scan was circa 11 minutes. Water suppression was achieved with the sequence for water suppression with adiabatic-modulated pulses (SWAMP), an adiabatic analogue of the conventional chemical shift-selective (CHESS) water suppression (de Graaf and Nicolay, 1998).

Perfusion MRI Perfusion MRI was conducted to confirm blood supply to the brain during infusion of ^{13}C-labeled glucose. Immediately following ^{1}H /^{13}C MRS experiments, we performed single-slice dynamic susceptibility contrast-enhanced MRI using single-shot gradient recalled echo planar imaging (EPI) in combination with injection of the intravascular contrast agent Combidex (10-30 mg/kg Fe in 10 mg/ml) (TR/TE = 250/14 ms; data matrix = 64 x 64; voxel resolution = 0.3 x 0.3 x 2.0 mm^3; number of acquisitions = 180-300). The slice position was adjusted according to the selected MRSI volume. Relative cerebral blood volume (CBV) values were determined from the intravascular contrast-induced change in transverse relaxation rate, ΔR_2^* (Hamberg et al., 1996).

Data analysis

Ischemic lesion area Brain tissue with significantly prolonged T_2 after stroke correlates with infarcted tissue (Palmer et al., 2001; Peeling et al., 2001). Therefore the ischemic lesion was defined as the ipsilateral area where T_2 > mean T_2 + 2 SD in contralateral tissue.

Metabolite concentrations MR spectra were used for quantification of metabolite concentrations and ^{13}C fractional enrichments (FE) using the LCModel algorithm (Provencher, 1993). In short, the LCModel algorithm models the *in vivo* MR spectrum as a superposition of a basis set *in vitro* MR spectra of pure metabolite solutions. To complete the spectral basis set for LCModel fitting, the macromolecular baseline was determined from a measurement on a healthy rat (Behar and Ogino, 1993). MRS signals from lipids have been shown to significantly increase after ischemic brain injury (Gasparovic et al., 2001). Therefore, three macromolecular signals observed at ~0.8, ~1.3 and ~2.7 ppm in ischemic areas were added to the model. Total metabolite concentrations were determined from individual ^{1}H-^{13}C MR spectra prior to infusion of [U-^{13}C]glucose assuming the concentration of total creatine, as an internal standard, to be 10 mM (Pfeuffer et al., 1999). In the lesion at 24 h and 3 weeks, and in the lesion borderzone at 3 weeks, the concentration of total creatine was significantly reduced and the internal concentration standard total creatine of the contralateral homologues VOI was used for metabolite quantification. The ^{1}H surface coil's B_1 profile did not show consistent dif-

ferences between the left and right side. Furthermore, equivalent B_1 fields in ipsi- and contralateral homologues regions were ascertained by positioning the coil symmetrically over the brain midline, parallel to the selected MRSI column.

Metabolite turnover To determine the kinetics of [4-^{13}C]Glu and [4-^{13}C]Gln enrichment, as well as [3-^{13}C]Lac formation, individual spectra from animals at 24 h (n = 6) or 3 weeks post-stroke (n = 8) were added for each volume-of-interest (VOI) and time-point, and fitted with LCModel. Subsequently, the metabolite turnover time-courses were fitted with a one-phase exponential: $y = y_{max}(1\text{-}\exp(-kx))$, where x is time after onset of [U-^{13}C]glucose infusion; y is FE (of [4-^{13}C]Glu or [4-^{13}C]Gln) or concentration (of [3-^{13}C]Lac); y_{max} is steady state FE or concentration, and k is the turnover rate constant. Because Gln synthesis is limited by Glu supply, FE of [4-^{13}C]Gln is unlikely to exceed FE of [4-^{13}C]Glu. Therefore, y_{max} was thresholded at the calculated steady state FE of [4-^{13}C]Glu for fitting of the [4-^{13}C]Gln turnover time-courses.

Region-of-interest analysis MRI and MRSI data were analyzed in different VOIs that incorporated distinct tissue conditions based on the extent of the lesion. The 16 MRSI voxels were overlaid on the corresponding T_2 maps. Circa 8 voxels fell within the brain volume and could be used for further analysis. Voxels that included tissue outside the brain were discarded. VOIs included: i) the ipsilateral lesion area (T_2 > mean contralateral T_2 + 2SD) (IL_{lesion}), ii) the ipsilateral lesion borderzone (MRSI voxel adjacent to T_2-lesion area) (IL_{border}), and iii) ipsilateral non-ischemic tissue (MRSI voxel(s) with normal T_2 values, adjacent to lesion borderzone voxel) (IL_{normal}). Depending on the lesion size, VOIs consisted of 1-3 MRSI voxels. MR spectra of voxels within the same VOI were added for further analysis. Contralateral counterparts served as control VOIs (CL_{lesion}, CL_{border} and CL_{normal}). Figure 1 shows location of the VOIs with respect to the T_2-lesion area.

Statistics All values are expressed as mean ± SD. The error of the LCModel fitting was calculated for each metabolite MR signal by Monte Carlo Simulation with 13 iterations. Differences in functional status were analyzed with a one-way repeated measures analysis-of-variance (ANOVA) with post-hoc multiple comparison *t*-testing with Bonferroni correction. Differences between ipsi- and contralateral FE (for [4-^{13}C]Glu and [4-^{13}C]Gln) and concentration (for [3-^{13}C]Lac) at the latest time-point were analyzed using a one-way repeated measures ANOVA followed by a Student-Newman-Keuls test. Differences between VOIs were analyzed using a one-way ANOVA with post-hoc multiple comparison *t*-testing with Bonferroni correction. $P < 0.05$ was considered significant.

Results

Neurological status

All rats demonstrated substantial functional deficits at day 4 after stroke (neurological score: 7.3 ± 1.3 (vs. 0.1 ± 0.4 at day 0; $P < 0.05$); adhesive removal time: 56.0 ± 7.5 s (vs. 7.4 ± 6.3 s at day 0; $P < 0.05$), which significantly improved towards day 21 after stroke (neurological score: 5.1 ± 1.3; adhesive removal time: 22.5 ± 13.6 s) ($P < 0.05$ vs. day 4).

Ischemic lesion area

Unilateral ischemic lesions were characterized by a significant increase in T_2 and were included in part of the MRSI column, e.g. the affected somatosensory cortex (Figure 1). T_2 values in the different VOIs are shown in Table 1. T_2 was significantly prolonged in the lesion as compared to contralateral. In the lesion borderzone and in non-ischemic ipsilateral tissue, T_2 values were not significantly different from contralateral values. The coordinates of the lesion borderzone VOI were not significantly different between the 24h (2.2 ± 0.4 mm lateral from midline) and 3w groups (2.5 ± 0.9 mm lateral from midline).

Relative CBV values (% of contralateral) in the lesion and borderzone VOIs were 126 ± 37% and 139 ± 53%, respectively, at 24 h, and 86 ± 56% and 68 ± 25%, respectively, at 3 weeks post-stroke. For all VOIs, there were no significant differences in relative CBV values between the 24h and 3w groups.

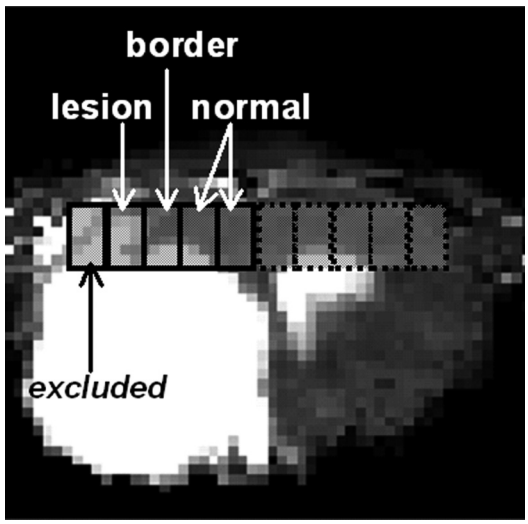

Figure 1

MRSI column displaying volumes-of-interest (ipsilateral lesion (lesion); ipsilateral lesion borderzone (border); ipsilateral nonischemic tissue (normal); and their contralateral counterparts) overlaid on an average T_2 map of five adjacent brain MRI slices (corresponding with the coverage of the MRSI volume) at 3 weeks after stroke. The lesion is characterized by a prolonged T_2. Note that voxels outside the lesion, particularly in the borderzone, include part of the lateral ventricle, which was largely equal in size and signal intensity between ipsi- and contralateral voxels.

Table 1	T_2 ± SD (ms) in ipsi- (IL) and contralateral (CL) VOIs at 24 h (24h) and 3 weeks (3w) after stroke. *P < 0.05 as compared to contralateral. Note that T_2 values in the borderzone (IL and CL) are elevated due to partial inclusion of ventricles.					
	Normal		*Borderzone*		*Lesion*	
	IL	*CL*	*IL*	*CL*	*IL*	*CL*
24h	36.9 ± 4.1	39.7 ± 5.5	45.2 ± 8.2	46.5 ± 8.7	55.1 ± 2.9*	40.6 ± 5.0
3w	47.1 ± 3.7	45.6 ± 3.9	53.6 ± 3.3	49.9 ± 5.0	80.0 ± 8.1*	44.0 ± 3.8

Metabolic alterations

Total metabolite concentrations. MRS data quality, accuracy of LCModel fitting and the severity of stroke-induced metabolic changes are demonstrated in Figure 2, which shows representative measured and fitted ^{1}H MR spectra obtained from a healthy brain region (CL_{normal} at 24 h post-stroke; Figure 2A) and from a lesioned area at 3 weeks after stroke (IL_{lesion}; Figure 2B). Most of the metabolite signals, except for the lactate/lipids (Lac/Lip) and lipids peaks at ~1.3 and ~0.8 ppm, respectively, were clearly diminished inside the lesion.

Total concentrations of metabolites as calculated with the LCModel algorithm, are presented in Table 2. The last column in Table 2 presents the uncertainties of a typical fit of a ^{1}H MR spectrum from a non-ischemic VOI as determined by a Monte Carlo simulation with 100 iterations. Only metabolites fitted with uncertainties <15% were included in our analysis. At 24 h after stroke, we found significant reductions in the concentration of Gln, choline (Cho) and N-acetyl aspartate (NAA), and an increase in Lac/Lip signal in IL_{lesion}. Cho and NAA levels were significantly reduced in IL_{border}, while Gln levels were increased in this area. A decrease in Cho signal was detected in IL_{normal}.

At 3 weeks after stroke, Glu, Gln, and NAA levels were significantly decreased, and Lac/Lip was still increased in IL_{lesion}. In IL_{border}, Glu was decreased and Lac/Lip was increased. There were no significant changes in IL_{normal}. At both time-points we found no changes in myo-inositol (Ins) and taurine (Tau) concentrations in any of the VOIs.

Table 2 **Total metabolite concentrations (mean ± SD (mmol/l)) in ipsi- and contralateral VOIs at 24 h (24h) and 3 weeks (3w) after unilateral stroke. *P < 0.05 as compared to contralateral. The last column represents the error (%) of a typical fit of a MR spectrum from CL_{normal} calculated by Monte Carlo Simulation.**

		Normal		*Borderzone*		*Lesion*		*Uncertainty (%)*
		IL	*CL*	*IL*	*CL*	*IL*	*CL*	
Cho	24h	6.5±0.8*	9.3±1.3	8.0±2.2*	10.7±1.3	4.5±1.6*	8.1±0.9	9.0
	3w	7.2±1.7	7.8±3.2	9.0±4.1	8.1±3.2	5.2±2.7	6.6±1.8	
Gln	24h	3.9±1.0	3.8±1.1	5.1±0.6*	3.6±1.2	1.1±0.9*	3.8±0.5	7.7
	3w	4.8±0.8	4.2±0.7	4.5±1.0	4.5±1.0	3.0±1.0*	4.7±1.3	
Glu	24h	9.2±1.2	9.0±0.5	10.2±2.4	8.6±1.8	8.7±2.5	8.7±1.0	4.2
	3w	8.7±1.0	8.6±1.0	5.7±1.7*	8.3±1.3	1.7±1.0*	8.0±1.0	
Ins	24h	7.0±0.4	7.7±1.0	7.9±1.3	8.3±0.6	7.5±2.4	7.7±1.1	1.3
	3w	11.0±1.0	9.1±0.8	12.3±1.0	10.4±1.1	8.3±2.0	9.2±1.2	
Lac/ Lip	24h	3.0±1.5	2.2±0.8	7.7±4.0*	1.8±0.7	13.1±2.8*	0.8±0.2	12.0
	3w	2.4±0.7	1.0±0.5	14.5±9.8*	2.6±2.5	26.4±14.0*	1.5±0.6	
NAA	24h	8.9±1.1	10.3±0.5	7.4±1.0*	10.3±0.7	3.9±1.0*	10.9±0.9	5.8
	3w	10.5±2.1	10.8±1.4	9.2±1.1	10.0±1.1	5.6±1.5*	11.5±0.9	
Tau	24h	7.9±0.5	7.7±0.9	9.2±1.0	8.2±0.6	8.2±3.1	8.0±0.6	2.1
	3w	8.8±0.7	8.0±1.2	9.2±0.9	9.2±1.2	7.6±1.4	8.7±0.8	

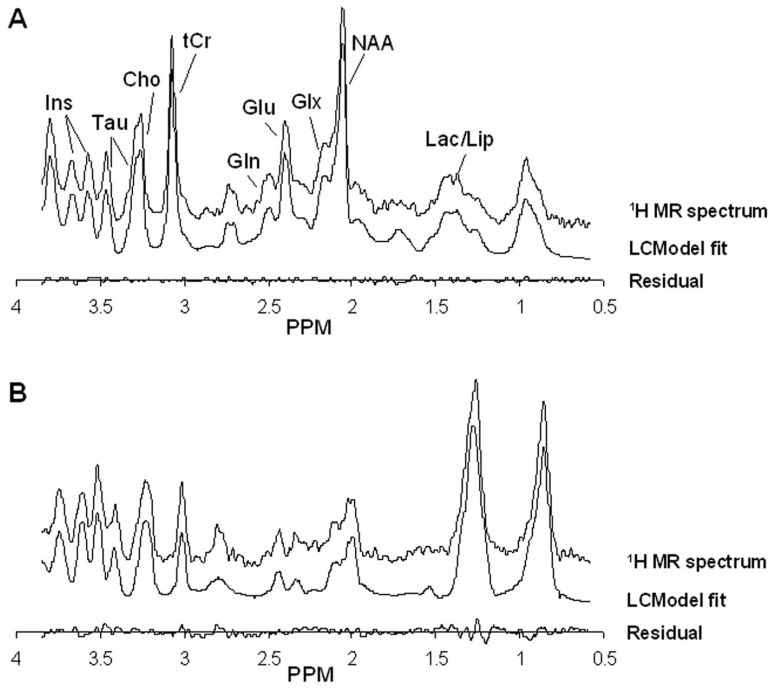

Figure 2

Measured and fitted ^{1}H MR spectra from CL_{normal} at 24 h (A) and IL_{lesion} (B) at 3 weeks after stroke. The residual signal is the difference between the experimentally measured and LCModel fitted spectra. Cho: choline; tCr: total creatine; Glu: glutamate; Gln: glutamine; Glx: glutamate + glutamine; Ins: inositol; Lac/Lip: lactate + lipids; NAA: N-acetyl aspartate; Tau: taurine.

Dynamic metabolite formation Figure 3 shows localized ^{1}H/^{13}C MR spectra from the different VOIs obtained at 132 ± 2 minutes after onset of infusion of [U-^{13}C]glucose at 24 h and 3 weeks after stroke. Excellent sensitivity and optimal spectral resolution of the ^{1}H/^{13}C MR spectra allowed separate detection of [4-^{13}C]Glu and [4-^{13}C]Gln signals. Clearly, Glu and Gln formation were equal in IL_{normal} and CL_{normal}. Inside the lesion, Glu and Gln signals were considerably reduced, particularly at 3 weeks after stroke. In IL_{border}, formation of Glu and Gln was moderately decreased as compared to contralateral at 24 h post-stroke, but the [4-^{13}C]Gln signal was normalized after 3 weeks. [3-^{13}C]Lac formation was evident in IL_{lesion} and IL_{border} after 24 h, which largely diminished after 3 weeks.

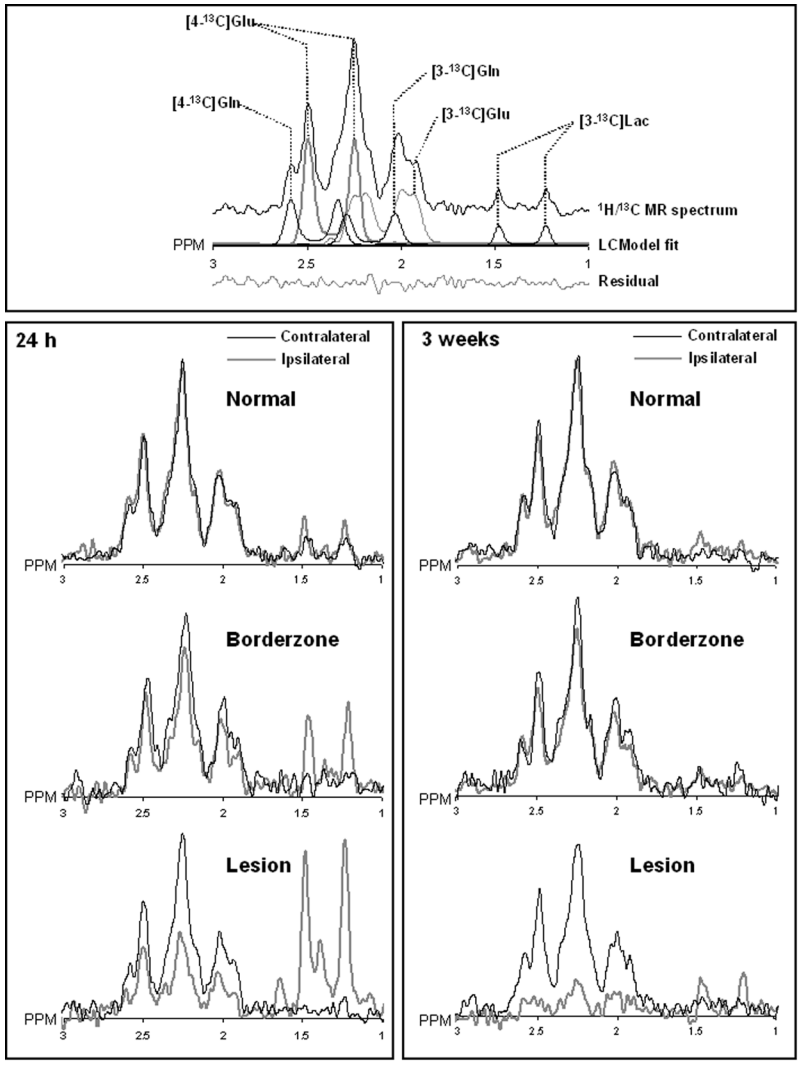

Figure 3

Top: Measured and calculated $^{1}H/^{13}C$ MR spectra obtained by adding all $^{1}H/^{13}C$ MR spectra from all contralateral VOIs at 24 h after stroke. The residual signal is the difference between the calculated and measured spectra. Below; $^{1}H/^{13}C$ MR spectra from the ipsilateral lesion area, lesion borderzone and non-ischemic tissue, and their contralateral counterparts at 24 h (left) and 3 weeks after stroke (right). Spectra are the sum of individual spectra acquired at the last time-point, i.e. 132 ± 2 min after onset of [U-^{13}C]glucose infusion. Note that all resonances appear as doublet signals due to the absence of broadband heteronuclear decoupling.

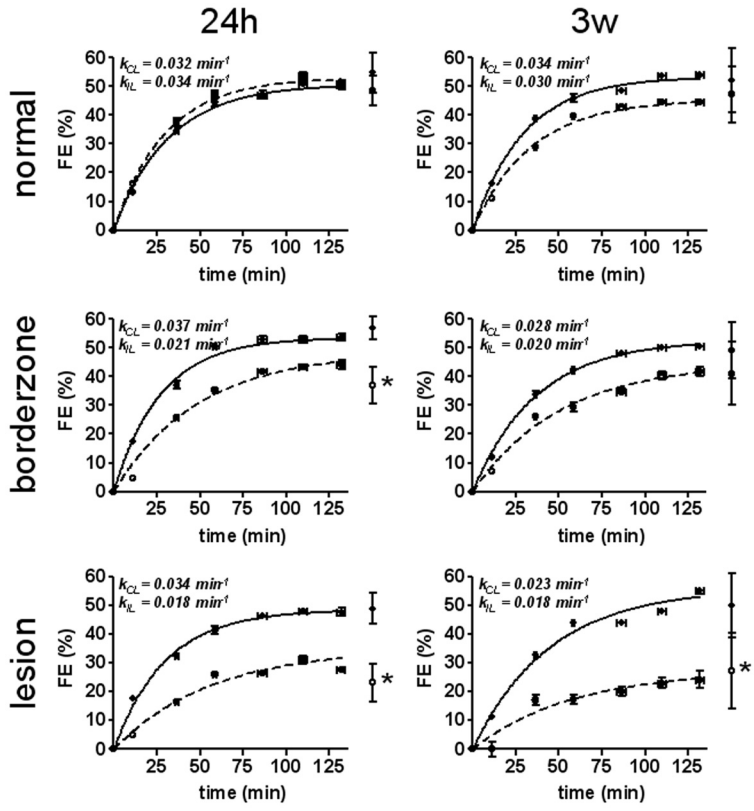

Figure 4

[4-^{13}C]glutamate turnover curves for contra- (closed circles; —) and ipsilateral (open circles; - - -) VOIs (top: normal; middle: borderzone; bottom: lesion) at 24 h (left) and 3 weeks after stroke (right). Curves were obtained using a single-exponential fitting procedure based on data from group-wise summed spectra. Turnover rate constants for the ipsi- (k_{IL}) and contralateral VOIs (k_{CL}) are displayed in the graphs. Data points at the right of the graphs represent FE at the latest time-point as calculated from individual spectra (mean ± SD). *P < 0.05 as compared to contralateral.

FE time-courses and rate constants for Glu and Gln for all VOIs, calculated from group-wise summed spectra, are shown in Figure 4 and 5, respectively. Both for Glu and Gln, turnover curves were comparable in IL_{normal} and CL_{normal} at both time-points. At 24 h after stroke, FE of Glu and Gln at the latest time-point ($FE_{t[max]}$) were significantly reduced in IL_{lesion} and IL_{border} as compared to their contralateral counterparts. Turnover rate constants (k) for Glu and Gln were also clearly decreased in these areas. After 3 weeks, $FE_{t[max]}$ of Glu and Gln was still significantly reduced in IL_{lesion}, but not in IL_{border}. For Glu, k remained decreased in both these VOIs after 3 weeks. However, k of Gln had recovered in IL_{border} at this time-point.

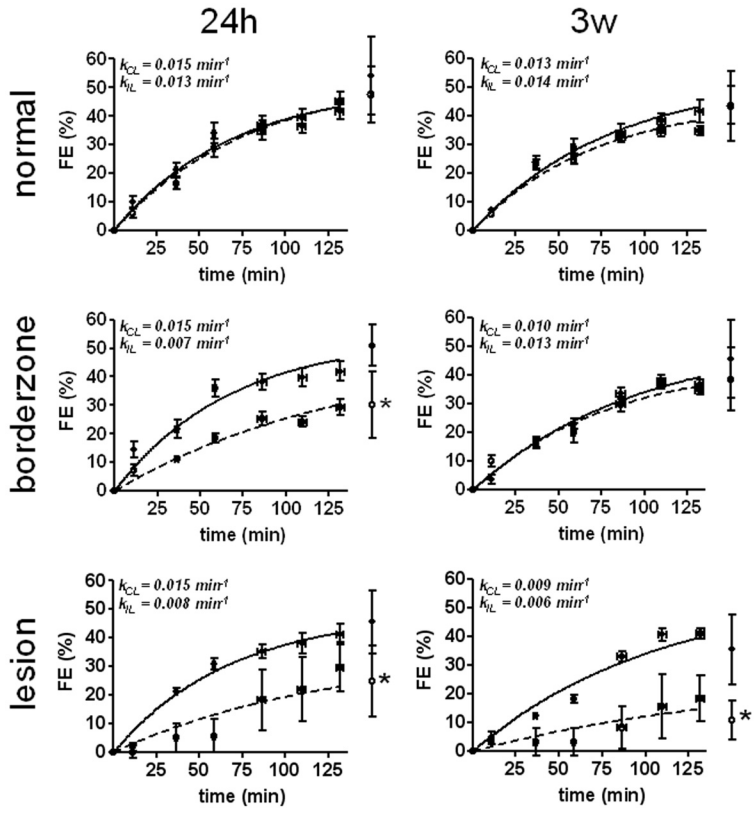

Figure 5

[4-^{13}C]glutamine turnover curves for contra- (closed circles; —) and ipsilateral (open circles; - - -) VOIs (top: normal; middle: borderzone; bottom: lesion) at 24 h (left) and 3 weeks after stroke (right). Curves were obtained using a single-exponential fitting procedure based on data from group-wise summed spectra. Turnover rate constants for the ipsi- (k_{IL}) and contralateral VOIs (k_{CL}) are displayed in the graphs. Data points at the right of the graphs represent FE at the latest time-point as calculated from individual spectra (mean ± SD). *P < 0.05 as compared to contralateral.

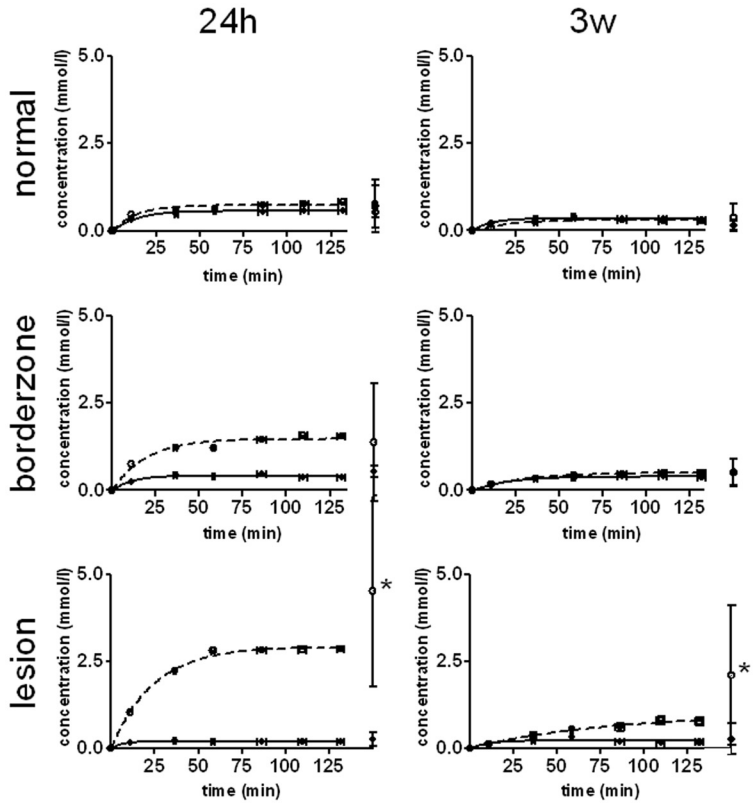

Figure 6

[3-^{13}C]lactate turnover curves for contra- (closed circles; —) and ipsilateral (open circles; - - -) VOIs (top: normal; middle: borderzone; bottom: lesion) at 24 h (left) and 3 weeks after stroke (right). Curves were obtained using a single-exponential fitting procedure based on data from group-wise summed spectra. Data points at the right of the graphs represent concentration at the latest time-point as calculated from individual spectra (mean ± SD). *P < 0.05 as compared to contralateral.

Time courses of [3-^{13}C]Lac formation are shown in Figure 6. Clear Lac turnover was detected in IL_{lesion} and Il_{border} at 24 h after stroke, which was still existing after 3 weeks in IL_{lesion}, but not in IL_{border}.

Discussion

In this study we combined ultrahigh-field *in vivo* $^{1}H/^{13}C$ MRSI and MRI to characterize changes in glucose metabolism and glutamatergic neurotransmission in relation to brain tissue status and functional recovery after experimental stroke. Baseline metabolite concentrations, and dynamic forma-

tion of Glu, Gln and Lac were measured in lesional, perilesional and unaffected brain areas at 24 h and 3 weeks post-stroke. Our main finding is that (semi-)acutely impaired brain metabolism in perilesional tissue recovers at chronic stages, which may play a fundamental role in retrieval of neuronal function after early stroke-induced dysfunction. Below we describe differences in brain tissue condition after cerebral ischemia and discuss how changes in neuronal and glial metabolism may account for functional loss and subsequent recovery.

Ischemic lesion Transient unilateral MCA occlusion resulted in a lesion with highly prolonged T_2 and marked decrease in NAA, indicative of severe neuronal injury. Concentrations of most other detectable metabolites were also significantly reduced. Glu levels, on the other hand, were maintained at 24 h post-stroke. This may reflect its well-described increased extracellular release and/or reduced uptake after ischemia (see Nishizawa (2001) for a review), or its accumulation in glial cells where it is not further metabolized into Gln due to depressed glutamine synthetase (Ottersen et al., 1996). In accordance with the latter, Gln levels were significantly diminished. After 3 weeks, Glu levels were drastically reduced, consistent with severe neuronal death. Both at 24 h and 3 weeks Glu turnover was significantly diminished in the ischemic core reflective of strongly reduced glycolysis and tricarboxylic acid (TCA) activity in neuronal tissue. Importantly, reduced formation of glycolytic products could not be explained by lack of glucose supply since CBV was preserved in the lesion (and in other brain VOIs) at both timepoints.

Astrocytes play an important role in glutamatergic neurotransmission as these brain cells are responsible for the recycling of Glu. Extracellular Glu is taken up by specific transporters and subsequently converted into Gln by the enzyme glutamine synthetase through the Glu-Gln cycle. We detected reduced levels of Gln, along with diminished Gln enrichment and turnover rate at 24 h after stroke, which pointed toward astroglial injury. The partial recovery of Gln levels after 3 weeks may be explained by reactive astrocytosis, which typically arises in chronic, structurally damaged ischemic tissue (Petito et al., 1990). Yet, our data suggest that such proliferation of glial cells is not accompanied by enhanced Gln synthesis.

Lactate/lipid signals were highly elevated after 24 h and 3 weeks in the lesion area. Significant [3-^{13}C]Lac production, reflective of ongoing anaerobic glycolysis, was particularly evident after 24 h. Considerably reduced lactate formation from infused ^{13}C-glucose at 3 weeks after temporary ischemia in the largely necrotic lesion core, suggests that MRS-detectable lipids strongly contribute to the ^{1}H MR signals around 1.3 ppm, which is in agreement with Gasparovic et al. (2001) and Harada et al. (2007). High amount of lipids probably reflects accumulation of membrane degradation products inside infiltrated macrophages (Gasparovic et al., 2001).

Lesion borderzone It is not surprising that the above-described cerebral ischemic damage resulted in significant functional deficits. Nevertheless, de-

spite severe and irreversible tissue impairment in the ischemic lesion, all animals displayed considerable improvement of neurological function over time. This may be related to recovery of neuronal function, subsequent to initial deficiency, in brain tissue just outside the ischemic lesion core. At 24 h after stroke we detected clear signs of neuronal dysfunction in perilesional areas: NAA levels were lowered and Glu and Gln turnover were reduced. Nevertheless, the levels of reduction of fractional enrichment and turnover rate of [4-^{13}C]Glu were clearly less in the lesion borderzone as compared to the lesion core, suggestive of preserved oxidative glucose metabolism in surviving neurons. Furthermore, anaerobic glycolysis, evident from active [3-^{13}C]Lac formation, was considerably less than in the lesion core.

Gln formation and Cho levels were significantly reduced in the lesion borderzone after 24 h. However, Gln turnover was still ongoing and we detected elevated baseline Gln levels. This suggests that despite astroglial impairment, cells remained metabolically active. Previous studies in acute rat stroke models have provided evidence that preservation of astrocytic metabolism may be crucial for neuronal survival (Haberg et al., 2001; Thoren et al., 2005). Active neuronal-glial interaction is important for maintenance of brain homeostasis and critical changes in the metabolic coupling between these two compartments may directly affect neuronal viability after stroke (Liu et al., 1999).

After 3 weeks there were clear indications of substantial neuronal and glial recovery in the lesion borderzone. Futhermore, the absence of significant Lac production suggested normal oxidative glycolysis. At this time point NAA, Cho and Gln levels were normalized, Glu turnover was maintained, and Gln turnover had returned to control levels. The latter reflects recovery of the Glu-Gln neurotransmitter cycle between glutamatergic neurons and astroglia. Functional imaging studies in stroke patients and animal stroke models have reported reinstatement of neuronal activation responses in perilesional sensorimotor cortex, in association with spontaneous recovery of sensorimotor function (Dijkhuizen et al., 2001; Dijkhuizen and Nicolay, 2003; Tombari et al., 2004; Jaillard et al., 2005). For example, in the same rat model as used in the current study, Dijkhuizen et al. (2003) have observed that stimulus-induced brain activation in perilesional sensorimotor cortex is lost at 24 h after stroke, but returns after 2 weeks. Morphologically, this region may undergo structural plasticity, including sprouting of neurites and synaptogenesis (Keyvani and Schallert, 2002; Carmichael, 2003; Nudo, 2006). Our current data indicate that (semi-)acute functional 'silence' of perilesional tissue is related to deficiency of energy metabolism and Glu-Gln neurotransmitter cycling. More chronically, oxidative glycolysis normalizes and glutamatergic neurotransmission recovers, which is vital to reinstatement of neuronal function and may underlie subsequent behavioral recovery.

In conclusion, we have demonstrated that ^{1}H/^{13}C MRSI offers a fine tool to detect regionally specific impairment and recovery of neuronal and glial metabolism after stroke. To the best of our knowledge, this study is the first to show *in vivo* metabolic alterations in perilesional tissue that may explain

post-stroke loss and reinstatement of neuronal function. Future studies with this methodology may enable measurement of absolute metabolic fluxes and further improved regional confinement (de Graaf et al., 2004), as further improvements in MR acquisition methods, e.g. heteronuclear decoupling (de Graaf et al., 2003b), will allow detection of more metabolites with increased signal-to-noise ratio, thereby enabling analysis with advanced mathematical metabolic models (Mason and Rothman, 2004).

Acknowledgements

- This research was financially supported by fellowships from foundation 'De Drie Lichten' (JvdZ), the Netherlands Organisation for Scientific Research (JvdZ), and the Royal Netherlands Academy of Arts and Sciences (RD). We thank Bei Wang for excellent technical assistance.

References

Behar KL, Ogino T (1993). Characterization of macromolecule resonances in the 1H NMR spectrum of rat brain. Magn Reson Med 30:38-44.

Carmichael ST (2003). Plasticity of cortical projections after stroke. Neuroscientist 9:64-75.

Choi JK, Dedeoglu A, Jenkins BG (2007). Application of MRS to mouse models of neurodegenerative illness. NMR Biomed 20:216-237.

de Graaf RA, Nicolay K (1998). Adiabatic water suppression using frequency selective excitation. Magn Reson Med 40:690-696.

de Graaf RA, Brown PB, Mason GF, Rothman DL, Behar KL (2003a). Detection of [1,6-13C2]-glucose metabolism in rat brain by in vivo 1H-[13C]-NMR spectroscopy. Magn Reson Med 49:37-46.

de Graaf RA, Mason GF, Patel AB, Behar KL, Rothman DL (2003b). In vivo 1H-[13C]-NMR spectroscopy of cerebral metabolism. NMR Biomed 16:339-357.

de Graaf RA, Mason GF, Patel AB, Rothman DL, Behar KL (2004). Regional glucose metabolism and glutamatergic neurotransmission in rat brain in vivo. Proc Natl Acad Sci U S A 101:12700-12705.

Dijkhuizen RM, Nicolay K (2003). Magnetic resonance imaging in experimental models of brain disorders. J Cereb Blood Flow Metab 23:1383-1402.

Dijkhuizen RM, de Graaf RA, Garwood M, Tulleken KA, Nicolay K (1999). Spatial assessment of the dynamics of lactate formation in focal ischemic rat brain. J Cereb Blood Flow Metab 19:376-379.

Dijkhuizen RM, Ren J, Mandeville JB, Wu O, Ozdag FM, Moskowitz MA, Rosen BR, Finklestein SP (2001). Functional magnetic resonance imaging of reorganization in rat brain after stroke. Proc Natl Acad Sci U S A 98:12766-12771.

Dijkhuizen RM, Singhal AB, Mandeville JB, Wu O, Halpern EF, Finklestein SP, Rosen BR, Lo EH (2003). Correlation between brain reorganization, ischemic damage, and neuro-

logic status after transient focal cerebral ischemia in rats: a functional magnetic resonance imaging study. J Neurosci 23:510-517.

Garwood M, DelaBarre L (2001). The return of the frequency sweep: designing adiabatic pulses for contemporary NMR. J Magn Reson 153:155-177.

Gasparovic C, Rosenberg GA, Wallace JA, Estrada EY, Roberts K, Pastuszyn A, Ahmed W, Graham GD (2001). Magnetic resonance lipid signals in rat brain after experimental stroke correlate with neutral lipid accumulation. Neurosci Lett 301:87-90.

Haberg A, Qu H, Sonnewald U (2006). Glutamate and GABA metabolism in transient and permanent middle cerebral artery occlusion in rat: importance of astrocytes for neuronal survival. Neurochem Int 48:531-540.

Haberg A, Qu H, Haraldseth O, Unsgard G, Sonnewald U (1998). In vivo injection of [1-13C]glucose and [1,2-13C]acetate combined with ex vivo 13C nuclear magnetic resonance spectroscopy: a novel approach to the study of middle cerebral artery occlusion in the rat. J Cereb Blood Flow Metab 18:1223-1232.

Haberg A, Qu H, Saether O, Unsgard G, Haraldseth O, Sonnewald U (2001). Differences in neurotransmitter synthesis and intermediary metabolism between glutamatergic and GABAergic neurons during 4 hours of middle cerebral artery occlusion in the rat: the role of astrocytes in neuronal survival. J Cereb Blood Flow Metab 21:1451-1463.

Hamberg LM, Boccalini P, Stranjalis G, Hunter GJ, Huang Z, Halpern E, Weisskoff RM, Moskowitz MA, Rosen BR (1996). Continuous assessment of relative cerebral blood volume in transient ischemia using steady state susceptibility-contrast MRI. Magn Reson Med 35:168-173.

Harada K, Honmou O, Liu H, Bando M, Houkin K, Kocsis JD (2007). Magnetic resonance lactate and lipid signals in rat brain after middle cerebral artery occlusion model. Brain Res 1134:206-213.

Igarashi H, Kwee IL, Nakada T, Katayama Y, Terashi A (2001). 1H magnetic resonance spectroscopic imaging of permanent focal cerebral ischemia in rat: longitudinal metabolic changes in ischemic core and rim. Brain Res 907:208-221.

Jaillard A, Martin CD, Garambois K, Lebas JF, Hommel M (2005). Vicarious function within the human primary motor cortex? A longitudinal fMRI stroke study. Brain 128: 1122-1138.

Keyvani K, Schallert T (2002). Plasticity-associated molecular and structural events in the injured brain. J Neuropathol Exp Neurol 61:831-840.

Koch KM, McIntyre S, Nixon TW, Rothman DL, de Graaf RA (2006). Dynamic shim updating on the human brain. J Magn Reson 180:286-296.

Liu D, Smith CL, Barone FC, Ellison JA, Lysko PG, Li K, Simpson IA (1999). Astrocytic demise precedes delayed neuronal death in focal ischemic rat brain. Brain Res Mol Brain Res 68:29-41.

Longa EZ, Weinstein PR, Carlson S, Cummins R (1989). Reversible middle cerebral artery occlusion without craniectomy in rats. Stroke 20:84-91.

Mason GF, Rothman DL (2004). Basic principles of metabolic modeling of NMR (13)C isotopic turnover to determine rates of brain metabolism in vivo. Metab Eng 6:75-84.

Nishizawa Y (2001). Glutamate release and neuronal damage in ischemia. Life Sci 69:369-381.

Novotny EJ, Jr., Fulbright RK, Pearl PL, Gibson KM, Rothman DL (2003). Magnetic

resonance spectroscopy of neurotransmitters in human brain. Ann Neurol 54 Suppl 6: S25-31.

Nudo RJ (2006). Mechanisms for recovery of motor function following cortical damage. Curr Opin Neurobiol 16:638-644.

Ottersen OP, Laake JH, Reichelt W, Haug FM, Torp R (1996). Ischemic disruption of glutamate homeostasis in brain: quantitative immunocytochemical analyses. J Chem Neuroanat 12:1-14.

Palmer GC, Peeling J, Corbett D, Del Bigio MR, Hudzik TJ (2001). T2-weighted MRI correlates with long-term histopathology, neurology scores, and skilled motor behavior in a rat stroke model. Ann N Y Acad Sci 939:283-296.

Pascual JM, Carceller F, Roda JM, Cerdan S (1998). Glutamate, glutamine, and GABA as substrates for the neuronal and glial compartments after focal cerebral ischemia in rats. Stroke 29:1048-1056; discussion 1056-1047.

Peeling J, Corbett D, Del Bigio MR, Hudzik TJ, Campbell TM, Palmer GC (2001). Rat middle cerebral artery occlusion: correlations between histopathology, T2-weighted magnetic resonance imaging, and behavioral indices. J Stroke Cerebrovasc Dis 10:166-177.

Petito CK, Morgello S, Felix JC, Lesser ML (1990). The two patterns of reactive astrocytosis in postischemic rat brain. J Cereb Blood Flow Metab 10:850-859.

Pfeuffer J, Tkac I, Choi IY, Merkle H, Ugurbil K, Garwood M, Gruetter R (1999). Localized in vivo 1H NMR detection of neurotransmitter labeling in rat brain during infusion of [1-13C] D-glucose. Magn Reson Med 41:1077-1083.

Provencher SW (1993). Estimation of metabolite concentrations from localized in vivo proton NMR spectra. Magn Reson Med 30:672-679.

Schallert T, Fleming SM, Leasure JL, Tillerson JL, Bland ST (2000). CNS plasticity and assessment of forelimb sensorimotor outcome in unilateral rat models of stroke, cortical ablation, parkinsonism and spinal cord injury. Neuropharmacology 39:777-787.

Thoren AE, Helps SC, Nilsson M, Sims NR (2005). Astrocytic function assessed from 1-14C-acetate metabolism after temporary focal cerebral ischemia in rats. J Cereb Blood Flow Metab 25:440-450.

Thoren AE, Helps SC, Nilsson M, Sims NR (2006). The metabolism of C-glucose by neurons and astrocytes in brain subregions following focal cerebral ischemia in rats. J Neurochem 97:968-978.

Tombari D, Loubinoux I, Pariente J, Gerdelat A, Albucher JF, Tardy J, Cassol E, Chollet F (2004). A longitudinal fMRI study: in recovering and then in clinically stable sub-cortical stroke patients. Neuroimage 23:827-839.

van der Zijden JP, Bouts MJ, Wu O, Roeling TA, Bleys RL, van der Toorn A, Dijkhuizen RM (2008). Manganese-enhanced MRI of brain plasticity in relation to functional recovery after experimental stroke. J Cereb Blood Flow Metab 8:832-840.

Weber R, Ramos-Cabrer P, Justicia C, Wiedermann D, Strecker C, Sprenger C, Hoehn M (2008). Early prediction of functional recovery after experimental stroke: functional magnetic resonance imaging, electrophysiology, and behavioral testing in rats. J Neurosci 28:1022-1029.

Chapter 6 General Discussion

6 General Discussion

Elucidating the long-term structural and functional cerebral changes involved in post-stroke loss and recovery of function is essential for the development of therapeutical strategies aimed at the improvement of final functional outcome. Studies in experimental stroke models have shown to be important in providing more insights into structural as well as functional brain plasticity (Nudo and Friel, 1999). Until recently, examination of structural alterations related to plasticity usually required invasive methods and was limited to cross-sectional measurements at a single time point (Carmichael, 2003). Furthermore, studies on plasticity-associated changes in neuronal function are often limited to invasive measurements in restricted parts of the brain (e.g., electrophysiology measurements) (see Carmichael (2003)).

The studies described in this thesis focussed on the characterization of long-term alterations in brain morphology and function after experimental stroke with the use of *in vivo* MR imaging and spectroscopy techniques, in relation to behavioural assessment of functional recovery. Special attention was given to the potential of advanced MR methods to study long-term *in vivo* structural reorganization, and changes in glucose metabolism and glutamatergic neurotransmission in perilesional areas. We applied manganese-enhanced MRI (MEMRI), diffusion tensor imaging (DTI) and $^{1}H/^{13}C$ MRS to detect neuronal remodelling in areas that appeared unaffected on conventional MRI. In this thesis it is demonstrated that i) MEMRI provides a tool to detect loss, recovery and (re-)arrangement of neuronal connectivity (Chapters 2 and 3); ii) DTI enables one to assess changes in tissue architecture and white matter integrity (Chapter 4); and iii) $^{1}H/^{13}C$ MRS can be used to measure loss and recovery of glucose metabolism and glutamergic neurotransmission (Chapter 5).

The process of neuroplasticity includes a number of structural and physiological changes that may ultimately compensate for lost function. Early on, plasticity involves unmasking and/or strengthening of existing, but functionally inactive pathways. When ischemic damage to a functional network is incomplete, initially affected areas may regain their function (Dijkhuizen et al., 2001; Dijkhuizen and Nicolay, 2003; Weber et al., 2008). After complete disruption, the only alternatives remain substitution by activation of functionally related networks (Seitz and Freund, 1997) or establishment of

new connections. The latter develops more chronically after ischemia, since the structural changes that lead to the formation of new connections involve long-term processes, such as axonal sprouting and synaptogenesis (Carmichael et al., 2001; Keyvani and Schallert, 2002; Carmichael, 2006; Nudo, 2006).

Our studies have revealed a series of changes in tissue morphology (Chapter 4), neuroanatomy (Chapters 2-4) and metabolism (Chapter 5) at subacute and chronic stages after experimental stroke. Based on our data, we propose to roughly categorize the temporal pattern of alterations in perilesional areas that undergo brain plasticity after stroke in three distinct stages (obviously, the exact timing of these changes may vary depending on species and stroke model):

1 ***Acute stage:*** *initiation of fractional structural and functional damage*
   - edema formation (Chapter 4)
   - impaired energy metabolism and neurotransmission (Chapter 5)
   - disturbed neuronal connectivity (Chapters 2 and 3)
2 ***Subacute stage:*** *structural and functional recovery*
   - resolution of edema (Chapter 4)
   - restoration of oxidative glycolysis and glutamatergic neurotransmission (Chapter 5)
   - restitution of ipsilesional connections (Chapter 3)
3 ***Chronic stage:*** *enhanced neuroanatomical connectivity*
   - remodelling of white matter (Chapter 4)
   - increase in structural interhemispheric neuronal connectivity (Chapter 3)

Assumably, during the subacute and chronic stages, the brain adapts to the initial injury and plastic alterations become evident. In the next part of this chapter we will discuss the spatiotemporal profile of changes in neuronal network properties in perilesional areas and the potential role of these changes in functional recovery. Lastly, we will discuss potentials and pitfalls of the applied *in vivo* MR techniques regarding future studies on plasticity after brain injury.

Brain plasticity after stroke

Alterations in perilesional areas

Ischemia causes a sequence of pathophysiological mechanisms such as excitotoxicity, inflammation and apoptosis. Ischemic damage can be identified on conventional T_2- and diffusion-weighted MR images (Hoehn-Berlage et al., 1995). Inside the chronic ischemic lesion, T_2 and ADC_{av} are increased due to severe tissue degeneration and interstitial fluid accumulation (see Dijkhuizen and Nicolay (2003) and references therein) (Chapter 2-5). However stroke-induced damage is not restricted to the ischemic area. Prolonged depression in neuronal activity, blood flow and metabolism may also be

induced in portions of the brain that are connected to but at distance from the site of injury, i.e. diaschisis (Feeney and Baron, 1986; Carmichael et al., 2004). Although diaschisis involves impairment of brain function, it may also trigger restorative processes that may be involved in plasticity (Li et al., 1998; Witte et al., 2000; Carmichael, 2006).

In Chapter 4, a large lesion area with T_2 prolongation was evident acutely after stroke. The apparent lesion size, however, decreased on T_2 maps after a few days. This may be due to partial resolution of vasogenic edema, which usually occurs in the first weeks after ischemia (see Dijkhuizen and Nicolay (2003) and references therein). Nevertheless, our studies indicate, that neurons were still affected in perilesional areas outside the T_2 lesion area. There was delayed and decreased managenese transport to subcortical regions of the sensorimotor network connected to the cortical lesion borderzone, suggestive of a sensorimotor network disruption, after 2 weeks post-stroke (Chapter 2 and 3). In addition, in the cortical area bordering the infarct, there was metabolic deprivation early after stroke (Chapter 5).

As mentioned before, initial damage in perilesional areas may induce restorative processes with beneficial effects in the long run (Feeney and Baron, 1986; Witte and Stoll, 1997; Kury et al., 2004). Early perilesional damage may trigger a phase, in which neuronal networks adapt to the effects of deafferentiation to compensate for loss of function. The studies in this thesis clearly depict long-term changes in neuroanatomy and neuronal function in perilesional areas in parallel with functional recovery. The unfolding of plasticity became prominent at the subacute stage after stroke. Alterations in brain metabolism, tissue architecture and neuronal connectivity were identified in perilesional areas. After three weeks, indication of restitution of previously impaired glutamatergic neurotransmission and oxidative glycolysis was detected in the perilesional cortex (Chapter 5). The early deficiency of energy metabolism and Glu-Gln neurotransmitter cycling may have reduced the metabolic demand and thereby may have allowed later reinstatement of neuronal function (Dijkhuizen et al., 2001; Dijkhuizen et al., 2003; Tombari et al., 2004; Jaillard et al., 2005; Weber et al., 2008). Metabolic recovery in the peri-infarct cortex tied in with resolution of initial tissue damage (Chapter 4) and an improvement of connectivity from the sensorimotor cortex (Chapter 3). Restoration of neuronal network properties observed during the first weeks after stroke may indicate an unmasking or disinhibition of existing pathways rather than formation of new connections (see for reviews Lee and van Donkelaar (1995); Nudo and Friel (1999)). Structural adaptations, however, which are known to develop during weeks to months after stroke (see for reviews Nudo and Friel (1999); Carmichael (2003)), were indicated by enhancement of interhemispheric neuronal connectivity (Chapter 3) and rearrangement of white matter integrity (Chapter 4) at 10 weeks after stroke. These observations are more likely to be related to formation of new connections. Previous studies using histological microscopy techniques have shown comparable results. Several factors involved in the formation of new connections have been shown to be upregulated within the first weeks after cerebral ischemia, including growth-associated protein

43 (GAP-43), synaptophysin, synaptic density and dendritic spines (Stroemer et al., 1995; Li et al., 1998; Ito et al., 2006; Brown et al., 2007). Despite the induction of these processes, actual effective establishment of new connections with the perilesional cortex may take weeks after stroke (Carmichael et al., 2001), which is supported by our studies (Chapter 4).

Correlation with functional recovery

In the previous paragraph three important processes that may contribute to post-stroke loss and recovery of function have been discussed: i) resolution of initial tissue damage, ii) reinstatement of neuronal network properties through restoration of metabolic activity and improvement of neuronal connectivity, and iii) potentiation or formation of existing or new pathways through rearrangement of white matter and enhancement of intra- and interhemisperic neuronal connectivity. These post-stroke cerebral alterations were correlated with changes in sensorimotor function, assessed with a behavioural test providing a neurological score and/or an adhesive removal test. A speculative overview of the time-course of functional recovery along with potentially underlying neuronal alterations described in this thesis is shown in Figure 1.

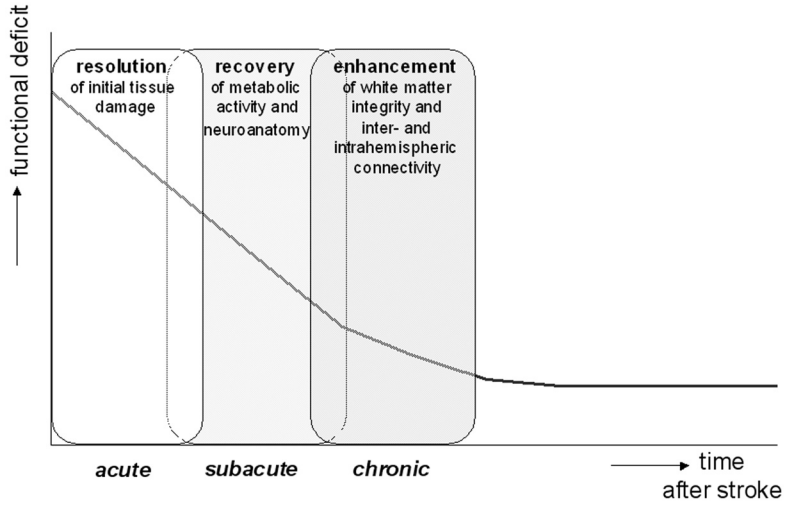

Figure 1

Sequence of structural and functional alterations in perilesional areas during the time course of functional recovery after stroke.

This thesis emphasizes that post-stroke plasticity is a multi-factorial phenomenon. The mechanisms contributing to plasticity each follow a certain time-dependent pattern. It is therefore difficult to directly correlate each of these separate adaptations to functional recovery. More likely, these may all

be individually part of an interacting complex of alterations ultimately leading to the establishment of functional networks responsible for functional recovery (see Figure 1).

Early structural injury and functional disturbances in the sensorimotor network induce direct impairment of sensorimotor function, which usually starts to improve after a few days (Reglodi et al., 2003). In our stroke model, initially impaired sensorimotor function also improved within the first days, which is likely to be the result of the resolution of acute tissue damage (see Lee and van Donkelaar (1995); Carmichael (2003)). Early ischemia-induced changes that are reflective of tissue degeneration, i.e. prolonged T_2 and decreased FA, normalized in the perilesional areas causing the apparent lesion size to decrease (Chapter 4). While early functional recovery is paralleled by a decrease in the apparent lesion size, neuronal connectivity remains largely impaired up to at least 2 weeks after stroke (Chapter 2 and 3). Nevertheless, early factors involved in plasticity, such as neuronal hyperexcitability, disinhibition, dendritic sprouting and synaptic adaptations (see for a review Kreisel et al. (2006)) may already have been initiated.

In the following weeks to months, when the permanent lesion is fully established, sustained functional recovery is more likely to be due to the process of neuroplasticity in regions outside the ischemic zone (see for reviews Nudo and Friel (1999); Kreisel et al. (2006); Rodriguez-Gonzalez et al. (2007)). In this thesis such plastic changes were characterized by recovery of perilesional metabolic activity (Chapter 5) and neuronal intra- and interhemispheric connectivity (Chapter 3).

The long-term processes of structural and functional remodelling described in this thesis provide insights in mechanisms that may be responsible for post-stroke loss and recovery of function. Our findings further suggest that maximal functional recovery is achieved when lost innervation is effectively taken over by existing pathways and/or new connections.

MRI and MRS of brain plasticity

The studies in this thesis demonstrate that MRI provides an *in vivo*, multiparametric tool to examine the spatiotemporal dynamics of brain reorganization after stroke. Despite these promising results that were obtained with these MRI methodologies, several limitations should be considered as well.

MEMRI

In Chapters 2-4, MEMRI was applied to track changes in neuronal pathways of the sensorimotor network after stroke. We have shown that MEMRI enables detection of loss and/or dysfunction of neuronal connections (Chapter 2), as well as reorganization of ipsi- and contralateral pathways (Chapter 3).

The experimental protocol of MEMRI-based *in vivo* neuronal tract tracing is relatively easy and manganese accumulation can be quantified by calcula-

tion of changes in R_1, which are proportional to manganese concentration (Chapters 2-4). Despite the advantages of MEMRI, the specificity of this technique is inferior to that of conventional tract tracing techniques. MEMRI is a macroscopic technique to visualize (changes in) neural pathways without discriminating between anterograde or retrograde distribution of the tracer (Pautler et al., 1998; Pautler, 2004). Thereby, it does not provide straightforward information on the exact anatomical characteristics underlying the observed changes in connectivity (i.e. axonal sprouting, synaptogenesis or dendritic sprouting). Furthermore, due to the relatively large thickness of MRI slices and the partially non-specific distribution of manganese (see Chapter 3), the spatial extent of manganese enhancement is larger than the area labeled with a conventional tract tracer.

Another limitation of MEMRI is that the tissue wash-out of manganese is relatively slow. As shown in Chapter 2, manganese could still be detected at 8 days after injection. This complicates longitudinal MEMRI measurements, which are particularly important in understanding the dynamics of post-stroke plasticity.

The unique properties of manganese, i.e. its paramagnetic character and ability to enter neurons through voltage-gated Ca^{2+} channels, have also led to alternative applications of MEMRI (see for a review Silva et al. (2004)). First, MRI in combination with intravenous infusion of manganese can be used to detect neuronal activation during pharmacological or somatosensory stimulation (Lin and Koretsky, 1997). This technique has been termed activity-induced manganese-enhanced (AIM-MRI). In contrast to BOLD fMRI, which is generally used to map regional brain activation by measuring the hemodynamic response, this technique enables imaging of a parameter directly related to neuronal activity (i.e. calcium influx into neurons). In addition, it induces strong signal enhancement in active brain regions (>50 % instead of 2-5% with BOLD fMRI) (see for review Aoki et al. (2004a)). However, this technique is invasive as it requires opening up the blood-brain barrier in order to achieve rapid manganese accumulation.

Second, MEMRI can be applied to improve detection of details of the neuroarchitecture (Aoki et al., 2004b). After systemic administration, manganese accumulates in specific areas in the brain, which results in strong contrast enhancement of specific structures on MR images (Watanabe et al., 2002). Contrast enhancement largely relies on the regional accessibility through the blood-brain barrier. The application of this technique in stroke research may be complicated, since the focal disruption of the blood-brain barrier after ischemia may affect the manganese distribution.

A major drawback of all MEMRI applications is that manganese acts as a (neuro)toxin at high concentrations. Acute overexposure may cause hepatic failure (Chandra and Shukla, 1976) or cardiac toxicity (Wolf and Baum, 1983), and chronic exposure may eventually lead to neurological disorders (Pal et al., 1999). In the studies described in Chapters 2-4, no behavioural abnormalities were observed in any of the control animals. In addition, neurotoxic effects due to chronic exposure were not an issue, given that manganese was injected only once and rats were studied up to 8 days after the injection. Our

studies show that MEMRI can be safely applied to detect changes in neural pathways after brain injury in laboratory animals. Still, due to the potential neurotoxic effects and the invasiveness of the manganese injection, extension of MEMRI for use in clinical practice remains challenging.

Despite the abovementioned restrictions, MEMRI provides a promising technique for *in vivo* imaging of functional and structural plasticity in animal models of brain injury. Future studies should focus on i) increasing the sensitivity of manganese detection (see Chuang and Koretsky (2006)), and/or ii) development of non-invasive ways to deliver manganese directly to the target organ. Thereby, doses of manganese necessary to get the desired amount of contrast can be reduced to increase specificity, and to minimize toxicity and wash-out time. This may open up opportunities for longitudinal measurements as well as clinical purposes.

DTI

Diffusion Tensor Imaging (DTI) can be used to examine tissue microstructure in the human (Basser et al., 1994) and rodent brain (Xue et al., 1999), and can provide information about the spatial and temporal evolution of stroke that is distinct from other MR techniques (see for a review Sotak (2002)). It enables measurement of spatial characteristics of diffusion of tissue water (i.e. diffusion anisotropy), which are affected by the presence and orientation of barriers, such as cell membranes and myelinated fibres. Hence, changes in the integrity of these structures, e.g. due to cerebral ischemia, may be detected with DTI. In addition, DTI is able to distinguish between gray and white matter and may allow separate assessment of the response of these tissue types to ischemic injury. It has recently been applied to detect modifications of white matter integrity in post-ischemic rat brains (Jiang et al., 2006; Shen et al., 2007). In Chapter 4, DTI was applied in order to track longitudinal changes in structural integrity of brain tissue after stroke. Initial decrease in fractional anisotropy (FA) recovered over time. Moreover, a progressive FA increase in white matter areas was detected, suggestive of white matter rearrangement. These results, however, remain incompletely resolved and must be interpreted carefully. First of all, the exact mechanisms responsible for late FA increase at 10 weeks after stroke described in Chapter 4 remain to be elucidated. Microscopical histological evaluation is required to determine to what extent white matter reorganization and gliosis contribute to chronic post-stroke FA increase. In addition, fluctuations in FA measurements may occur due to the high sensitivity of FA maps to noise and the anatomical variations across the regions-of-interest. Notwithstanding, DTI provides a unique *in vivo* tool to non-invasively track longitudinal changes in structural integrity after stroke. Future studies should be aimed at the improvement of spatial resolution, which may include advanced data acquisition to increase signal-to-noise ratio. In addition, advanced data processing, such as fibre tracking algorithms, and histological evaluation will improve DTI results and the interpretation thereof. Although these matters

are challenging, *in vivo* DTI promises to play an important role for the evaluation of ischemic brain injury, both in experimental and human stroke.

$^{1}H/^{13}C$ MRS

$^{1}H/^{13}C$ MRS in combination with infusion of ^{13}C-labeled glucose can be used to dynamically measure ^{13}C-accumulation in cerebral metabolites. The study in Chapter 5 is the first to describe successful application of *in vivo* $^{1}H/^{13}C$ MRS to detect dynamics of changes in glucose metabolism and glutamatergic neurotransmission in areas with a different degree of ischemic damage. Evidence findings suggest that early functional 'silence' of perilesional tissue is related to deficiency of energy metabolism and Glu-Gln neurotransmitter cycling. More chronically, oxidative glycolysis normalizes and glutamatergic neurotransmission recovers, which may be vital to reinstatement of neuronal function.

In MRS studies, quantification of metabolite concentrations and metabolite turnover requires high signal-to-noise ratios. Individual spectra may be summed to increase the signal-to-noise ratios and the accuracy of fitting of metabolite signals in small volumes. Still, future studies should be aimed improvements in MR acquisition methods (e.g. heteronuclear decoupling) in order to enhance signal-to-noise ratios, thereby enabling individual measurement of metabolite turnover and absolute metabolic fluxes (Patel et al., 2005). Another methodological difficulty is due to partial volume effects. The signal acquired is a superposition of signals originating from different tissue types such as gray and white matter. These regional variations in tissue composition may induce differences in glucose metabolism. Yet, this may be overcome by direct comparison to an area with a similar tissue composition (i.e. homologous contralateral area). Nevertheless, the high sensitivity and spectral resolution shown in the study in Chapter 5 holds great potential for extending $^{1}H/^{13}C$ MRS to study metabolic changes in other brain diseases. Also, it provides an alternative measurement of functional brain activity and may therefore be used as a correlate for other functional imaging studies after stroke.

The MR imaging and spectroscopy methodologies applied in this thesis have shown to offer sensitive means for detecting structural and functional changes in areas in and outside the ischemic lesion. An increasing progress in the field of MR research may lead to an increasing use of MRI and MRS in stroke research, diagnosis and treatment monitoring. Nevertheless, future studies should be aimed at the improvement of experimental protocols and validation of MR methodologies. Specifically, longitudinal, multi-parametric MR protocols in combination with histological evaluation and behavioural assessment may play a key role in resolving the complex pattern of post-stroke neuronal reorganization in relation to functional recovery.

Conclusion

This thesis contributes to an improved knowledge about the neural mechanisms that may underlie post-stroke loss and recovery of function. We have demonstrated evolving neuroanatomical and metabolic remodeling after stroke using multiparametric MR techniques. The spatio-temporal profile of neuronal remodeling suggests that perilesional and connected areas play a key role in neuroplasticity and recovery of function, which continues for months following stroke. This may open up possibilities for long-term treatment of stroke patients directed at the improvement of functional outcome.

References

Aoki I, Naruse S, Tanaka C (2004a). Manganese-enhanced magnetic resonance imaging (MEMRI) of brain activity and applications to early detection of brain ischemia. NMR Biomed 17:569-580.

Aoki I, Wu YJ, Silva AC, Lynch RM, Koretsky AP (2004b). In vivo detection of neuroarchitecture in the rodent brain using manganese-enhanced MRI. Neuroimage 22:1046-1059.

Basser PJ, Mattiello J, LeBihan D (1994). MR diffusion tensor spectroscopy and imaging. Biophys J 66:259-267.

Brown CE, Li P, Boyd JD, Delaney KR, Murphy TH (2007). Extensive turnover of dendritic spines and vascular remodeling in cortical tissues recovering from stroke. J Neurosci 27: 4101-4109.

Carmichael ST (2003). Plasticity of cortical projections after stroke. Neuroscientist 9:64-75.

Carmichael ST (2006). Cellular and molecular mechanisms of neural repair after stroke: making waves. Ann Neurol 59:735-742.

Carmichael ST, Wei L, Rovainen CM, Woolsey TA (2001). New patterns of intracortical projections after focal cortical stroke. Neurobiol Dis 8:910-922.

Carmichael ST, Tatsukawa K, Katsman D, Tsuyuguchi N, Kornblum HI (2004). Evolution of diaschisis in a focal stroke model. Stroke 35:758-763.

Chandra SV, Shukla GS (1976). Role of iron deficiency in inducing susceptibility to manganese toxicity. Arch Toxicol 35:319-323.

Chuang KH, Koretsky A (2006). Improved neuronal tract tracing using manganese enhanced magnetic resonance imaging with fast T(1) mapping. Magn Reson Med 55:604-611.

Dijkhuizen RM, Nicolay K (2003). Magnetic resonance imaging in experimental models of brain disorders. J Cereb Blood Flow Metab 23:1383-1402.

Dijkhuizen RM, Ren J, Mandeville JB, Wu O, Ozdag FM, Moskowitz MA, Rosen BR, Finklestein SP (2001). Functional magnetic resonance imaging of reorganization in rat brain after stroke. Proc Natl Acad Sci U S A 98:12766-12771.

Dijkhuizen RM, Singhal AB, Mandeville JB, Wu O, Halpern EF, Finklestein SP, Rosen BR, Lo EH (2003). Correlation between brain reorganization, ischemic damage, and neurologic status after transient focal cerebral ischemia in rats: a functional magnetic resonance imaging study. J Neurosci 23:510-517.

Feeney DM, Baron JC (1986). Diaschisis. Stroke 17:817-830.

Hoehn-Berlage M, Eis M, Back T, Kohno K, Yamashita K (1995). Changes of relaxation times (T1, T2) and apparent diffusion coefficient after permanent middle cerebral artery occlusion in the rat: temporal evolution, regional extent, and comparison with histology. Magn Reson Med 34:824-834.

Ito U, Kuroiwa T, Nagasao J, Kawakami E, Oyanagi K (2006). Temporal profiles of axon terminals, synapses and spines in the ischemic penumbra of the cerebral cortex: ultrastructure of neuronal remodeling. Stroke 37:2134-2139.

Jaillard A, Martin CD, Garambois K, Lebas JF, Hommel M (2005). Vicarious function within the human primary motor cortex? A longitudinal fMRI stroke study. Brain 128: 1122-1138.

Jiang Q, Zhang ZG, Ding GL, Silver B, Zhang L, Meng H, Lu M, Pourabdillah-Nejed DS, Wang L, Savant-Bhonsale S, Li L, Bagher-Ebadian H, Hu J, Arbab AS, Vanguri P, Ewing JR, Ledbetter KA, Chopp M (2006). MRI detects white matter reorganization after neural progenitor cell treatment of stroke. Neuroimage 32:1080-1089.

Keyvani K, Schallert T (2002). Plasticity-associated molecular and structural events in the injured brain. J Neuropathol Exp Neurol 61:831-840.

Kreisel SH, Bazner H, Hennerici MG (2006). Pathophysiology of stroke rehabilitation: temporal aspects of neuro-functional recovery. Cerebrovasc Dis 21:6-17.

Kury P, Schroeter M, Jander S (2004). Transcriptional response to circumscribed cortical brain ischemia: spatiotemporal patterns in ischemic vs. remote non-ischemic cortex. Eur J Neurosci 19:1708-1720.

Lee RG, van Donkelaar P (1995). Mechanisms underlying functional recovery following stroke. Can J Neurol Sci 22:257-263.

Li Y, Jiang N, Powers C, Chopp M (1998). Neuronal damage and plasticity identified by microtubule-associated protein 2, growth-associated protein 43, and cyclin D1 immunoreactivity after focal cerebral ischemia in rats. Stroke 29:1972-1980; discussion 1980-1971.

Lin YJ, Koretsky AP (1997). Manganese ion enhances T1-weighted MRI during brain activation: an approach to direct imaging of brain function. Magn Reson Med 38:378-388.

Nudo RJ (2006). Mechanisms for recovery of motor function following cortical damage. Curr Opin Neurobiol 16:638-644.

Nudo RJ, Friel KM (1999). Cortical plasticity after stroke: implications for rehabilitation. Rev Neurol (Paris) 155:713-717.

Pal PK, Samii A, Calne DB (1999). Manganese neurotoxicity: a review of clinical features, imaging and pathology. Neurotoxicology 20:227-238.

Patel AB, de Graaf RA, Mason GF, Rothman DL, Shulman RG, Behar KL (2005). The contribution of GABA to glutamate/glutamine cycling and energy metabolism in the rat cortex in vivo. Proc Natl Acad Sci U S A 102: 5588-5593.

Pautler RG (2004). In vivo, trans-synaptic tract-tracing utilizing manganese-enhanced magnetic resonance imaging (MEMRI). NMR Biomed 17:595-601.

Pautler RG, Silva AC, Koretsky AP (1998). In vivo neuronal tract tracing using manganese-enhanced magnetic resonance imaging. Magn Reson Med 40:740-748.

Reglodi D, Tamas A, Lengvari I (2003). Examination of sensorimotor performance following middle cerebral artery occlusion in rats. Brain Res Bull 59:459-466.

Rodriguez-Gonzalez R, Hurtado O, Sobrino T, Castillo J (2007). Neuroplasticity and cellular therapy in cerebral infarction. Cerebrovasc Dis 24 Suppl 1:167-180.

Seitz RJ, Freund HJ (1997). Plasticity of the human motor cortex. Adv Neurol 73:321-333.

Shen LH, Li Y, Chen J, Zacharek A, Gao Q, Kapke A, Lu M, Raginski K, Vanguri P, Smith A, Chopp M (2007). Therapeutic benefit of bone marrow stromal cells administered 1 month after stroke. J Cereb Blood Flow Metab 27:6-13.

Silva AC, Lee JH, Aoki I, Koretsky AP (2004). Manganese-enhanced magnetic resonance imaging (MEMRI): methodological and practical considerations. NMR Biomed 17:532-543.

Sotak CH (2002). The role of diffusion tensor imaging in the evaluation of ischemic brain injury - a review. NMR Biomed 15:561-569.

Stroemer RP, Kent TA, Hulsebosch CE (1995). Neocortical neural sprouting, synaptogenesis, and behavioral recovery after neocortical infarction in rats. Stroke 26:2135-2144.

Tombari D, Loubinoux I, Pariente J, Gerdelat A, Albucher JF, Tardy J, Cassol E, Chollet F (2004). A longitudinal fMRI study: in recovering and then in clinically stable subcortical stroke patients. Neuroimage 23:827-839.

Watanabe T, Natt O, Boretius S, Frahm J, Michaelis T (2002). In vivo 3D MRI staining of mouse brain after subcutaneous application of MnCl2. Magn Reson Med 48:852-859.

Weber R, Ramos-Cabrer P, Justicia C, Wiedermann D, Strecker C, Sprenger C, Hoehn M (2008). Early prediction of functional recovery after experimental stroke: functional magnetic resonance imaging, electrophysiology, and behavioral testing in rats. J Neurosci 28:1022-1029.

Witte OW, Stoll G (1997). Delayed and remote effects of focal cortical infarctions: secondary damage and reactive plasticity. Adv Neurol 73:207-227.

Witte OW, Bidmon HJ, Schiene K, Redecker C, Hagemann G (2000). Functional differentiation of multiple perilesional zones after focal cerebral ischemia. J Cereb Blood Flow Metab 20:1149-1165.

Wolf GL, Baum L (1983). Cardiovascular toxicity and tissue proton T1 response to manganese injection in the dog and rabbit. AJR Am J Roentgenol 141:193-197.

Xue R, van Zijl PC, Crain BJ, Solaiyappan M, Mori S (1999). In vivo three-dimensional reconstruction of rat brain axonal projections by diffusion tensor imaging. Magn Reson Med 42:1123-1127.

Summary

There is increasing evidence that spontaneous functional recovery after stroke is associated with structural and functional changes in non-injured brain circuitry. This thesis "MR Imaging and Spectroscopy of Brain Plasticity after Experimental Stroke" was devoted to unravelling the complex pattern of neural reorganization after stroke, using multi-parametric *in vivo* MR methods. Studies were aimed at the detection of long-term functional and/or structural alterations in perilesional and remote areas that contribute to post-stroke loss and recovery of function. Special focus was given to the potential of advanced MRI and MRS techniques to study post-stroke reorganization.

A general introduction on the subject of this thesis is presented in **Chapter 1**. In *the first paragraph* the potential role of brain plasticity in spontaneous functional recovery after stroke is discussed. Characterization of the spatio-temporal pattern of functional and structural changes underlying spontaneous functional recovery may hold great potential for new therapeutic strategies. Using animal models of focal cerebral ischemia, a combination of multiple experimental methods, including invasive techniques, can be applied to assess the temporal characteristics of brain injury and recovery after stroke.

The second paragraph introduces different advanced MR imaging and spectroscopy methods that can be used to study brain plasticity after stroke. Conventional MR methods, such as T_2 and diffusion-weighted MRI, are able to demonstrate tissue degeneration and can be used to determine the extent and location of the ischemic lesion. Manganese-enhanced MRI (MEMRI) and diffusion tensor imaging (DTI) can inform on neuronal connectivity and microstructural integrity, respectively, and may be able to detect neuroanatomical reorganization. In addition, functional MRI (fMRI) and $^{1}H/^{13}C$ MR spectroscopic imaging ($^{1}H/^{13}C$ MRSI) can depict changes in functional tissue status. The combination of these MR methodologies may provide unique information on morphological as well as functional alterations in brain tissue, which can be measured over time and correlated with functional recovery.

Chapter 2 is aimed at the validation of MEMRI as a technique to depict changes in connectivity within the sensorimotor network chronically after focal cerebral ischemia in rats. To that aim, the dynamics of manganese distribution were characterized by repetitive measurement of manganese-induced changes in R_1 ($1/T_1$) in different brain regions after injection into the spared sensorimotor cortex at 2 weeks after stroke. The MEMRI results were compared with results from a conventional neuronal tract tracing technique based on *post mortem* detection of wheat-germ agglutinin horseradish peroxidase (WGA-HRP) labeling in the brain.

Manganese was transported to distinct regions of the connective pathway between cortex, caudate putamen, substantia nigra and thalamus. In rats with a two-week old unilateral stroke, delayed and decreased manganese accumulation was detected in brain network regions that are connected to the sensorimotor cortex. The reduced build-up of manganese in these regions points toward disturbed connectivity within the sensorimotor network. WGA-HRP labeling was found in the same regions of the ipsilateral sensorimotor pathway as detected with MEMRI. In correspondence with our MEMRI data, after stroke a reduction of WGA-HRP-labeled cells was found in subcortical areas. These data show that MEMRI provides an *in vivo* neuronal tract tracing method to detect changes in neuronal connectivity after experimental stroke.

Chapter 3 describes temporal changes in neuroanatomical connectivity in relation to functional recovery after experimental stroke. Combined neuronal tract tracing with MEMRI and WGA-HRP immunohistochemistry were performed to assess changes in intra- and interhemispheric sensorimotor network connections at different time-points after stroke in rats. We measured the spatial distribution of both neuronal tracers 4 days after injection in the perilesional sensorimotor cortex at 2, 4 and 10 weeks post-stroke along with repetitive behavioural testing.

Manganese enhancement and WGA-HRP staining were decreased in subcortical areas of the ipsilateral sensorimotor network at 2 weeks post-stroke. After 4 and 10 weeks, when rats had reached a plateau stage of functional recovery, ipsilateral sensorimotor pathways were restored and manganese enhancement in connected contralateral regions was increased. These findings suggest that remodelling of intra- and interhemispheric neuronal networks effectively contributes to post-stroke functional recovery.

In **Chapter 4**, the time-course of structural remodelling in perilesional areas was characterized in relation to recovery of neuronal connectivity after unilateral stroke in rats. Repetitive *in vivo* T_2-weighted MRI and DTI measurements were performed from 3 hours to 10 weeks after stroke, followed by MEMRI at 10 weeks.

Early ischemia-induced changes that are reflective of tissue degeneration, i.e. prolonged T_2 and decreased fractional anisotropy (FA), normalized at chronic time-points in the lesion borderzone. In areas where T_2 recovered over time, there was a progressive FA increase in some white matter regions,

suggestive of alterations in fibre structure. This was accompanied by significant manganese enhancement in subcortical regions that had been part of the T_2 lesion at early time points after stroke. This suggests that resolution of initial ischemic damage may be accompanied by remodelling of white matter structure and preservation or restoration of neuronal connectivity, which may be critical factors in post-stroke functional recovery.

Chapter 5 reports on regionally specific alterations in glycolysis and glutamatergic neurotransmitter metabolism at semi-acute and chronic time-points after stroke in relation to functional recovery. Ultrahigh-field *in vivo* $^{1}H/^{13}C$ MRSI during ^{13}C-labeled glucose infusion and MRI were performed at 24 hours and 3 weeks after stroke in rats. Baseline metabolite levels and dynamic formation of glutamate (Glu) and glutamine (Gln) were determined in areas with different degrees of ischemic injury.

Inside the lesion we detected significant reductions in baseline metabolite levels and minimal active Glu and Gln formation at both time-points, indicative of irreversible functional tissue damage. In perilesional areas, early ischemia-induced decreases in *N*-acetyl aspartate (NAA) levels and Glu and Gln turnover were suggestive of neuronal dysfunction. After 3 weeks, when animals showed significant neurological improvement, NAA and Gln levels were normalized. Furthermore, oxidative glycolysis and glutamatergic neurotransmission recovered over time, which is essential for reinstatement of neuronal function. Loss and recovery of brain metabolism in the lesion borderzone may contribute to post-stroke loss and recovery of function.

The findings on long-term structural and functional remodelling after stroke and the potential role thereof in functional recovery are discussed in **Chapter 6**. Also, the MR imaging and spectroscopy techniques applied in this thesis are evaluated.

Changes in tissue morphology, neuroanatomy and metabolic function in (sub)acute and chronic stages after stroke are described, which can be categorized in three distinct stages. At the acute stage, critically impaired sensorimotor function is accompanied by edema formation, reduced energy metabolism and neurotransmission, and disturbed neuronal connectivity. In the following period, early ischemia-induced structural and functional damage recovers in conjunction with restoration of sensorimotor function. Then, at chronic stages after stroke, when functional recovery has reached a plateau stage, there is a further enhancement in neuroanatomical connectivity. This spatiotemporal profile of neural remodelling suggests that perilesional and connected areas play a key role in neuroplasticity and recovery of function, which continues for months following stroke.

Although this thesis contributes to an improved knowledge about the neural mechanisms that may underlie post-stroke loss and recovery of function, future studies are needed to determine the exact correlation between the complex pattern of plasticity and functional recovery remains to be elucidated.

Combination of different magnetic resonance (MR) methodologies offers a

versatile approach to measure mechanisms involved in post-stroke reorganization. Several MR modalities were shown to be able to provide specific information on post-stroke reorganizational changes, which are not detectable with MR techniques that are generally used for clinical applications. MEMRI can detect changes in neuronal connectivity, DTI enables examining of white matter integrity and $^{1}H/^{13}C$ MRS can demonstrate changes in metabolic activity. Future studies should be aimed at the improvement of experimental protocols and validation of MR methodologies. Nevertheless, longitudinal, multi-parametric MR protocols in combination with histological evaluation and behavioural assessment may play a key role in resolving the complex pattern of post-stroke neuronal reorganization in relation to functional recovery.

Samenvatting

Er is steeds meer bewijs dat spontaan functioneel herstel na een hersenberoerte samenhangt met structurele en functionele veranderingen in onbeschadigde hersennetwerken. Dit proefschrift "MR beeldvorming en spectroscopie van hersenplasticiteit na een experimentele beroerte", handelt over het complexe proces van neurale reorganisatie na een hersenberoerte, bestudeerd met behulp van multi-parametrische MR methoden. De onderzoeken waren gericht op het in kaart brengen van langdurige functionele en/of structurele veranderingen in perilesionale en verder gelegen gebieden, die bijdragen aan functioneel verlies en herstel. Speciale aandacht is uitgegaan naar de potentie van nieuwe, geavanceerde MR 'imaging' (MRI) en spectroscopie (MRS) technieken om reorganisatie na een hersenberoerte te bestuderen.

In **Hoofdstuk 1** wordt een algemene introductie gegeven over het onderwerp van dit proefschrift. De potentiële rol van hersenplasticiteit in het spontaan functioneel herstel na een beroerte wordt beschreven in *de eerste paragraaf*. Karakterisering van het spatiotemporele patroon van functionele en structurele veranderingen die bijdragen aan spontaan functioneel herstel kan belangrijk zijn voor het ontwikkelen of verbeteren van therapeutische strategieën. Door gebruik te maken van diermodellen voor focale cerebrale ischemie, kunnen meerdere experimentele methoden worden gecombineerd, waaronder invasieve technieken, om diverse karakteristieken van hersenschade en –herstel na een beroerte te bestuderen.

De tweede paragraaf introduceert verscheidene geavanceerde MR beeldvorming en spectroscopie methoden, die gebruikt kunnen worden om hersenplasticiteit na een beroerte te kunnen onderzoeken. Conventionele MR methoden, zoals T_2- en diffusie-gewogen MRI, zijn geschikt om weefselschade te lokaliseren en kunnen gebruikt worden om het volume van de ischemische lesie te bepalen. MRI met contrast versterking met mangaan (manganese-enhanced MRI (MEMRI)) en diffusie tensor beeldvorming (DTI) kunnen informatie geven over respectievelijk neuronale connectiviteit en microstructurele integriteit van het weefsel, en zijn daarmee mogelijk in staat om neuroanatomische reorganisatie te detecteren. Daarnaast kunnen functionele MRI (fMRI) en $^{1}H/^{13}C$ MR spectroscopische beeldvorming ($^{1}H/^{13}C$

MRSI) veranderingen in de functionele status van het weefsel in kaart brengen. Door deze MR methoden te combineren, kan er unieke informatie verkregen worden over zowel morfologische als functionele aanpassingen in het hersenweefsel. Dergelijke metingen kunnen herhaald uitgevoerd worden over lange periodes en rechtstreeks gecorreleerd worden aan functioneel herstel.

In **Hoofdstuk 2** wordt MEMRI gevalideerd als een techniek om chronische veranderingen in connectiviteit in het sensorisch-motorisch netwerk na focale cerebrale ischemie in ratten te detecteren. Door herhaalde metingen van mangaan-geïnduceerde veranderingen in R_1 ($1/T_1$) in verschillende hersengebieden na injectie in de gespaarde sensorische/motorische cortex werd de dynamiek van mangaan distributie op twee weken na een beroerte bestudeerd. De MEMRI resultaten werden vergeleken met resultaten van een conventionele neuronale tracing techniek gebaseerd op de *post mortem* detectie van 'wheat-germ agglutinine horseradish peroxidase' (WGA-HRP).

Mangaan werd getransporteerd naar verschillende gebieden met projectiebanen tussen de sensorische/motorische cortex, caudate putamen, substantia nigra en de thalamus. In ratten met een 2-weken oude unilaterale beroerte, werd er vertraagde en verminderde mangaan accumulatie gevonden in netwerk regio's die in verbinding staan met de sensorische/motorische cortex. De verminderde ophoping van mangaan in deze regio's wijst op een verstoorde connectiviteit in het sensorisch-motorisch netwerk. WGA-HRP werd gedetecteerd in dezelfde hersengebieden van het ipsilaterale sensorisch-motorisch netwerk als mangaan. In overeenstemming met onze MEMRI resultaten werd er na een beroerte een verminderd aantal WGA-HRP gelabelde cellen gedetecteerd in de subcorticale gebieden. Deze data laten zien dat MEMRI een unieke *in vivo* neuronale tract tracing techniek is om veranderingen in neuronale connectiviteit na een experimentele beroerte zichtbaar te maken.

Hoofdstuk 3 beschrijft de relatie tussen temporele veranderingen in neuroanatomische connectiviteit en functioneel herstel na een experimentele beroerte. Gecombineerde neuronale 'tract tracing' met MEMRI en WGA-HRP immunohistochemie werd toegepast om veranderingen in intra- en interhemisferische connecties in het sensorisch-motorisch netwerk te bepalen op verschillende tijdspunten na een beroerte in ratten. De spatiële distributie van beide neuronale tracers werd gemeten 4 dagen na injectie in de perilesionale sensorisch-motorische cortex op 2, 4 en 10 weken na een beroerte. Tevens werden er herhaalde gedragsmetingen uitgevoerd.

Twee weken na een beroerte was er een afname van mangaan contrast versterking en WGA-HRP aankleuring in subcorticale regiós van het ipsilaterale sensorisch-motorisch netwerk. Na 4 en 10 weken, als ratten een plateau fase van functioneel herstel hadden bereikt, wezen de MEMRI en WGA-HRP data op herstel van de ipsilaterale sensorische/motorische projecties en werd er verhoogde mangaan contrast versterking gevonden in verbonden contralaterale gebieden. Deze bevindingen suggereren dat reorganisatie van

intra- en interhemisferische neuronale netwerken effectief bijdragen aan functioneel herstel na een beroerte.

Hoofdstuk 4 behandelt het tijdsverloop van structurele reorganisatie in perilesionale gebieden in relatie tot herstel van neuronale connectiviteit na een unilaterale beroerte in ratten. Herhaalde *in vivo* T_2-gewogen MRI en DTI metingen werden uitgevoerd van 3 uur tot 10 weken na een beroerte.

Vroege door ischemie geïnduceerde veranderingen die duiden op weefsel degeneratie, namelijk een verlenging van de T_2 en een afname van de fractionele anisotropie (FA) van water diffusie, normaliseerden op chronische tijdspunten in het grensgebied van de lesie. In gebieden waar T_2 herstel over de tijd optrad, werd een progressieve toename van FA in sommige witte stof gebieden gevonden, wat duidt op aanpassingen in vezelstructuur. Dit ging gepaard met significante mangaan contrast versterking in subcorticale regio's die deel uitmaakten van de T_2 lesie op vroege tijdstippen na een beroerte. Dit suggereert dat verdwijning van initiële ischemische schade gepaard gaat met reorganisatie van witte stof structuur en behoud of herstel van neuronale connectiviteit, welke kritische factoren kunnen zijn voor functioneel herstel na een beroerte.

Hoofdstuk 5 beschrijft regio-specifieke metabole veranderingen in glycolyse en glutamaterge neurotransmissie op semi-acute en chronische tijdspunten na een beroerte in relatie tot functioneel herstel. Ultrahoog-veld *in vivo* $^{1}H/^{13}C$ MRSI tijdens infusie van ^{13}C-gelabeld glucose en MRI werden uitgevoerd op 24 uur en 3 weken na een beroerte in ratten. Basisniveaús van metaboliet concentraties en dynamische vorming van glutamaat (Glu) en glutamine (Gln) werden bepaald in gebieden met verschillende mate van ischemische schade.

In de lesie werden significante afnames in metaboliet concentraties en minimale aktieve Glu en Gln vorming gevonden op beide tijdspunten na een beroerte, duidend op ernstige functionele weefselschade. In perilesionale gebieden wezen vroege door ischemie geïnduceerde afnames in *N*-acetyl aspartaat (NAA) concentratie, alsmede verminderde Glu en Gln omzetting, op neuronale dysfunctie. Na 3 weken, wanneer de dieren een significante neurologische verbetering lieten zien, waren NAA en Gln waarden genormaliseerd. Bovendien herstelde oxidatieve glycolyse en glutamaterge neurotransmissie over de tijd, hetgeen essentieel is voor herstel van neuronale functie. Verlies en verbetering van hersenmetabolisme in het perilesionale gebied zou een belangrijke rol kunnen spelen bij functie verlies en herstel na een beroerte.

De bevindingen over chronische structurele en functionele reorganisatie na een beroerte en de potentiële rol ervan in functioneel herstel worden bediscussieerd in **Hoofdstuk 6.** Tevens worden de toegepaste MR beeldvorming en spectroscopie technieken geëvalueerd.

Veranderingen in weefselmorfologie, neuroanatomie en metabole functie in (sub)acute en chronische fases na een beroerte, zoals beschreven in dit

proefschrift, kunnen ingedeeld worden in drie verschillende stadia. In het acute stadium gaat ernstige verstoring van sensorische/motorische functie gepaard met oedeem vorming, afgenomen energie metabolisme en neurotransmissie, en verstoorde neuronale connectiviteit. In de daaropvolgende periode herstellen vroege door ischemie geïnduceerde structurele en functionele schade tegelijk met verbetering in sensorisch/motorisch functioneren. Daarna, in het chronische stadium na een beroerte, wanneer functioneel herstel een plateau fase heeft bereikt, is er een verdere versterking van neuronale connectiviteit. Dit spatiotemporele patroon van neurale reorganisatie suggereert dat perilesionale en overige verbonden gebieden een belangrijke rol spelen in neuroplasticiteit en herstel van functie, hetgeen maanden na een beroerte aanhoudt.

Hoewel dit proefschrift bijdraagt aan een verbetering van kennis over neurale mechanismen die ten grondslag liggen aan functie verlies en herstel na een beroerte, zullen verdere onderzoeken nodig zijn om de exacte correlatie tussen het complexe patroon van plasticiteit en herstel van functie op te helderen.

De combinatie van verschillende magnetische resonantie (MR) methoden biedt een veelzijdige benadering om mechanismen die betrokken zijn bij reorganisatie na een beroerte te meten. De verscheidene MR modaliteiten die beschreven zijn, kunnen specifieke informatie geven over plastische veranderingen na een beroerte, die niet bestudeerd kunnen worden met MR technieken die doorgaans worden gebruikt voor klinische doeleinden. MEMRI kan veranderingen in neuronale connectiviteit zichtbaar maken, DTI kan gebruikt worden om witte stof integriteit te bestuderen en $^{1}H/^{13}C$ MRS kan veranderingen in metabole aktiviteit onthullen. Toekomstig onderzoek zal zich moeten richten op de verbetering van experimentele protocollen en validatie van MR methodologieën. Desalniettemin, longitudinale, multi-parametrische MR protocollen in combinatie met histologische validatie en gedragsmetingen kunnen een essentiële rol spelen in het ontcijferen van het complexe patroon van neuronale reorganisatie in relatie tot functie herstel na een hersenberoerte.

List of Publications

Van der Zijden J, Dijkhuizen RM. "Assessment of functional and neuroanatomical reorganization after experimental stroke using MRI." *In: Tavitian, Leroy-Willig and Ntziachristos, eds. International Textbook on in vivo Imaging in Vertebrates. Chichester: John Wiley & Sons, Ltd, July 2007: 239-242.*

Van der Zijden JP, Wu O, Van der Toorn A, Roeling TP, Bleys RLAW, Dijkhuizen RM. "Changes in neuronal connectivity after stroke in rats as studied by serial manganese-enhanced MRI." *Neuroimage 2007; 34 (4): 1650-7.*

Van der Zijden JP, Bouts MJRJ, Wu O, Roeling TAP, Bleys RLAW, Van der Toorn A, Dijkhuizen RM. "Manganese-enhanced MRI of brain plasticity in relation to functional recovery after experimental stroke." *Journal of Cerebral Blood Flow and Metabolism 2008; 28 (4): 832-40.*

Van der Zijden JP, Van der Toorn A, van der Marel K, Dijkhuizen RM. "Longitudinal *in vivo* MRI of alterations in perilesional tissue after transient ischemic stroke in rats." *Journal of Experimental Neurology; In press.*

Van der Zijden JP, de Graaf RA, van Eijsden P, Dijkhuizen RM. "$^{1}H/^{13}C$ MR spectroscopic imaging of regionally specific metabolic alterations after experimental stroke." *Submitted.*

Dankwoord

De afgelopen jaren heb ik met plezier gewerkt aan de totstandkoming van dit proefschrift. Dit was niet gelukt zonder de hulp, kennis en steun van vele mensen. Ik maak daarom graag van de gelegenheid gebruik om iedereen die een bijdrage heeft geleverd te bedanken. Een aantal mensen wil ik in het bijzonder noemen.

In de eerste plaats wil ik het woord richten tot mijn co-promotor, dr. R.M. Dijkhuizen. Beste Rick, de eindstreep is gehaald! Toen ik (iets meer dan) 4 jaar geleden begon aan mijn promotieonderzoek was de afdeling nog klein. De snelle groei die de *in vivo* NMR heeft gemaakt onder jou supervisie zegt genoeg over je kwaliteiten. Vooral je optimisme, toewijding en kritische blik maken je een bijzonder goede wetenschapper en een ware inspirator. Daarnaast bleek je ook een redelijke karaoke-zanger, en ben je de artiestennaam Ricky Martin Dijkhuizen meer dan waardig. Wat ik eigenlijk wil zeggen: bedankt voor je vakkundige begeleiding en de goede tijd!

Ook mijn promotor, prof. dr. ir. M.A.Viergever ben ik dankbaarheid verschuldigd. Beste Max, bedankt voor je vertrouwen en de mogelijkheid om te promoveren bij de meest fantastische afdeling van het ISI.

Dat ik elke dag weer met goede zin richting de Uithof vertrok, is voor een groot deel te danken aan mijn collega's van de *in vivo* NMR.

Raoul, er is een tijd van komen en een tijd van gaan. We hebben vanaf het eerste moment bloed, zweet en tranen met elkaar gedeeld; maar onze tijd van gaan is aangebroken. Erg fijn, dat ik altijd even mijn ochtendhumeur op je af mocht reageren. Ook de zeikkwartiertjes onder het genot van een senseootje zullen me atijd bijblijven. Gelukkig weet ik dat ik het niet zal hoeven missen en dat de talloze uitnodigingen eraan komen!

Annette, Master of Resonance Imaging. Geen vraag over MRI plaatjes, scanners of sequenties bleef onbeantwoord. Je hebt me de technische snufjes van MRI weten bij te brengen. Over hulp gesproken: Gerard, als we jou toch niet hadden. Het lijkt wel of jij alles uit je hoge hoed kan toveren, van afgebroken elektrodes tot omgebouwde strijkijzers, niets is jou te gek.

Wie ik ook nog even apart wil noemen is meneer "Landscape". Maurits, jij weet alles net even wat krommer te doen. Toch weet je er altijd weer mee weg

te komen. Kortom, de juiste persoon om het stroke/plasticiteits-roer over te nemen.

Mark (mark mark mark mark), ook al is het voor mij nog steeds *fuzzy what C means*, je hebt mijn data weten om te toveren tot een prachtig resultaat. Kajo, ook jouw *Mickey Mouse* analyses zijn onbeschrijflijk. Ik ben blij dat al mijn briefjes nog steeds een prominente plaats mogen innemen op de muur.

Beste Erwin, Ona, Ivo, Wim, Lisette, Casper, Erik, Angga, René, Maartje, Kim, de cardio's en alle studenten. Ik mag mij gelukkig prijzen met zulke collega's. Bedankt voor jullie interesse, gezelligheid, adviezen, zin en onzin.

Ook alle collega's van het ISI en de dierverzorgers van het GDL wil ik bedanken voor een goede tijd.

Een aantal experimenten beschreven in dit proefschrift zijn uitgevoerd op de afdeling Functionele Anatomie van het Rudolf Magnus Instituut. Ik ben prof. dr. Ronald Bleys erkentelijk dat ik van de faciliteiten van de afdeling gebruik heb mogen maken. Daarnaast wil ik alle mensen van de afdeling bedanken voor hun raad en ondersteuning en een aantal in het bijzonder. Allereerst Jan-Willem, jij hebt me wegwijs gemaakt op het lab. Je jarenlange ervaring met immunohistochemische kleuringen hebben me ontzettend geholpen. Ik ben ook veel dank verschuldigd aan Tom, want de Kleine Meander bleek vaak een groot probleem. Het maakte niet uit hoe druk je het had, altijd kon je een gaatje vinden om me te helpen.

Een gedeelte van het onderzoek beschreven in dit proefschrift is uitgevoerd in het Magnetic Resonance Research Center van Yale University School of Medicine, een geweldige ervaring. Beste Robin, bedankt dat je dit project voor me hebt mogelijk gemaakt. Ook ben ik je dankbaar voor alle hulp en gastvrijheid tijdens mijn verblijf in New Haven. Dankzij je inzicht, expertise en nauwkeurigheid heb je me in korte tijd veel weten bij te brengen over ^{13}C Spectroscopic Imaging.

Pieter, de hoeveelheid hulp die ik van jou heb gekregen bij dit project is te veel om op te noemen. Al voordat ik vertrok: het regelen van woonruimte, visum, dieraanvragen, noem maar op. Eenmaal gearriveerd heb je me wegwijs gemaakt in New Haven, waardoor ik me al snel thuis voelde. Vervolgens heb je me na terugkeer uit de brand geholpen met de uitwerking van de data die ik zo enthousiast verzameld had. Zonder jouw bijdrage had ik me geen raad geweten. In één woord: geweldig!

Dear Bei, Graeme, Kevin, Laura, Amy, Terry and all other MRRC-colleagues. Thank you for helping me out, keeping me company en making this into a great adventure for me!

De laatste loodjes wegen het zwaarst. Daarom wil ik mijn nieuwe collega's van de UvA en de studenten van PB1 en PB6 bedanken voor de goede atmosfeer waarin ik terecht ben gekomen. Jullie zijn een belangrijke drijfveer geweest om het proefschrift tot een goed einde te laten komen.

De totstandkoming en verdediging van dit proefschrift zijn mede mogelijk gemaakt door mijn geweldige paranimfen, vriendinnen, jaarclubgenoten en teamgenoten: Dani en Turk (sorry Caro!). Ik zou mij geen beter tweetal aan mijn zijde kunnen wensen voor deze grote gebeurtenis. Ik heb genoten van onze gezellige etentjes, dansavonden, grove grappen-uurtjes en goede gesprekken. Chaotisch en volume op 100, super! Daarnaast wil ik jou, Turk, speciaal bedanken voor het produceren van dit proefschrift.

Om nog even bij de jaarclub te blijven: Houg, Brak, Q en Li. Ik heb jullie gezelschap altijd op prijs gesteld. Ik hoop dat we de jc-etentjes en borrels nog vele jaren blijven volhouden.

Dan mijn Tjelse vriedinnetjes: Maaike, Marjo, Mijk, Fem, Sai en Jan, ik vind het bijzonder dat we na al die jaren nog zo dik zijn met elkaar. Jullie zijn toppers!

Als ware appendix achteraan de lijst: Maris. Van huisgenoot tot gala date, je bent van alle markten thuis.

Je schoonfamilie heb je niet voor het kiezen. Daarom denk ik dat ik mij gelukkig mocht prijzen met die van mij. Lieve Eem, Luc, Cas en Rik: jullie vormen een warm nest, waar ik me als een *ratje in het water* voelde. Van pittige discussies tot rare ratelende rijmende sinterklaasgedichten: ik heb ervan genoten.

Last but not least wil ik het woord richten tot mijn naasten. Lieve pap en mam, wat een bofkont ben ik met zulke ouders. Zonder jullie onvoorwaardelijke steun, liefde en vertrouwen had ik dit niet voor elkaar kunnen boksen.

Lieve broer en zussen, aanhang en kids, een beter stelletje ongeregeld kan ik me niet wensen. Kit en Peter, erg prettig om jullie in de buurt te hebben. Ik denk wel dat Mats Utrecht veel te gezellig vindt en liever niet gaat verhuizen. Mette en Stan, nu heb ik weer tijd om op te komen passen. Dan kunnen Joost en Linda eindelijk een keertje met zijn tweeën uit eten. Ja-maar-Jannie, ook al weet de rest van de wereld het nog niet: je bent de gaafste!

Dan mijn rots in de branding: lieve Jeroen, wat had ik zonder jou gemoeten. Door dik en dun, jij was er altijd. Je positieve energie, liefde en vertrouwen zijn de belangrijkste bron van kracht voor me geweest. Woorden schieten te kort om te zeggen wat jij voor me betekend hebt: je bent de liefste!

Curriculum Vitae

Johanna Petra (Jet) van der Zijden werd geboren op 18 mei 1979 te Tiel. Na het behalen van haar VWO diploma aan het GSG Lingecollege in Tiel, begon zij in 1997 aan de studie Biologie aan de Universiteit Utrecht. Tijdens deze studie deed zij een hoofdvakstage bij de afdeling Neurobiologie onder leiding van dr. R.J.A. van Wezel en dr. I. Hooge, waarbij ze de interactie tussen verschillende oogbewegingen tijdens het volgen van een circulaire stimulus onderzocht. Hierna volgde een onderzoeksstage bij TNO voeding in Zeist onder leiding van dr. C. Krul en prof. dr. W. Seinen, waarbij de genetische toxiciteit van de darminhoud op darmcellen werd onderzocht. Op 20 februari 2003 werd het doctoraal diploma behaald.

Per 1 mei 2003 trad zij in dienst als assistent in opleiding (AIO) bij de afdeling Image Sciences Institute van het Universitair Medisch Centrum Utrecht. Het onderwerp van haar onderzoek was de toepassing van magnetische resonantie technieken om hersenplasticiteit na een hersenberoerte te bestuderen. Het onderzoek werd hoofdzakelijk uitgevoerd op de afdeling Biomedical MR Imaging and Spectroscopy (BMRIS). Daarnaast is een gedeelte van het onderzoek uitgevoerd aan de Yale University School of Medicine (New Haven, CT, USA) onder leiding van dr. R.A. de Graaf. De resultaten van het onderzoek, dat onder supervisie stond van dr. R.M. Dijkhuizen en prof. dr. ir. M.A. Viergever, zijn beschreven in dit proefschrift.

Sinds Februari 2008 werkt ze als Tutor Psychobiologie aan de Universiteit van Amsterdam.